Room temperature ammonia sensors

POLITECNICO DI TORI

Department of Applied Science
and Technology

Room temperature amm
sensors

PhD Thesis

XXVI Cycle-2013)

Supervisor: Prof. M.Tulliani

Co-Supervisor: Prof F. Geobaldo

Candidate: Mirko Borgna

December 2013

Summary

In this thesis, different materials were used to make ceramic sensors to ammonia, obtained by screen printing, working at room temperature. The main objective is to apply these devices to food chemistry, in order to evaluate quantitatively the alteration products of certain food categories, for example meat, which tends to generate biogenic amines, such as cadaverine, putrescine, histamine and others.

Since the ammonia is the simplest amino group, it was decided to characterize ceramic sensors in ammonia atmosphere.

The ceramic materials used for the realization of sensors are ZnO, WO_3 and Bi_2O_3. However, the tests performed have shown that the ceramic oxides were not sufficient to ensure good electrical responses. So, we have functionalized sensors mainly with carboxyl groups, in order to improve the electrical response to ammonia. The best results were obtained by functionalization of glass ceramic with canforquinone (CQ) and benzophenone (BP) via plasma. These sensors give a good response in ammonia atmosphere starting from few ppm.

Acknowledgements

Completing a PhD is truly a marathon event, and I would not have been able to complete this journey without the aid and support of several people over the past three years.
Foremost, I would like to express my sincere gratitude to my supervisor, Prof. Jean Marc Tulliani for the continuous support during my PhD study and research, for his patience, motivation and great knowledge. His guidance helped me all the time during writing of this thesis.
In addition, I would like to thank Prof. Geobaldo for acting to be my co-supervisor in this project and for his insightful comments.

My sincere thanks also goes to Prof. Montanaro: I couldn't forget her excellent advices during LINCE meetings.
I'd like to thank the many colleagues I have worked with in LINCE's group and the ones with whom I have shared the office: Giorgio, Andrea, Chiara, Mohamed and Ahmed.

I thank my family for instilling in me confidence and a drive for pursuing my PhD.

My sincere gratitude also goes to my family in law, for his support and for giving me such a great gift,.

And for last but not least, a great thanks goes to Clara, my beloved life. Without her, this journey would not have ever started ... and these three years would not have been so wonderful. Thank you!

The journey is ended: thanks for having made this moment special! When one door closes, one gate opens.

Table of Contents

Part I

Preface

In recent decades there have been many important changes in lifestyle and food in global market.

It is now common to purchase food in shopping malls, where the food supply is increasing in size and diversity. For this reason it is necessary to adapt and improve controls about the safety and the quality of food. During years, food processing technology has made great strides in agriculture and respectively the population increased. For these reasons, issues concerning food safety have become very complex. The complexity concerns variable quality related to food products, new food products, their conservation and fraud.

In addition, the production processes for food preservation have become very important due to the need to store food for long periods, to avoid chemical and microbiological deterioration, infestation of insects and pathogenic contamination [1]. Today, the producers aim is to introduce innovative products to the market at shorter time intervals, trying to prevent health risks, product losses and disputes. In addition, consumers expect a wide range of competitively priced, highly processed and convenient food products of high quality. They requires fresh, nutritious, healthy, tasty and overall sure food.

On the other hand, consumers have no direct means for their expectations verification and have to rely completely to the supervisory authorities. So food control is fundamental both for the consumers protection and for food industry that intends to gain the trust of consumers.

For these reasons the aim we need to achieve is to prevent the food spoilage, in order to ensure high quality products. It is possible to find many ways to assess and prevent spoilage, using chromatographic and spectrometric techniques, which are the most common tools, or even using ceramic , optical, composite or biochemical sensors.

This thesis deals with the research of ceramic materials, adopted in the food industries to monitor the quality of the food, using thin layers to detect gases. There are many works, easily available in literature, which have been already made about the realization of ceramic materials used for sensing.

The features that distinguish the sensors presented in this thesis from the previous ones are simplicity, speed and low cost to make them.

The first chapter of this thesis presents a detailed description of the main ceramic sensors. Chapter 1 ends with ceramic sensors to ammonia, with a special attention to those who work at room temperature, because sensors aimed to evaluate food spoilage should be used at room temperature.

The second chapter is entirely focused on food chemistry principles and, in particular, on the state of art methods for the determination of food spoilage.

The third chapter deals with the materials studied during this PhD as CO_2 and ammonia sensors and focuses on screen printing technique. The materials studied were designed to be applied to a limited category of spoiled food, particularly those that produce biogenic amines; for this reason, the analysis that will be presented tests the measures of variation of electrical resistances of the sensors with respect to the variation of the concentration of moisture and ammonia, the simplest amino group taken as a reference.

Part II

Bibliographic chapters

Chapter 1

Ceramic Sensors

1.1 Introduction

In the last years the development of new sensors has rapidly grown especially in control systems, for the improvement of industrial processes and of human lifestyle.
The concept of ceramic sensors include all sensors produced using ceramic technology. The reason why these materials are widely used is due to the fact that they exhibit a number of specific features which enable their cost to become lower and their reliability to increase, thus occupying a significant position in sensor technology [1].
In this introduction a very general approach on sensors and ceramic sensors will be treated, dealing with their technology, classification, the types of materials used for their manufacturing, the methods of checking their features and the areas of application. This part will culminate with the focusing on ammonia sensors, whose topic is the main subject of this Ph.D. thesis.

1.2 Classifications and properties of sensors

In general, sensors are devices able to convert physical or chemical quantities into electrical signals [2]. The definition of the IEC (International Electrotechnical Committee) states that the sensor is the primary part of a measuring chain which converts the input variable into a signal suitable for measurement, [3].
It is possible to find basically two kinds of sensors: active and passive. The active one can convert one form of energy directly into another without the need of an external source, while the passive one is not able to convert the energy directly, but it checks the energy or the excitation from another source.
Certain requirements are set for sensors, according to their operating principle and their construction, in general the sensors must be characterized by:

- high sensitivity
- high accuracy
- reproducibility
- high response rate
- selectivity
- broad range of measurement and operating temperatures
- high reliability
- long period of operation
- resistance to ageing and to the ambient influences (vibration, water, dust)
- safety
- low price and small dimensions
- weight
- strength

The aim of a sensor is to carry out a quantitative conversion of a certain property of the substance or the process: the substance may be a solid, a liquid or a gas, while the property registered may be detected in different ways and it may have a physical or a chemical nature.

Sensors can be classified into two families: physical and chemical sensors.

Figure 1.2.1. Flow chart of physical and chemical sensors.

It is possible to find many applications in which these sensors can be used: Table 1.2.1 presents some examples of these applications and the corresponding principles of operation exploited. From Table 1.1 it emerges that sensors can be classified also according to their purpose: so we can find pressure and force sensors, sensors for level, speed sensors, sensors for acceleration, sensors for vibrations, sensors for magnetic field, sensors for vacuum, sensors for displacement, temperature sensors, humidity sensors, gas sensors, biosensors, sensors for radioactive radiation.

Type of sensor	Principle of operation	Quantity being measured
Thermistor (NTC), semiconductor sensor	Resistance€s change	Force, mass, pressure, acceleration, temperature, humidity gas
Capacitance sensor	Capacitance€s change	Force, mass, pressure, acceleration, level, humidity
Inductive sensor	Inductance change	Force, mass, pressure, acceleration, magnetic field torque
Hall sensor	Hall effect	Angle, number of revolutions force, magnetic field
Piezo/ultrasonic sensor	Piezoelectric effect	Pressure, acceleration, distance
Pyroelectric sensor	Pyroelectric effect	Smoke, fire, thermal distribution.
Optoelectronic sensor	Optoelectronic effect	Radiation, angle, torque, number of revolutions, displacement

Table 1.2.1. Possible applications and corresponding quantity being measured of different sensors classified according to their principles of conversion.

Sensors can be classified from different points of view: the materials, the principles of the conversion, the type of output signals, the technology of their production. The classification of the sensors from the point of view of the material used, the devices can be

divided according to the nature of the sensing material: metals, ceramics, polymers and composites.

Finally, sensors can be classified according to their manufacturing technology: so we can find integrated, thin films, thick films and ceramic sensors. Thin film sensors are obtained by depositing an appropriate sensitive thin film onto a dielectric substrate (the basis).

Thick film sensors are realized by depositing an appropriate sensitive paste on a ceramic substrate, most often made of alpha alumina (α-Al_2O_3), followed by a heat treatment in order to shape the thick film.

1.2.1 Classification of ceramic sensors

Ceramic materials are inorganic, non-metallic materials, mainly resulting from the combination of metal and non metal elements by strong bonds (covalent or ionic). They can be crystalline or partially crystalline. They are formed by the action of heat and subsequent cooling [4].

The use of ceramics in sensors application is determined by many properties of the material [5], as for example:

- their microstructure can be controlled over their composition and the firing conditions, in fact the microstructure exerts an evident influence over different properties of the ceramics, such as electrical, optical, magnetic, thermal and mechanical properties;
- these materials can be used for high-temperature applications, thanks to their high temperature resistance and to the ambient influence;
- ceramics are produced by means of relatively simple operations, such as mixing the pristine components, pressing and firing at high temperatures;
- ceramics are produced starting from cheap materials, giving rise to relatively cheap sensors

In general ceramic materials have structural properties connected with the crystal grains (called bulk), the separation surface of near crystal grains (grain boundaries), the separation surface of crystal grains and space (surface) and the pores in the structure. Thanks to these features, both bulk and surface properties can be exploited in the production of ceramic sensors.

Ceramic materials used for sensors application can be classified mainly into three families:

- ceramics exploited for physical properties of the grains;
- ceramics exploited for properties of the grain boundaries;
- ceramics exploited for surface properties;

Standing at this general classification, ceramic sensors exploiting these properties are reported in Table 1.2.1.1.

Exploited attribute	General application	Functional property
Bulk	Temperature sensor	Negative temperature coefficient thermistor (NTC)
	Oxygen gas sensor	Solid electrolyte and semiconduction
	Pressure sensor	Piezoelectricity
	Infrared sensor	Pyroelectricity
	Ultrasonic sensor	Piezoelectricity
	Capacitance temperature sensor	Ferroelectricity
	Magnetic temperature sensor	Ferromagnetic
	Critical temperature senso	Semiconduction
Grain† boundary properties	Temperature sensor	Positive temperature coefficient thermistor(PTC)
	Gassensor	Semiconduction
	Pressure sensor	Semiconduction
Surface properties	Humidity sensor	Conduction/semiconduction

Table 1.2.1.1. Classification of ceramic sensors according to materials properties [6]

Type of sensor	Output signal	Effect	Material
Temperature sensor	Change in resistance	Change in the concentration of t temperature carriers	NiO, CoO, FeO, MnO, MnO-NiOCoO

		Thermistor effect with a negative or positive temperature coefficie	$CoO-Al_2O_3-CaSiO_3$
		Phase transition, barrier effect	$BaTiO_3$
		Phase transition semiconductormetal	VO_2, V_2O_3
	Change in magnetization	Phase transition ferromagnet/paramagnet	Ferrites on the basis of Mn-Zn, Ni-Zn, Mn-Cu
	Change in capacitance	Temperature change the dielectric permittivity of ferroelectrics	$(Ba_{1-x}Sr_x)TiO_3$, $BaTiO_3$, PZT
Gas sensor	Change in resistance	Thermal reaction of the catalytic combustion of gases	Pt catalyst/Al_2O_3/ Pt conductor
		Change in electric charge with adsorption-desorption of gases	SnO_2, ZnO, In_2O_3, WO_3, Fe_2O_3, NiO, Cr_2O_3, TiO_2, etc.
		Temperature variations	Thermistors
Humidity sensor	Change in resistance	Ionic conduction with humidity adsorption	LiCl, ZnO-Li_2O, etc.
		Electron conduction with humidity adsorption	TiO_2, ZnO, $MgCr_2O_4$-TiO_2, Fe_2O_3, etc.
	Change in capacitance	Change the dielectric permittivity with humidity absorption	RuO_2
Optical sensor	Electromotive force	Pyroelectric effect	$SrTiO_3$, $LiNbO_3$, $PbTiO_3$, PZT, etc.
Ultrasonic sensor	Difference in phases of waves	Piezoelectric effect	$PbTiO_3$, $PbZrO_3$, PZT
Sensors for force, pressure	Change in resistance	Piezoresistive effect	ZnO-NiO-Li_2O, ZnO-TiO_2-B_2O_3,

and acceleration			V_2O_5
	Change output voltage	Piezoelectric effect	$PbTiO_3$, $PbZrO_3$, PZT
Piezoresonance sensor	Change in frequency	Piezoelectric effect	$PbTiO_3$, $PbZrO_3$, PZT

Table 1.2.1.2. Ceramic sensors, exploited effects and materials [6].

1.2.2 Parameters of ceramic sensors

The most important parameters for gas sensors are the following ones:

- Sensor resistance in function of gas concentration: it illustrates the influence of gas concentration Cg on the sensor resistance (Rs) or on the conductivity (Gs); the concentration of the gas is usually measured in ppm. At low concentrations of gas in atmosphere and at fixed constant temperature, the conductivity can be described by equation (1.2.2.1)

$$G_s = KC_g^{\alpha} \qquad (1.2.2.1)$$

where K and α are constant and Cg stands for the gas concentration parameters in air.

- Sensor response to gas: it is defined as the relative variation of the starting resistance, comparing it with the resistance measured in gas atmosphere:

$$SR = (R_{Pgas} - R_{Pgas_{air}0}) / R_{Pgas_{air}0} \qquad (1.2.2.2)$$

where $R(P_{gas})$ is the total resistance of the material when exposed to $P(_{gas})$ partial pressure and $R(P_{gas_{air}0})$ is the measured resistance when the gas partial pressure tends to zero. It is function of gas concentration.

- Sensitivity: it is represented by the slope of the calibration curve of the sensor response in function of the gas concentration [7].
- Response characteristic: it is a resistance/time relationship taken down at sharp changes of gas concentration; the response is measured at definite temperature and gas concentration values.

- Operating temperature: it should be specific for any sensor; it is function of the ceramic composition and of the gas to be detected. It is important to define this parameter because with respect to every single gas, the sensor reaches the maximum of its sensitivity at a given temperature.
- Selectivity: it is the ability of a sensor to give response only to a certain gas (Figure 1.2.2.1); it is correlated to a definite gas and it is closely connected with its operating temperature [8].

Figure 1.2.2.1. Schematic representation of the target (triangle) identification in a mixture (rhombus = species of interference).

- Porosity: an important requirement in the production of ceramic materials for sensors application is checking the pores' size: in the case of piezoceramics, ferrite ceramics, PTC and NTC thermistors, varistors and ferroelectric ceramics, the pores' volume is reduced to minimum values, while the role of the pores is particularly important for gases and humidity ceramic sensors [9].

In particular, pores are empty spaces between the ceramic grains which play a very important role on the properties of a ceramic sensor. Concerning the number of pores, it is possible to find pores having three different natures: the open passage pores, which pass through the bulk of the material from a surface to another one, or which start from one surface, go around a certain volume and come back to the same initial surface; the open dead-end pores, which start from a surface and reach to a certain depth in the bulk; internal pores, which are present in the bulk and do not have an outlet on the surface. Besides, pores can have different kinds of shapes, mainly cylindrical, rectangular, split and square. Actually, the structure of the pore system is much more complicated with respect to the

ones that has just been discussed, because the real structure is a combination of the types above defined.

According to their size, it is possible to refer to microporosity when the pore size is below 2 nm, mesoporosity when the pore size is between 2 and 50 nm, and macroporosity for pore sizes over 50 nm [10]. This terminology was developed to classify the porosity of the materials by the IUPAC. Another very important factor connected to the pores is the porosity, defined as [11]:

$$P = V_p/V \qquad (1.2.2.3)$$

where Vp represents the total pore volume and V is the ceramic bulk volume.

For ceramic sensors the last basic concept to define is the specific surface area s, defined as:

$$s = S/m \qquad (1.2.2.4)$$

where [s] = m^2/g, S is the total surface, that is the sum of the ceramic external surface S_S and the surface of the internal pores Sp ($S_S \equiv Sp$).

The specific surface area indicates the reactivity degree of a surface: a large value of s in a ceramic material guarantees a high sensitivity of the sensor, giving rise to a large change in electrical resistance or capacitance.

All these factors (size, porosity and specific surface area) are important in the production of ceramic sensors: they can be controlled by choosing either a suitable temperature regime or by introducing suitable additives which stimulate the pore formation.

1.3 Electrical properties of ceramic sensors

The response of ceramic sensors to an external phenomenon, such as water vapor, gases, pressure, temperature and so on, gives an electrical response, by varying their resistance or the electrical current [12]. For this reason it is fundamental to determine the electrical properties of ceramic oxides in order to explain the ceramic sensors' operation principles.

The specific structure of the ceramics determines the following basic factors, on which its electrical resistance depends: grain bulk, grain surface and grain boundaries.

1.3.1 Electrical conductivity in ceramic sensors

In general the electrical conduction may be of two different natures: electrical and ionic, differing between them from the typology of the species responsible for the conduction. Considering the electron conduction mechanism, in each crystal lattice, the atoms are arranged in a definite order; the atoms of each chemical element in ceramic oxides occupy well defined positions in the lattice site. If all these sites for metal and oxygen atoms are occupied, the material is a perfect crystal.
In order to understand the basic principles of the electrical conduction in ceramic materials, let us consider a particular case, that refers to a semiconducting perfect crystal, whose band structure is shown in Fig. 1.3.1.1.

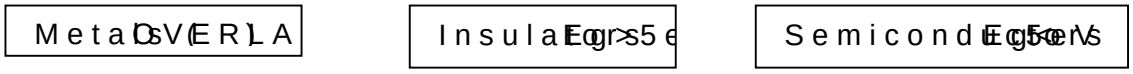

Figure 1.3.1.1 Energy bands characteristic of a conductor, an insulator and a semiconductor.

Eg is the energy gap and represents the width of the forbidden band and it is defined as the difference between the bottom of the conduction band (Ec) and the top of the valence band (Ev), so Eg = Ec – Ev. In semiconductors the value of Eg is approximately 1 eV, while in insulators it may reach 7 eV.
At T = 0 K, the valence band (VB) is completely filled by the electrons, while the conduction band (CB) is completely empty. This deals with a particular case in which a semiconductor material behaves as an insulator one. However T ≠ 0 K, so if the thermal energy increases, the electrons of the VB start to have a sufficient energy to pass the gap so to move to CB: the higher the temperature, the easier the movement of the electrons to pass from a band to another one. As electrons (e) pass to the CB, they leave holes (h) in the VB, which can be seen as positive electrical charges. So at T > 0 K heat generates an e-h couple

with a probability defined by Boltzmann factor exp(-Eg/2kT), where k is the Boltzmann constant (k = 1.38 × 10^{-23} J/K).

The concentrations of electrons (n) and holes (p) generated by temperature are equal: such semiconductor is called intrinsic, characterized by concentrations intrinsic of electrons (n_i) and holes (p_i), defined by equation 1.3.1.1:

(1.3.1.1)

where m_n and m_p are the effective masses of the electrons and holes, respectively, while ħ = 1.05 × 10^{-34} Js (ħ = h/2π) is the normalized Planck's constant.

Once defined n_i and p_i, the electrical conductivity of an intrinsic semiconductor (σ_0) is defined as the sum of the partial conductivities of electrons and holes:

$$\sigma_0 = \sigma_{n_i} + \sigma_{p_i} = q n_i \mu_n + q p_i \mu_p \qquad (1.3.1.2)$$

where μ_n and μ_p are the electron and hole mobilities, respectively.

As n_i and p_i increase exponentially with a rise in temperature, σ_0 also increases following an exponential law.

This feature is exploited in the NTC thermistors, which are sensors whose electrical resistance decreases after an increase in temperature.

Considering the equation 1.3.1.1, the most important factor is the constant of the exponential:

$$B = E_g/2k \qquad (1.3.1.3)$$

The aim is to obtain a high value of B, in order to have high values of n_i and p_i, so a high σ_0. That is possible by choosing either semiconductor materials with a wide E_g if we want to work at high temperatures, or semiconductor materials with a narrow E_g if we want to consider low temperatures applications.

1.3.1.1 Ionic conduction mechanism

Now let us take in consideration the mechanism of ionic conduction [13].

From the point of view of energy, atoms in lattice sites are located in potential wells. If T > 0K, there is a definite probability for some atoms to receive enough heat energy to leave lattice sites. So an intrinsic ionic disorder occurs, as the periodicity of ions in the lattice is disturbed. In this case we use the term ion instead of atoms because the chemical bond is partially or completely ionic and the atoms have a certain electric charge.

These local disturbances are called point defects of the lattice. In particular, two different mechanisms of point defect formation are possible, according to the place the atoms locate after leaving the lattice sites: Frenkel and Schottky defects.

Frenkel defect occurs when atoms A, after leaving the lattice sites, pass in the interstices. This kind of movement can be described by the following equation:

$$0 \rightarrow A_A + V_i \rightarrow V_A + A_i \qquad (1.3.1.1.1)$$

where 0 denotes the perfect crystal, A_A is the atom A occupying its due place in a certain site, V_i is the non-occupied interstice, V_A the non-occupied site by the atom A (so it is a vacancy) and A_i is the atom A located in an interstice. This mechanism is represented in Fig. 1.3.1.1.1.

Figure 1.3.1.1.1. Defect formation mechanism in a crystal having a composition AB: a) Frenkel and b) Schottky types.

The vacancy concentration [VA] is equal to the atom concentration in the interstices [A_i] and can be quantified by the following equation:

$$[V_A] = [A_i] = (N\ N_i)^{1/2} \cdot \exp(-\Delta H_F/2kT) \qquad (1.3.1.1.2)$$

where ΔH_F is the enthalpy of the Frenkel defect formation, N is the number of sites for the atom A, N_i is the number of interstices which may be occupied by atoms A.

However this kind of mechanism not always occurs: in order to have Frenkel defect it is necessary that the dimensions of A are such that they can be placed in the interstices. If such arrangement does not verify, the defects in the lattice are formed according to the Schottky mechanism, shown in Fig. 1.3.1.1.1b.

In this case, the atoms A, after releasing the sites, come out on the crystal surface and the mechanism can be explained by the following equation:

$$0 \rightarrow V_A + A \qquad (1.3.1.1.3)$$

where A indicates the atom A on the surface and V_A the vacancy formed by A.

The concentration of these vacancies is equal to the atom concentration and it is equal to:

$$[V_A] = [A_i] = N \exp(-\Delta H_S/2kT) \qquad (1.3.1.1.4)$$

where N is the number of sites and ΔH_S is the enthalpy of the Schottky defect formation.

Considering both the defect mechanisms, vacancies are formed in the crystal sites and atoms A can occupy the free places located in the near borough. From equations 1.3.1.1.2 and 1.3.1.1.4 it can be evidenced that, as the temperature increases, $[V_A]$ tends to $(NN_i)^{1/2}$ or to N in the case of Frenkel or Schottky mechanism, respectively.

So for $T > 0K$ atoms in the lattice of oxides have an electric charge and due to the mechanisms above described they build the lattice like ions: the metal and the oxygen ions are positively and negatively charged respectively.

In absence of an electric field, ions motion in the sublattice with vacancies is chaotic and it is carried out by hopping from one site to another one. On the contrary, by applying an external electric field, the ionic motion becomes directed and an electric current is generated and starts flowing through the crystal lattice.

This type of electric conduction is called intrinsic ionic conduction

In presence of defects in the sublattices of the metal and the oxygen, the intrinsic ionic conductivity is given by the sum of the conductions of the two types of ionic species:

$$\sigma_{io} = q n_{+} \mu_{+} + q n_{-} \mu_{-} \qquad (1.3.1.1.5)$$

where n_{+} and n_{-} are the vacancy concentrations in the sublattices of the metal and the oxygen, while μ_{+} and μ_{-} are the mobilities of the metal and the oxygen, respectively.
From equations 1.3.1.1.2 and 1.3.1.1.4 it is possible to note that the intrinsic ionic conduction has an activation nature, whose energy is nothing but the enthalpy of the defect formation (ΔH_F and ΔH_S for the Frenkel and Schottky mechanisms, respectively).
So the intrinsic ionic conduction is a sum of the cationic (metal ions) and anionic (oxygen ions) conduction and the crystals characterized by this type of conduction are called ionic conductors or solid electrolytes

1.3.1.2 Extrinsic electron conduction mechanism

Usually, the intrinsic electron conduction is low, for this reason suitable impurities are intentionally introduced inside the crystal in order to increase the conduction [14]. This approach is known as the doping method
In particular, let us consider the case of a generic ceramic oxide characterized by the chemical formula MO, where M is a metal of second valency (e.g. ZnO, MgO, CdO, NiO): if we replace some of the atoms M by the atoms belonging to a metal of third valency, such as Al, the aluminum gives up three electrons instead of two.
Two of these electrons fill the VB, while the third is redundant and connected with the aluminum atom, whose energy level E_d is situated above the middle of the forbidden band E_g, near the bottom of the CB.
At T = 0K the crystal behaves as an insulator and all positions of E_d are occupied by electrons, but when T > 0K part of these electrons in this level have a sufficient energy to pass from E_d to CB, as a result of heat excitation. It is possible to express the electrons concentration in function of the temperature as follows:

$$n = (2N_d)^{1/2} \cdot (m_n kT/2\pi\hbar^2)^{3/4} \cdot \exp(-\Delta E_d/2kT) \qquad (1.3.1.2.1)$$

where N_d is the concentration of donor atoms and $\Delta E_d = E_c - E_d$ is the energy needed to the electrons to pass from E_d to E_c.
So the passage of electrons from E_d to the CB leads to an increase of electric conductivity, determined by the motion of these electrons. This type of semiconductor, characterized by

impurities having a valence number higher than the crystal's atoms, leads to a n-type semiconductor, where n indicates the presence of negative charges responsible for the electric conduction of the material.

The impurities which introduce electrons to the CB are called donors and the E_d represents the donor level.

Let us consider now the opposite situation: if the bivalent metal atom M is replaced by some univalent atoms, i.e. Li, there is a shortage of one electron for each impurity atom for the band atom to be filled. As a consequence, the free energy level in the VB is created and rises above its top: this level (E_a) is situated below the middle of the forbidden band, near the top of the VB. This kind of impurity gives rise to holes in the VB and is called acceptor, while E_a is the acceptor level. This type of doping leads to define the p-type semiconductor, as electrical conductivity is determined by the motion of the holes; p, the indicates that the responsibles for electrical conduction are positive electrical charges (in particular the holes).

The hole concentration in the VB is defined in a similar way as the electron in the CB for a n-type semiconductor:

$$p = (2N_a)^{1/2} \cdot (m_p kT/2\hat{}\ddagger 2)^{3/4} \cdot \exp(\ldots E_a/2kT) \qquad (1.3.1.2.2)$$

where N_a is the concentration of acceptor atoms and $E_a = E_a \ldots E_v$ is the energy needed to the electrons to pass from E_a to E_v.

A schematic representation of the n-type and p-type semiconductors is reported in Fig. 1.3.1.2.1.

Once n and p have been determined, it is possible to define the electrical conductivity for n-type (σ_n) and p-type (σ_p) semiconductors:

$$\sigma_n = qn\check{S}_n \text{Œ} N_d^{1/2} \cdot (m_n T)^{3/4} \cdot \exp(\ldots E_d/2kT) \qquad (1.3.1.2.3)$$

$$\sigma_p = qn\check{S}_p \text{Œ} N_a^{1/2} \cdot (m_p T)^{3/4} \cdot \exp(\ldots E_a/2kT) \qquad (1.3.1.2.4)$$

Figure 1.3.1.2.1. Energy band diagram of n-type and p-type semiconductors. The full circles indicate the electrons, while the empty ones are the holes.

The concentration of free carriers is higher than the intrinsic concentration, because the activation energy of the impurity levels is smaller than the semiconductor forbidden band width.

So by introducing impurities, from eq. 1.3.1.2.3 and 1.3.1.2.4 we can note that relevant conduction can be obtained at lower temperatures than the intrinsic conduction, because n_n and p_p are function of E_d and E_a respectively, which are smaller than E_g of an intrinsic semiconductor.

The doping of semiconductor crystals can be applied to lots of ceramic sensors, such as metal oxide varistors, as ZnO, SnO_2, TiO_2 and $SrTiO_3$, PTC-thermistors, as $BaTiO_3$, humidity ceramic sensors and ceramic sensors for gases. For varistors, the aim is to increase the conductivity of the ceramic grains within definite limits, while for thermistors the main purpose is to achieve low resistance at room temperature. For humidity ceramic sensors doping is carried out both to reduce the electrical resistance at low humidities (in this case sensors' resistance, below 30% RH, exceeds 1 MΩ, making their application below these limits difficult) and to increase the sensor sensitivity by means of secondary impurities. Finally, for ceramic gas sensors, doping lets to increase the sensitivity to a particular gas by means of an appropriate selected impurity.

In general real oxide crystals are nonstoichiometric, that means that the relation between metal cations and oxygen anions is not fulfilled in accordance to their chemical formula.

The deviation from stoichiometry depends on ambient atmosphere and temperature [15]. Often, a certain number of oxygen atoms passes from crystal to the surrounding atmosphere, according to the reaction:

MO ðîñòà $MO_{1-x} + x/2\ O_2$ (1.3.1.2.5)

where x indicates the site of an oxygen atom: from eq. 1.3.1.2.5 x parts remain unoccupied and these vacancies arise in the oxygen sublattice. This process can be chemically summarized by the following reaction:

$O_2 \rightarrow V_0^{2+} + 2e^{-} + 1/2O_2$ (1.3.1.2.6)

As oxygen ions have a negative charge, their corresponding vacancies formed are positively charged. For the valence electrons given up from these parts of the metal atoms no free places in the VB are present. Their energy levels usually situated very close to the bottom of the CB. At medium and high temperatures lots of electrons, situated on this level, pass to the CB. So, the electron concentration is given by the equation:

$n = 2[V_0]$ (1.3.1.2.7)

Thus, oxygen vacancies behave as donor impurities and the corresponding oxide semiconductors is a n-type semiconductor, which includes for example ZnO, CdO, SnO_2, CeO_2, TiO_2, V_2O_5, Nb_2O_5, Ta_2O_5 and WO_3.

In other metal oxides the opposite case can emerge, that means that there may be a shortage of metal atoms in the crystal. In this case the equation 1.3.1.2.5 becomes:

$MO \rightarrow M_{1-x}O + xM$ (1.3.1.2.8)

$M_M \rightarrow V_M^{2-} + 2h^{+} + M$ (1.3.1.2.9)

The metal vacancies are negatively charged and act as acceptor impurities. For each vacancy there is a shortage of two electrons for the VB to be filled and the free energy locates close to the top of the VB. At medium and high temperatures electrons shall leave VB giving rise to holes characterized by a concentration $p = 2[V_M]$.

These materials are p-type semiconductors and include Ag_2O, CoO, MnO, Cr_2O_3, NiO and Cu_2O.

Now let us take into account the ceramic materials' electric properties depending on grain surface.

Different factors influence the electrical features of the ceramic grain, such as the properties of the grain bulk, which has just been discussed above, the interruption of the lattice in the grain boundaries and secondary atoms or molecules on the surface [16].
As this thesis deals with sensitive materials for humidity and gas sensing, the last property will be deepened.
When atoms or molecules coming from the surrounding atmosphere approach to the ceramic grains, they are captured on the surface of the materials giving rise to the phenomenon of adsorption. Depending on the mechanism of this process, it is possible to identify a physical and chemical types of adsorption. The reverse process is called desorption.
In the case of physical adsorption, the atoms and molecules retain their individuality: the forces of their interaction with the surface have mainly an electrostatic nature. They are small and the binding energy with the surface does not exceed 0.1 eV. That explains why the physical adsorption and desorption are carried out at relatively low temperatures.
On the other hand in the chemical adsorption the atoms or molecules are chemically bonded with the crystal: the binding energy is above 1 eV and this kind of bond is predominantly covalent and partially ionic. In this case the adsorption and desorption take place at high temperatures.
Regardless of the type of adsorption, the adsorbed atoms or molecules form donor or acceptor surface levels.
It is not aways possible to differentiate the mechanisms of physical and chemical adsorption strictly: in many real cases the adsorption has a mixed nature.
Let us examine now the influence of the surface states over the band diagram and the electrical properties of the surface layer: in particular, as a starting point, let us take in consideration the cases of the surface layers of intrinsic semiconductors.
For these materials the Fermi level E_F is situated in the middle of the forbidden band and their band diagram is reported in Fig. 1.3.1.2.2.

Figure 1.3.1.2.2. Energy band diagram of an intrinsic semiconductor characterized by a) acceptor and b) donor surface states.

In particular, Fig. 1.3.1.2.2a presents the band diagram in acceptor surface states. They catch electrons from the surface layer, which becomes depleted of electrons and enriched in holes, so bending upwards the energy levels in CB€s bottom and the VB€s top. On the surface, a potential barrier is formed having a height φ_s, of which the electrons must overcome in order to leave the crystal bulk.
In this case the surface layer is enriched in holes having an additional concentration Δp_s, producing an additional electrical conduction occurring in the surface layer, surface conduction, defined as:

$$\sigma_{ps} = q \Delta p_s \mu_{ps} \qquad (1.3.1.2.10)$$

where μ_{ps} is the mobility of the holes in the surface layer.
On the contrary, Fig. 1.3.1.2.2b shows the band diagram of a crystal with donor surface levels: in these levels the electrons pass into the CB in a thin surface level, which is enriched in electrons and depleted in holes. In this case the energy levels bend downwards. For crystals with donor surface levels, being the surface layer enriched in electrons, having an additional concentration Δn_s, an additional electrical conduction occurs, defined in a similar way as 1.3.1.2.10:

$$\sigma_{ns} = q \Delta n_s \mu_{ns} \qquad (1.3.1.2.11)$$

where μ_{ns} is the mobility of the electrons in the surface layer.

Concerning the n-type semiconductors, the Fermi level (E_F) is located below the CB bottom, as it is shown in the band diagrams in the left side of Fig. 1.3.1.2.3a: considering the case of acceptor surface levels, the electrons from the surface layer are captured by the acceptor surface levels. The surface is negatively charged and has a surface density of Q_s. The surface layer having a thickness d_n is depleted of electrons and their concentration may be assumed to zero. This layer is called depletion layer, or area of bulk charge. The energy levels at the bottom of CB and the top of VB in the surface layer bend upwards, leading to the formation of a potential barrier on the surface with a height $q\varphi_s$, which depends on the concentration of electrons in the bulk n and on the concentration of the acceptor surface states N_{as}:

$$j_s = qnd_n^2/2\varepsilon_0\varepsilon = qN_{as}^2/2\varepsilon_0\varepsilon = Q_s^2/2q\varepsilon_0\varepsilon \qquad (1.3.1.2.12)$$

where ε is the relative dielectric constant and $\varepsilon_0 = 8.85 \times 10^{-12}$ F/m. From equation 1.3.1.2.12 the height of the potential barrier depends on the surface and bulk properties of the grains. The depletion layer with a thickness d_n is positively charged and an electrostatic field is formed in it, whose potential change from 0 in the bulk to φ_s on the surface.
The concentration of electrons in this layer is different from zero and changes according to its thickness as follows:

$$n = n_0 \cdot \exp(q\varphi/kT) \qquad (1.3.1.2.13)$$

In the steady state, the Fermi level is constant for the whole bulk of the crystal.
In Fig. 1.3.1.2.3b a band diagram in acceptor surface states is presented: it considers the case when the electron concentration is very low or the surface state concentration is very high. In this case the deformation of the bands is so large that the Fermi level in a thin surface layer passes into the lower half of the forbidden band. This state of the Fermi level corresponds to the p-type semiconductor: the layer so formed, having a hole conductivity in a n-type semiconductor, is called inverse layer and leads to the formation of an p-n junction near the surface.

Figure 1.3.1.2.3 Energy band diagram of n-type and p-type semiconductors characterized by surface states: a) n-type and acceptor surface states; b) p-type and acceptor surface states with an inverse layer; c) n-type and donor surface states acceptor; d) p-type and donor surface states; e) p-type and donor surface states with an inverse n-layer; f) p-type and acceptor surface states.

The conduction of the inverse layer may surpass the bulk conduction.

On the other hand Fig. 1.3.1.2.3c presents the band diagram in donor surface levels: the surface layer, having a thickness d_n, is enriched with electrons and the energy levels are bent downwards, occurring an additional surface conductivity:

$$\Delta\sigma_{ns} = q\Delta n_s \check{S}_{ns} \qquad (1.3.1.2.14)$$

where Δn_s is the additional electrons' concentration in the enriched layer. This effect occurs on the basis of the operation principle of some semiconductor sensors for humidity and gases sensing. Taking into account the case of a p-type semiconductor, the bending of the energy bands is a mirror-image of the n-type semiconductor's bending. So in Fig.

1.3.1.2.3d, 1.3.1.2.3e and 1.3.1.2.3f the cases are examined in parallel and the bending can be mathematically defined as:

$$j_s = qpd_p^2/2\varepsilon_0\varepsilon = qN_{ds}^2/2\varepsilon_0\varepsilon n = Q_s^2/2q\varepsilon_0\varepsilon p \qquad (1.3.1.2.15)$$

where N_{ds} is the concentration of the donor surface states not occupied by the electrons and p is the concentration of the holes in the bulk.

So, for all the cases above mentioned, in order to explain the mechanism of sensing, it is necessary to take in consideration the impurities' concentration (donors or acceptors), the forbidden band width and the dielectric constant. In particular the concentration of the impurities influences the potential barrier height in the formation of the depletion surface layer or the relative share of the surface conduction in the formation of an enriched surface layer. The width of the forbidden band affects the possibility of forming an inverse layer. Finally the dielectric constant influences the potential barrier height and the depletion layer width.

In the production of some sensors, ceramics are used in which potential barriers are formed on the grain surface. In some cases the barriers are formed under an external influence. These potential barriers on the grain surface influence the electrical properties of ceramics, as they prevent the electrons to pass from one grain to another one, so affecting the conduction.

According to the grain binding mechanism, three types of boundaries between them can be differentiated:

- type A: the impurity atoms or non-stoichiometric vacancies, forming the surface layer, are located on the grain surface. These atoms get on the surface either during the ceramics firing process, or by means of diffusion after that. The layer's thickness is disregarded and the boundary is regarded as a direct contact between two grains. The band diagram resulting is shown in Fig. 1.3.1.2.4a. From the energy's point of view, these are two Schottky barriers connected back-to-back and this model is typical of the metal-oxide varistors (MOV), such as ZnO, SnO_2 and TiO_2;
- type B: in the grain boundaries a second phase is formed, whose physical and chemical properties are different from their bulk properties. The layer formed between the grains is thick 1-10 nm and structurally it is crystalline or amorphous. This layer is formed when there is a great amount of impurities: some of them cause surface states and

others decrease the firing temperature and increase the ceramic density (Fig. 1.3.1.24b). This is the typology typical of some varistors and PTC thermistors;

- type C: this type of grain boundary is more complicated and is a combination of the two types above described. One of the probable mechanisms for producing an intermediated layer is a diffusion between the grains or a segregation from the bulk to the surface. One of the materials characterized by this type of boundary is $SrTiO_3$.

The width of the grain boundaries is determined by the sum of the widths of the depletion layers in the contacting grains and by the thickness of the dielectric layers between the grains, if such layers exist. At low voltages, the mechanism of conduction between the grains is a thermionic emission across the Schottky barrier.
The density of the current through the barrier is:

$$j = A \cdot \exp(-q j_s/kT)[1 - \exp(-qV/kT)] \qquad (1.3.1.2.16)$$

where A is the Schottky-Richardson constant and V is the voltage applied. From the equation 1.3.1.2.16 it is possible to determine the potential barrier height by measuring temperature dependence of the current at a constant voltage. At high voltages the conduction of the contacts between the grains is determined by the tunnelling through the barriers.

Figure 1.3.1.2.4 Energy band diagram of the boundary a) of type A and b) type B or C between two ceramic semiconductor grains.

The typical current-voltage characteristic is symmetrical, nonlinear and typical of MOV, presented approximately in the form of:

$$I = CV^{\alpha} \qquad (1.3.1.2.16)$$

where C is constant and α is the nonlinear exponent describing the nonlinearity of the current-voltage characteristic. So the electrical resistance can be expressed as:

$$R = 1/CV^{\alpha-1} \qquad (1.3.1.2.17)$$

1.3.2 Properties of semiconductors

The surrounding atmosphere influences the electron conductivity of ceramic materials, by changing the conductivity of the bulk, the grain surface and the height on the grain boundary potential barriers [17]. In particular gas and water molecules behave as active particles in semiconductor ceramics creating donor and acceptor states of the grain surface or in their bulk.

The changes are evidenced either in the grain bulk or in a thin surface layer and these are the peculiarities which distinguish the semiconductor sensors from proton humidity sensors, for which the conduction has a protonic nature and is verified in the bulk of the adsorbed water vapors.

Ceramic sensors involve oxide ceramics, which is the reason why the influence of oxygen on the bulk properties of the grains plays an important role. Thanks to the oxygen pressure it is possible to control the relation between the metal and the oxygen ions in the lattice, so the concentration of defects in it. In this way electrons and holes' concentration is controlled.

For example, when zinc atoms are dominant in zinc oxide, they are located in the interstices, so ZnO conduction is n-type and depends on the oxygen pressure according to:

$$n \propto p_{O_2}^{-1/6} \qquad (1.3.2.1)$$

where, in this case, $\alpha = -1/6$ at T = 1100°C. If oxygen pressure increases, the type of conduction changes to p-type, as oxygen atoms have been introduced into the sites, acting

as acceptors, leading to an increase of conduction with the increase of pressure, so changing the parameter r from -1/6 to +1/6.

The influence of oxygen on the surface and grain boundaries' properties is very important for ceramic sensors, as the firing process is mostly carried out in air.
So, at high temperatures at which this process is verified, a chemical adsorption of oxygen atoms over the grain surface is carried out. It has been demonstrated that in ceramic varistors as ZnO, grains are covered by a monolayer of oxygen atoms, which act as acceptors according to the following reaction:

$$O_2 + 2e^{\cdot\cdot} \rightarrow 2O^{\cdot\cdot} \text{ or } O_2 + 2e^{\cdot\cdot} \rightarrow O_2^{2\cdot\cdot} \qquad (1.3.2.2)$$

As a consequence, the adsorbed oxygen atoms change the electron concentration in the surface layer, acting as oppositely in n-type and p-type semiconductor ceramics.
In p-type ceramics, the acceptor surface states capture electrons from an enriched surface layer, so increasing the conductivity. A possible model to represent this type of ceramics is shown in Fig. 1.3.2.1.

Figure 1.3.2.1. Model of p-type semiconductor ceramics with acceptor surface states.

The surface layers are in contact between them and create conductive channels, which determine the ceramic conduction. If oxygen pressure increases, the amount of adsorbed oxygen atoms increases and the enriched layers expand.

On the other hand, in n-type semiconductor ceramics, the adsorbed oxygen atoms tend to form depletion layers on the surface and potential barriers occur at the grain boundaries, as Fig. 1.3.2.2 shows.

The potential barrier height has been already defined by equation 1.3.1.11 and the depletion layer width is proportionally inverse to the electrons' concentration:

$$d_n = N_{as}/n = Q_s/qn = \sqrt{(2\varepsilon_0\varepsilon_s/qn)} \qquad (1.3.2.3)$$

In this case, the adsorbed oxygen increases the electrical resistance. In particular, in order to determine the resistance's value, it is necessary to write the current density, already defined by equation 1.3.1.2.16:

$$j \propto V \cdot \exp(-q\phi_s/kT) \qquad (1.3.2.4)$$

From equation 1.3.2.4, the resistance R of the grain boundary is approximated as:

$$R \propto \exp(q\phi_s/kT) = \exp(qN_{as}^2\phi_s/2\varepsilon_0\varepsilon kT) \qquad (1.3.2.5)$$

which depends exponentially on the adsorbed oxygen atoms' concentration.

Figure 1.3.2.2. Model of n-type semiconductor ceramics with potential barriers at the grain boundaries.

Usually, as a result of the oxygen acceptor action, in n-type ceramics barriers in the grain boundaries are formed more easily than those which can be formed in p-type ceramics, because for them donor impurities must be introduced in order to compensate the acceptor action of oxygen.

Before presenting the ceramic sensors for humidity and gases detection, it is important to understand what happens when water or gas molecules approach to a semiconductor ceramic material [18].

In the case of direct interaction with the surface of n-type ceramic semiconductor, the gas and the water molecules are directly adsorbed on the ceramic grain surface, acting as donors when combining with the surface.

Taking H_2 as an example of a reducing gas, the reaction which verifies is:

$$H_2(gas) - 2e^{\cdot\cdot} \rightarrow 2H^{+} \qquad (1.3.2.6)$$

while, if watermolecules approach, the reaction becomes:

$$H_2O(vapor) - e^{\cdot\cdot} \rightarrow H_2O^{+} \qquad (1.3.2.7)$$

So in n-type ceramics, these types of gases tend to reduce the potential barrier height at the grain boundary, by consequently increasing the conductivity, which depends on the pressure that the gas exert on the material's surface, as already shown in eq. 1.3.2.1; in particular in presence of water molecules the parameter β is equal to 1/2, while with reducing gases $\beta = 1/2 \ldots 1/3$ or $1/2 + 1/3$. So:

$$\sigma = \sigma_0 p^{1/2}_{water} \quad (1.3.2.8)$$

$$\sigma = \sigma_0 p^{\beta}_{reducing} \text{ with } \beta = 1/2, 1/3 \quad (1.3.2.9)$$

In p-type materials, the reducing gases and water vapor tend to form a depletion layer and to reduce the conduction.
The reducing gases and water molecules interact chemically with the grain surfaces, as this condition is advantageous from the energy's point of view.
If no oxygen vacancies are present, the reactions which occur at the surface are:

$$H_2 (gas) + O^{\cdot} \rightarrow H_2O + e^{\cdot} \quad (1.3.2.10)$$

$$H_2O (vapor) + O^{\cdot} \rightarrow 2OH + e^{\cdot} \quad (1.3.2.11)$$

On the contrary, if oxygen vacancies can be found, the reactions 1.38 and 1.39 become:

$$H_2O (vapor) + O^{3\cdot} + V_0^{\cdot} \rightarrow 2OH^{\cdot} + e^{\cdot} \quad (1.3.2.12)$$

$$H_2O (vapor) + O^{3\cdot} + V_0^{2\cdot} \rightarrow 2OH^{\cdot} + 2e^{\cdot} \quad (1.3.2.13)$$

Also in this case, the gases act as donors.

1.4 Ceramic humidity sensors

In the electrical characterizations the sensor responses in function of relative humidity (RH) are reported: in order to understand what is the meaning of RH, let us start to present some preliminary definitions, which can be found in ref. [19].

The water vapor pressure is defined as the part of the total pressure of a gas which is contributed by the water vapor component.

The saturation water vapor pressure is the maximum attainable water vapor pressure of a gas for a given temperature and pressure.

The specific humidity is the ratio of the amount of water vapor to the amount of dry carrier gas. Commonly it is expressed in parts per million by volume or weight.

The dew-point is the temperature at which condensation would occur if a gas were to be cooled at constant pressure.

Finally, RH is the ratio of the water vapor pressure to the saturated water vapor pressure at the same temperature; it is expressed as a percentage.

Table 1.4.1 shows the relationship between these units. In particular the RH scale occupies only a small part of the practical humidity scale and is the unit most commonly used in ambient measurement and also in higher concentration levels in, for example, environmental test specifications.

Dew Point (°C)	Saturated vapor pressure (Pa)	Relative humidity at 21°C (%)	Absolute humidity (ppm v/v)
-100	0.001		0.01
-90	0.010		0.10
-80	0.055		0.54
-70	0.262		2.58
-60	1.082		10.68
-50	3.940		38.89
-40	12.940		126.82
-30	38.020	1.5	375.40
-20	103.300	4.2	1,020.00
-10	259.900	10.5	2,572.00
0	611.200	24.6	6,069.00
10	1,227.000	49.4	12,267.00
20	2,339.000	94	23,625.00
30	4,245.000		43,729.00
40	7,381.000		78,571.00
50	12,344.000		138,740.00
60	19,933.000		244,900.00
70	31,177.000		444,450.00
80	47,370.000		878,120.00
90	70,000.000		2,247,000.00
100	101,000.000		Inf

Table 1.4.1. The humidity scale.

The unit ppm v/v indicates the number of parts of water to 1 million parts of dry gas, expressed by volume. Since standard atmospheric pressure is 101,325 Pa, this is expressed as:

$$(\text{ppm v/v}) = \text{svp(Pa)} / 101{,}325 \cdot \text{svp(Pa)} \qquad (1.4.1)$$

where *svp* stands for saturated vapor pressure.

In recent years, the use of humidity control systems has increased in the quality control of production processes and products in a wide range of industries, such as the production of electronic devices, precision instruments, textiles, foodstuffs and in many domestic applications, as for example the control of living environments in buildings, where humidity sensors are used to guarantee a comfortable humidity level and for cooling [20]. Each field requires different operating conditions, so different kinds of humidity sensors have been developed to meet the different requirements.

Different humidity-sensing mechanisms and operating principles have been identified for ceramics. The type of conduction may be ionic or electronic: most current humidity sensors are based on porous sintered bodies of p-type ionic humidity-sensitive ceramics. Other humidity sensors using different sensing mechanisms are of the solid-electrolyte type, or use the heterocontacts between p- and n-type semiconducting oxides.

When the oxides are kept in contact with humid air, water molecules chemisorb on the available sites of the oxide surface, mainly at the neck parts of the crystal grains, by a dissociative mechanism to form two hydroxyl ions for each water molecule, from whom the hydroxyl group adsorbs on metal cations located in the surface layer of the grains, which have high local charge density and a strong electrostatic field. The proton reacts with an adjacent surface $O_2^{\cdots}$ group to form a second $OH^{\cdots}$ group. The chemisorbed layer, once formed, is not further affected by exposure to humidity.

When the first layer of water molecules is formed, subsequent layers of water molecules are physically adsorbed on the first hydroxyl layer. The physisorbed water easily dissociates to form H_3O^+, because of the high electrostatic fields in the chemisorbed layer.

The first layer of physisorbed water molecules is characterized by double hydrogen bonding of a single water molecule. The physisorption changes from monolayer to multilayer when the water vapor pressure increases. Water molecules, in the succeeding physisorbed layers, are only single bonded and form a liquid-like network [21].

Therefore, single bonded water molecules can form dipoles and reorient freely under an externally applied electric field, so increasing the dielectric constant. Physisorption of water molecules can verify at temperatures lower than 100 °C, while, at higher temperatures, chemisorption of water molecules is the only responsible for changes in the electrical conductivity of ceramics.

The interaction between the porous structure and water must also be considered: the presence of open porosity lets water condensation in the capillary pores. The quantity of

condensed water depends on the available pore sizes and their distribution; it is possible to evaluate the pore radius at which capillary condensation occurs at different temperatures (T) by means of the Kelvin equation:

$$r_k = 2 \cdot M / -RT \ln(P_S/P) \qquad (1.4.2)$$

where r_k is the Kelvin radius, P is the water-vapor pressure, P_S is the water-vapor pressure at saturation, $\cdot$, – and M are the surface tension (72.75 dyn cm^{-1} at 20°C), density and molecular weight of water, respectively. Water condensation takes place in all the pores with radii up to r_k, at given temperatures and water-vapor pressures.
The smaller the r_k or the temperature, the more easily the condensation occurs.
These physical interaction mechanisms between water and oxide surfaces are largely recognized to be the basis of the operative mechanisms of a wide range of different humidity-sensor materials.
Now let us examine the case of gas-sensing mechanism of ceramic sensors, deepening in particular the behavior of ammonia on the oxide surfaces.

1.5 Ceramic gas sensors

Ceramic gas sensors can be classified according to different principles, such as the chemical properties of the gas, the sensitivity region of the ceramic material, the conductivity mechanism, the measured physical quantity and the field of application [22].
According to the chemical gas properties, we can find both oxidizing gas sensors, such as O_2, Cl_2 sensors, and reducing gas sensors, sensitive for example to H_2, CO, NH_3, CH_4.
Oxidizing gases form acceptor surface states in semiconductive sensors, while the reducing ones tend to form donor surface states.
According to the sensitivity regions of the ceramic material, gas sensors can be divided into surface and volume sensors: the surface sensors are the traditional semiconductive gas sensors, while the volume ones are all the devices made of solid electrolytes as well as some semiconductive sensors.
According to the conductivity mechanism, ceramic gas sensors behave similarly to the humidity ones: so we can find either the electronic, such as all the semiconductive sensors, and the ionic sensors, as for example those made of solid electrolytes.

According to the measured physical quantity sensitive to the influence of gases, we can define the resistive, potentiometric and amperometric sensors. The resistive sensors are nothing but the semiconductive ones and the sensors made of solid electrolytes; for them the resistance is a function of the gas atmosphere that they detect. The potentiometric and amperometric devices include mainly the solid electrolytes sensors. These kinds of sensors are also called concentration cells and electrochemical pumps.

According to the field of application, ceramic gas sensors can be classified into reducing gas sensors, toxic gas sensors, alcohol sensors, odor sensors, oxygen sensors and other gas sensors.

Not all the sensors just defined will be described: the ones on which we will focus are the semiconductive resistive gas sensors, able to detect reducing gas (in particular NH_3).

The characteristics of resistive gas sensors are not determined by a general approach: the devices are defined in different ways and conditions which must be specified [23].

The first parameter to define is related to the influence of the gas concentration, C_g, namely measured in ppm values (even if sometimes the measurements are carried out in volume percentages), on sensor's resistance R_S or on its conductivity G_S. At low concentration of the gas in air, at a certain temperature, the following equation is approximately valid:

$$G_S = KC_g^{\alpha} \qquad (1.5.1)$$

where K and α are constants and C_g represents the gas concentration in air.

When we speak about measurements performed in air, we mean that measurements are carried out either in clear air or at fixed temperature and humidity.

Another important parameter to define for resistive gas sensors is the sensitivity, defined as the degree of the influence of a gas on the sensor's resistance. This parameter can be defined as:

$$S_g = R_a / R_S \qquad (1.5.2)$$

where S_g is the sensitivity to the gas, R_a the resistance of the sensor in air and R_S the resistance of the sensor exposed to a gas having a concentration C_g.

In particular, if a sensor is exposed to oxidizing gases, its resistance rises (giving a value of $S_g < 1$), while when it is exposed to reducing gases its resistance decreases ($S_g > 1$).

However the definition 1.5.2 has some disadvantages: the sensor€s resistance to air is assumed to be a basic one and it is difficult to compare the sensor€s parameters when the resistance changes within different boundaries. Besides, the sensitivity defined this characterizes a given sensor at a fixed concentration of the gas, so it is a function of this concentration and not an universal parameter.

For this reason generally it is preferable to define the sensitivity of the gas as the relative variation, measured in %, between the resistance of the sensor in air, R_a, and the resistance of the sensor exposed to the gas, R_g

$$S_R(\%) = 100 \cdot ((R_a - R_g)/R_a) \qquad (1.5.3)$$

This last definition has been used for all the measurements done in this Ph.D. thesis

1.6 Ceramics materials

1.6.1 Zinc oxide

Zinc oxide is recognized as one of the most important semiconducting material used for different technological applications.

It is well known that these properties of ZnO are dependent on the crystallinity, preferential orientation, crystallite size, dislocation density, microstrain, texture coefficient and morphology [24]. Thin films of ZnO can be used as a window layer as well as one of the electrodes in solar cells.

Figure 1.6.1.1 Position of the conduction and valence bands of some semiconductors at pH = 1 and some redox potentials

It has a wide band gap energy (3.37 eV at room temperature) [25-26] (Figure 1.6.1.1) and it is a semiconductor with hexagonal wurtzite structure (Figure 1.6.1.2) in which several applications like solar cells, gas sensors, liquid crystal displays and photothermal conversion systems [27-28].

Figure 1.6.1.2 Wurzite structure

A vast amount of research papers, regarding the gas sensing properties of ZnO thick and thin films or nanostructures, have been published in recent years [13-29]. The role of

doping, with atoms of different elements, on the sensing properties of ZnO, was intensively investigated too [34].

1.6.2 Iron oxide

Fe_2O_3 has been widely studied due to its abundance, low cost, and interesting magnetic, semiconducting, and electrochemical properties [35-42].

„-Fe_2O_3 is a n-type semiconductor; it has been proven to be a good gas sensitive material for detection of toxic, combustible, explosive and harmful gases in both domestic and industrial applications, extensive studies have been carried out to improve the gas sensing performances of the €-Fe_2O_3 based sensor [43-44]. It is well-known that the shape and size of €-Fe_2O_3 have a significant influence on its gas sensing properties [43-45].

„-Fe_2O_3, hematite, with an experimental band gap of 2.2 eV [49] was identified as a charge transfer semiconductor [50-51].

Figure 1.6.2.1 Crystal structure of the corundum structure. The transition metal atoms are label as gray while O is red. (a) The rhombohedral primitive cell. (b) The hexagonal representation.

1.6.3 Tungsten oxide

Because of its interesting chemical, optical and electrical properties, tungsten oxide (WO_3), which is a n-type semiconductor, has been the object of extensive research. It was studied

in numerous fields such as electrochromism [52], photoelectrochemical [56-57] and particularly in gas sensor [58-63]. Pure WO_3 has good sensing properties to oxidizing gases such as NO and NO_2 [64-65], O_3 [66-67] and Cl_2 [68]. However for reducing gases (CO, NH_3, ethanol, methanol, etc.), the surface modification of WO_3 by noble catalyst (Pt, Au, and Pd) is required. The sensing mechanism of gas sensors based on modified metal oxides by noble metals (NM-MO) has been reported in the literature by several authors [69-70]. It is accepted that the sensing mechanism is associated to the change of the resistance in contact with the chemisorbed oxygen and gas species on the surface of the metal oxide. For NM-MO such as Pt-SnO_2, Pt-WO_3 and Pd-WO_3, the catalyst on the surface of the metal oxides favors the presence of oxygen species (O^-, O_2^- and O^{2-}) on the surface which depends strongly on the temperature [71]. The ionization of oxygen molecules by the capture of electrons from the conduction band of oxides results in an electron depletion region on the surface of the sensor material. When the surface of the gas sensors is exposed to reducing gases, the oxygen species react with the gases and electrons are given back to the semiconductor, which increases the sensor conductivity [75].

Figure 1.6.3.1 WO_3 lattice monoclinic, pseudocubic [76].

1.6.4 Bismuth oxide

The Bi_2O_3 is much more known transition metal oxide semiconductor.

It has been extensively investigated for various applications as photocatalyst [78], [77] conducting solid electrolyte [79], optical and electrical material in solid oxide fuel cells [80] and oxygen sensors, and selective sensing material for NO detection [81]. In the last decade, Bi_2O_3 has been reported with various morphologies, such as nanorods [82], nanotubes [83], nanowires and nanofibers [84]. Due to such morphology, Bi_2O_3 has found numerous modern applications in electronics and electrooptics [85], catalysis [86] and gas sensors [87].

Figure 1.6.4.1 Bi_2O_3 lattice.

1.7 Ammonia Sensors

1.7.1 High Temperature

There are many principles for measuring ammonia described in literature.
Among all, in this subsection the most frequently used techniques in commercial ammonia detectors are discussed: in particular metal oxide gas sensors and catalytic ammonia detectors are dealt with by considering the applications both at high and at low temperatures.
Let us examine the case of metal oxide ammonia sensors operating at high temperatures.
The ammonia sensors that have been manufactured in the largest quantities are without doubt metal oxide gas sensors, mostly based on SnO_2 sensors. A lot of research has been done on these types of gas sensors [88].

These devices are inexpensive and thus very promising to develop gas sensors.

Many models have been proposed that try to explain the functionality of these types of sensors [91]. It is well established by now that gas sensors operate on the principle of conductance change due to chemisorption of gas molecules on the sensing layer.
A common model is based on the fact that metal-oxide films consist of a large number of grains, contacting at their boundaries. The electrical behavior is governed by the formation of double Schottky potential barriers at the interface of adjacent grains, caused by charge trapping at the interface. The height of this barrier determines the conductance.
When exposed to a chemically reducing gas, like ammonia, adsorption and mutual interaction between the gas and the oxygen result in oxidation of the gas at the surface [92]. Removal of oxygen ions from the grain surface results in a decrease in barrier height. The energy band diagram at the grain boundaries is shown in Fig. 1.7.1.1.

Figure 1.7.1.1. Energy band diagram showing the Schottky barrier height at the grain boundary of tin oxide without and with a chemically reducing gas.

As it can be concluded from this model, metal-oxide sensors are not selective to one particular gas. Different approaches to make selective sensor systems have been applied, like principle component analysis, or artificial neural networks, also known as the artificial nose, or conductance scanning at a periodically varied temperature.
Varying the temperature changes the current density through a Schottky barrier but chemisorption is also a function of the temperature. It is shown that these two effects have a different temperature dependency for different gases. Techniques have been shown to

create micromachined isolated hotplates that can be used to miniaturize and integrate these types of sensors on a chip.

A different approach to make selective metal oxide gas sensors is by using metals or additives that enhance the chemisorption of specific gases.

WO_3 based sensing material is demonstrated to respond to NH_3 and NO [93]. Many materials have been added to this sensing material in order to enhance the sensitivity and the selectivity towards these two gases. Known additives for optimizing the ammonia sensitivity of SnO_2 based ammonia sensors are Pd, Bi and $AlSiO_3$ or Pt and SiO_2. The lowest ammonia detection limit found in literature is 1 ppm, by using WO_3 ammonia sensor with Au and MoO_3 additives. The sensor is operated at an elevated temperature of more than 400°C. Most sensors have even higher detection limits. Normal detection limits of these sensors range from 1 to 1000 ppm. These sensors are commercially available and are mainly used in combustion gas detectors or gas alarm systems, for instance for reliable ammonia leakage detection in refrigeration systems, or for monitoring the ventilation into the passenger compartment in cars.

Another type of ceramic material used for ammonia detection is ZnO [94]: because of its high chemical stability, low dielectric constant, large electromechanical coupling coefficient and high luminous transmittance, ZnO based materials have been widely used as dielectric ceramic, pigment, catalyst and sensing material. As gas sensing material, it is one of the earliest discovered and most widely applied oxide gas sensing material.

It is sensitive to many sorts of gases and has satisfactory stability. However, ZnO based sensors are not selective for a particular gas and various attempts are being made to improve their selectivity. One approach is to use dopants and additives which can modulate the gas-sensing characteristics to some extent. In reference [94] the authors proposed a comparison between pure ZnO, RuO_2-doped ZnO and surface ruthenated ZnO sensors for ammonia detection. The sensing materials were deposited by means of screen-printing technique and the resulting sensors were tested under 1000 ppm of ammonia at different operating temperatures (100, 150, 200, 250, 300 and 350°C). It was demonstrated that the dopants in the ZnO material are necessary in order to increase the sensor response under ammonia atmosphere.

In particular the sensor response is defined in equation 1.5.3, in this case R_a would be the resistance in air and R_g the resistance measured in ammonia atmosphere.

The response of unmodified ZnO to NH_3 was relatively poor with respect to the response of RuO_2-doped ZnO and, above all, with respect to the response of surface ruthenated ZnO (Fig. 1.7.1.2).

ZnO based sensors were found to be sensitive to the operating temperature, the firing temperature and the amount of additive. Let us take into consideration, for example, the case of ruthenated ZnO tested under 1000 ppm of ammonia operating under different temperatures: from the results shown in Fig. 1.6.1.2, the response increased with increasing the RuO_2 amount to attain the maximum (S = 386) at 0.37 wt%, and then decreased with a further increase of RuO_2. The 0.37 wt% RuO_2 would be an appropriate amount to cover the film surface and to make a sufficient number of Ru sites available for adsorption of oxy species which react with the target gas.

The gas-sensing mechanism on the doped ZnO can be explained as follows: atmospheric oxygen molecules are adsorbed on the surface of n-type semiconductor oxides in the forms of $O^{\cdots}$ and $O^{2\cdots}$ thereby decreasing the electronic conduction. Atmospheric oxygen molecules take electrons from the conduction band of n-type ZnO to be adsorbed as $O^{\cdots}$ on ZnO.

The reaction can be expressed as:

$$O_2(gas) + 2e^{\cdots} \rightarrow 2O^{\cdots}_{ZnO} \qquad (1.7.1.1)$$

The ZnO material is oxygen deficient. The excess zinc ions (due to oxygen vacancies) act as electron donors. When reducing gas molecules like NH_3 react with negatively charged oxygen adsorbates, the trapped electrons are given back to conduction band of ZnO. The energy released during decomposition of adsorbed ammonia molecules would be sufficient for electrons to jump up into the conduction band of zinc oxide, causing an increase in the conductivity of the sensor.

Figure 1.7.1.2 Variation in response to 1000 ppm of NH_3 of: a) pure ZnO fired at 500–700 °C, b) thick films doped with different amounts of RuO_2 and fired at 650 °C, c) with surface ruthenation, fired at 650 °C, at different operating temperatures.

The possible reaction is:

$$2NH_3 + 3O^{\cdots}_{ZnO} \rightarrow 3H_2O + N_2 + 3e^{\cdots} \qquad (1.7.1.2)$$

For this reaction to proceed to the right hand side, some amount of activation energy has to be provided thermally. An increase in operating temperature surely increases the thermal energy so as to stimulate the oxidation of NH_3 (equation 1.7.1.2).

The reducing gas (NH_3) donates electrons to ZnO, therefore the resistance decreases, and the conductance increases. This is the reason why the gas response increases with

operating temperature. The point at which the gas response reaches maximum is the actual thermal energy needed for the reaction to proceed.

However, the response decreases at higher operating temperatures, as the oxygen adsorbates are desorbed from the surface of the sensor. Also, at high temperatures the carrier concentration increases due to intrinsic thermal excitation, and the Debye length decreases. This may be one of the reasons for the decreased gas response at high temperatures. As the species are desorbed from the surface, oxygen is adsorbed again.

When the optimum amount of ruthenium oxide (0.37 wt%) is incorporated on the surface of ZnO film, the Ru species would be distributed uniformly throughout the surface of the film. Due to this not only the initial resistance of the film is high but this amount would also be sufficient to promote the catalytic reaction effectively and thelocalarge change in the resistance on exposure of ammonia gas leading to high sensitivity. When the amount of RuO_2 on the surface of the film is less than the optimum, the surface dispersion may be poor and the sensitivity of the film is observed to be decreased since the amount may not be sufficient to promote the reaction more effectively. On the other hand, as the amount of RuO_2 on the surface is more than the optimum, the Ru atoms would be distributed more densely. As a result, the initial resistance of the film would decrease and the overall change in the resistance on the exposure of gas would be smaller leading to lower response to the target gas.

Fig. 1.7.1.3 shows the adsorption of oxygen species on the surface of zinc oxide, abstracting electrons, and thus causing an increase in the potential barrier at grain boundaries.

Thus, by controlling the distribution and amount of the catalyst on the semiconductor oxide surface, it is possible to fabricate sensors with good sensing properties.

Figure 1.7.1.3. Gas-sensing mechanism of surface ruthenated samples: a) oxygen adsorption and b) under ammonia atmosphere.

Another very interesting article which deals with doped ZnO for gas-sensing application at high temperatures and which inspired the first part of the Ph.D. work was the reference [95]: thick films of pure ZnO and Fe_2O_3-modified ZnO were prepared by screen-printing and their results under ammonia atmosphere at 350 °C were compared. The doping of the ZnO films with Fe_2O_3 was obtained by dipping the surface of these films into an aqueous solution of ferric ammonium sulfate for different intervals of time; then the films were dried at 90 °C and fired at 500 °C for 24 h in air ambient. The ferric ammonium sulfate dispersed on the films would be oxidized in the firing process, and sensor elements with different mass % of Fe_2O_3 were obtained.

Upon exposure to NH_3 gas, the barrier height of Fe_2O_3-ZnO intergranular region decreases markedly due to the chemical transformation of Fe_2O_3 into ammonium ferric hydroxide, leading to a drastic increase in conductance, so to a decrease in electrical resistance. In particular the Fe_2O_3-modified films showed very high electrical resistance on the order of 1 GΩ in air and a lower resistance on the order of 10 MΩ upon exposure of 50 ppm NH_3 at 350 °C. The sample, with 0.74 mass % of ferric oxide, was observed to be the most sensitive of all. It showed a response of 178.6 to 50 ppm NH_3 at 350 °C.

The response could be attributed to the adsorption-desorption-type sensing mechanism.

The higher response of this sample as compared to other Fe_2O_3-modified samples may be due to the optimum number of Fe_2O_3 grains dispersed on the surface.

If the amount of α-Fe_2O_3 is smaller than the optimum (0.74 mass %), then the number of Fe_2O_3 misfits on the surface would be smaller. A small amount of oxygen would adsorb and an oxidation of target gas would be weak, giving a smaller response.

When the amount of α-Fe_2O_3 dispersed on the surface is larger than the optimum (0.74 mass %), only some part of Fe_2O_3 would be utilized for the adsorption of oxygen and unused Fe_2O_3 would remain idle, resisting the NH_3 gas to reach the Fe_2O_3-ZnO surface.

Due to this, the resistance of the sensor could not change considerably, giving a comparatively smaller response.

The responses of these sensors are shown in Fig. 1.7.1.4.

Figure 1.7.1.4. Response's variation with operating temperature.

In the case of both semiconductor like pure and modified ZnO, the surface oxygen ions give up electrons, acting as donors, which are completely ionized if they are near the CB; however, if the donor levels are slightly below the conduction band, then these levels are not completely ionized at room temperature but are ionized at higher temperature.

At high temperature, the atmospheric oxygen captures the electrons from the CB of the sensing material:

$$O_{2(air)} + 4e^{-}_{(CB)} \rightarrow 2O^{2-}_{(film)} \qquad (1.7.1.3)$$

This would result in decreasing conductivity of the film. When ammonia reacts with the surface of the film and adsorbed oxygen on the surface of the film, it gets oxidized to nitrogen oxide gas and ferric ammonium hydroxide, liberating free electrons in the CB. The following reaction takes place as:

$$Fe_2O_3 + 5NH_3 + 4O^{2-}_{(film)} \rightarrow [FeNH]_4(OH)_{3(film)} + 2NO_{2(gas)} + 8e^-_{(CB)} \quad (1.7.1.4)$$

This shows the n-type conduction mechanism. The generated electrons contribute to a sudden increase in the conductance of the thick film. The misfit regions dispersed on the surface would enhance the ability of base material to adsorb more oxygen species, giving high resistance in air ambient.
These sensors showed high response to ppm level of gas, high selectivity from mixed gases, quick response and fast recovery.

1.7.2 Room temperature

In foods industries' applications, in order to evaluate foods' quality, the sensors work at room temperature. So in this subparagraph the state-of-art of the most representative ammonia sensors working at room temperature is presented.
In reference [96] where pure ZnO (called S1) and doped ZnO (Zn/Pd, Fe-ZnO and Ru-ZnO, called from now S2, S3 and S4 respectively) were prepared, with whom thick film sensors were realized and tested for specific sensitivity to ammonia gas in air at room temperature.
It has been noted that the sensitivity increases with increasing concentration of NH_3 in all these elements. Among all, S2 gave the highest sensitivity with respect to the others. The sensor response under gas exposure was defined as:

$$S_g = (v_a \dagger v_g)/v_a \quad (1.7.2.1)$$

where v_a is the sensor voltage output in air and v_g that in the presence of the gas.
Moreover, at these operating conditions, all of the sensor elements are insensitive to other test gases such as H_2, CO, ethanol, methanol and acetone. Fig. 1.7.2.1 shows the response time of these elements to 30 ppm of NH_3 in air and at room temperature.

Figure 1.7.2.1. Sensitivity of S1, S2, S3 and S4 for 30 ppm of ammonia gas in air.

The Pd-ZnO (S2) sensor element had a fast response time of 64 s and high sensitivity when compared to S1, S3 and S4. The lack of a quick response to NH_3 of S1, S3 and S4 may be due to the low surface catalytic activity. The response time of S2 to NH_3 is repeatable for the measured concentrations and the time drift is less than 0.5 mV h^{-1}.

All of these elements adsorb H_2O in air (3000-3660 cm^{-1}) which is clearly indicated in the IR spectra. Upon exposure to NH_3 a noticeable decrease in the hydroxyl bands of these sensors has been observed which may be due to the surface reaction of NH_3 with physisorbed H_2O.

Figure 1.7.2.2. Sensitivity of S1, S2, S3 and S4 for 30 ppm of ammonia gas in air.

The resulted reaction product (NH_4OH) which is volatile in nature may be responsible for modulating the sensitivity.

Further, the negligible quantity of the surface reaction product and its high volatility indirectly indicated the observed fast response of these sensors to NH_3 and quick recovery to normal conditions. Moreover the observed insensitivity to other interfering gases and vapors clearly indicated the specificity to NH_3. The observed changes in the sensitivity in pure and doped sensor elements may be attributed to the particle size variations in the calcined powders. The PZnO sensor which showed high sensitivity to different NH_3 concentrations had lower average particle size when compared to the other materials[97 98].

1.8 Conclusion

In this section the basic principles of ceramic sensors are presented, starting from the general definitions related to these devices and the presentation of ammonia ceramic sensors used at room temperature, which constitute the main theme of this thesis.
A section of the chapter is focused on the semiconductor type p, because the sensors studied during this research work have shown these electric behaviors: so it was necessary to show the main semiconductors characteristics and the gas sensing mechanisms that occur on the surface of the sensitive material. A section of the chapter is related to the description of materials used to obtain ammonia sensors. Since the devices described in the following sections are potentially used for the investigation of food quality, it is important to focus the next chapter on the discussion of food chemistry and food spoilage, in order to understand why materials sensitive to ammonia at room temperature have been studied.

Bibliography

1. T. G. Nenov and S. P. Yordanov, Ceramic Sensors Technology and Applications, Technomic Publishing Co. Inc. (1996), p. xi.

2. T. G. Nenov and S. P. Yordanov, Ceramic Sensors Technology and Applications, Technomic Publishing Co. Inc. (1996), pp. 3-11.

3. Terms and Definitions in Industrial Process Measurement and Control, (IEC draft 65/84), International Electrotechnical Committee (1982).

4. T.G. Nenov and S.P. Yordanov, Ceramic Sensors, Technomic Publishing Company, Inc., USA, pp. 133-174

5. T. G. Nenov and S. P. Yordanov, Ceramic Sensors Technology and Applications, Technomic Publishing Co. Inc. (1996), pp. 1-10.

6. T.G. Nenov and S.P. Yordanov, Ceramic Sensors, Technomic Publishing Company, Inc., USA, pp. 234-240

7. K. Galatsis, L. Cukrov, W. Wlodarski, P. McCormick, K. Kalantar-zadeh, E. Comini and G. Sberveglieri, p- and n-type Fe-doped SnO2 gas sensors fabricated by the mechanochemical processing technique, Sensors and Actuators B (Chemical), v B93, n 1-3, (2003), 562-565

8. L.A. Currie, Nomenclature in evaluation of analytical methods including detection and quantification capabilities (IUPAC Recommendations 1995), Pure and Applied Chemistry, v 67, n 10 (1995), 1699-1723

9. T. G. Nenov and S. P. Yordanov, Ceramic Sensors Technology and Applications, Technomic Publishing Co. Inc. (1996), pp. 11-16.

10. P. Colombo, C. Vakifahmetoglu and S. Costacurta, Fabrication of ceramic-com ponents with hierarchical porosity, Journal of Materials Science 45 (2010), pp. 5425-5455.

11. T. G. Nenov and S. P. Yordanov, Ceramic Sensors Technology and Applications, Technomic Publishing Co. Inc. (1996), pp. 17-20.

12. T. G. Nenov and S. P. Yordanov, Ceramic Sensors Technology and Applications, Technomic Publishing Co. Inc. (1996), pp. 24-26.

13. T. G. Nenov and S. P. Yordanov, Ceramic Sensors Technology and Applications, Technomic Publishing Co. Inc. (1996), pp. 27-28.

14. T. G. Nenov and S. P. Yordanov, Ceramic Sensors Technology and Applications, Technomic Publishing Co. Inc. (1996), pp. 29-31.

15. T. G. Nenov and S. P. Yordanov, Ceramic Sensors Technology and Applications, Technomic Publishing Co. Inc. (1996), p. 33.

16. T. G. Nenov and S. P. Yordanov, Ceramic Sensors Technology and Applications, Technomic Publishing Co. Inc. (1996), pp. 40-49.

17. T. G. Nenov and S. P. Yordanov, Ceramic Sensors Technology and Applications, Technomic Publishing Co. Inc. (1996), pp. 66-67.

18. T. G. Nenov and S. P. Yordanov, Ceramic Sensors Technology and Applications, Technomic Publishing Co. Inc. (1996), pp. 68-69.

19. P. T. Moseley, J. O. W. Norris and D. E. Norris, Techniques and mechanisms in gas sensing, Adam Hilger Bristol, Philadelphia and New York (1991), pp. 188-189

20. E. Traversa, Ceramic sensors for humidity detection: the state-of-the-art and future developments, Sensors and Actuators B 23 (1995), pp. 135-156.

21. M. Egashira, M. Nakashima, S. Kawasumi and T. Seiyama, Temperature programmed desorption study of water adsorbed on metal oxides, Bulletin of the Chemical Society of Japan 51 (1978), pp. 3144-3149.

22. T. G. Nenov and S. P. Yordanov, Ceramic Sensors Technology and Applications, Technomic Publishing Co. Inc. (1996), pp. 133-134.

23. T. G. Nenov and S. P. Yordanov, Ceramic Sensors Technology and Applications, Technomic Publishing Co. Inc. (1996), pp. 34-136.

24. G.Yanfeng, N. Masayuki, Morphology Evolution of ZnO Thin Films from Aqueous Solutions and Their Application to Solar Cells, Langmuir 22 (2006) 3339-3346.

25. S. Ghosh, P. Srivastava, B. Pandey, S. Maurav, P. Bharadwaj, D.K. Avasthi, D. Kabiraj, S.M. Shivaprasad, Study of ZnO and Ni-doped ZnO synthesized by atom beam sputtering technique, Applied Physics A 90 (2008) 761–765.

26. B. Pandey, S. Ghosh, P. Srivastava, D. Kabiraj, T. Shripati, N.P. Lalla, Synthesis of nanodimensional ZnO and Ni-doped ZnO thin films by atom beam sputtering and study of their physical properties, Physica E 41 (2009) 1161–1168.

27. K.L. Chopra, S. Major, D. K. Pandya, Transparent conductors—A status review, Thin Solid Films 102 (1983) 1–46.

28. R. Mariappan, V. Ponnuswamy, M. Ragavendar, Influence of molar concentration on the physical properties of nebulizer-sprayed ZnO thin films for ammonia gas sensor Materials Science in Semiconductor Processing 16 (2013) 1335–1343.

29. B.L. Zhu, C.S. Xie, J. Wu, D.W. Zeng, A.H. Wang, X.Z. Zhao, Influence of Sb, In and Bi dopants on the response of ZnO thick films to VOCs, Materials Chemistry and Physics 96 (2006) 459–465.

30. P.P. Sahay, R.K. Nath, Al-doped zinc oxide thin films for liquid petroleum gas (LPG) sensors, Sensors and Actuators B: Chemical 133 (2008) 222–227.

31. Y.-J. Li, K.-M. Li, C.-Y. Wang, C.-I. Kuo, L.-J. Chen, Low-temperature electrodeposited Cu-doped ZnO nanorods with enhanced ethanol and CO sensing properties, Sensors and Actuators B: Chemical 161 (2012) 737–744.

32. X. Wang, M. Zhao, F. Liu, J. Jia, X. Li, L. Cao, C_2H_2 gas sensor based on Ni-doped ZnO electrospun nanofibers, Ceramics International 39 (2013) 2883–2887.

33. L. Han, D. Wang, Y. Lu, T. Jiang, L. Chen, T. Xie, Y. Lin, Influence of annealing temperature on the photoelectric gas sensing of Fe-doped ZnO under visible light irradiation, Sensors and Actuators B: Chemical 177 (2013) 403–409.

34. A.P. Rambu, L. Ursu, N. Iftimie, V. Nica, M. Dobromir, F. Iacomi, Study on Ni-doped ZnO films as gas sensors, Applied Surface Science 280 (2013) 694–698.

35. H. B. Wu, J. S. Chen, H. H. Hng, X. W. Lou,* Nanostructured metal oxide-based materials as advanced anodes for lithium-ion batteries, Nanoscale, 4, 2526–2542 (2012).

36. T. Yu, Y. Zhu, X. Xu, K.S. Yeong, Z. Shen, P. Chen, C.T. Lim, J.T.L. Thong, C.H. Sow, Simple nanoscience: Substrate-friendly synthesis of metal oxide nanostructures using a hotplate, Small 2 (2006) 80.

37. J. Chen, L. Xu, W. Li, X. Gou, α-Fe_2O_3 Nanotubes in Gas Sensor and Lithium-Ion Battery Applications Adv. Mater. 17 (2005) 582-586.

38. J. Sarradin, A. Guessous, M. Ribes, J., Synthesis and characterization of lithium intercalation electrodes based on iron oxide thin films, Power Sources 62 (1996) 149-154.

39. J. Morales, L. Sánchez, F. Martín, F. Berry, X. Ren, S. Synthesis and characterization of nanometric iron and iron-titanium oxides by mechanical milling: electrochemical properties as anodic materials in lithium cells, Electrochem. Soc. 152 (2005) A1748.

40. D. Larcher, D. Bonnin, I. Rivals, L. Personnaz, J.M. Tarascon,, Combined XRD, EXAFS, and Mössbauer Studies of the Reduction by Lithium of α-Fe_2O_3 with Various Particle Sizes, J. Electrochem. Soc. 150 (2003) A1643.

41. M.V. Reddy, T. Yu, C-H. Sow, Z. Shen, C.T. Lim, G.V. Subba Rao, B.V.R. Chowdari, α-Fe_2O_3 nanoflakes as an anode Material for Li-ion batteries, Adv. Funct. Mater. 17 (2007) 2792.

42. Huang, Bo; Tai, Kaiping; Dillon, Shen J, Structural evolution of Fe_2O_3 nanowires during lithiation and delithiation, Journal of Power Sources 245 (2014) 308-314

43. S.Wang,L.iWang,T.Yang,X.Liu,J.Zhang,B.Zhu,S.Zhang,W. Huang,S.Wu,Porous α-Fe_2O_3 hollow microspheres and their application for acetone sensor,Journal of Solid State Chemistry 183 (2010) 2868-2876.

44. L.Huo,Q.Li,H.Zhao,L.Yu,S.Gao,J.Zhao, Solgel routeto pseudo cubics haped a Fe_2O_3 alcohol sensor: preparation and characterization, Sensors and Actuators B107(2005)915-920.

45. S.Y.Wang,W.Wang,W.Z.Wang,Z.Jiao,J.H.Liu,Y.T.Qian, Characterization and gas sensing properties of nanocrystalline iron (III)oxide films prepared by ultrasonic spray pyrolysis on silicon, Sensors and Actuators B69(2000)212-217.

46. E.T.Lee,G.E.Jang,C.K.Kim,D.H.Yoon ,Fabrication and gas sensing properties of a Fe_2O_3 thin film prepared by plasma enhanced chemical vapor deposition (PECVD), Sensors and Actuators B77 (2001) 222-227.

47. Q.Hao,L.Li,X.Yin,S.Liu,Q.Li,T.Wang, Anomalous conductivity-type transition sensing behaviors of n-type porous a-Fe2O3 nanostructure stowards H_2S, Materials Science and Engineering B176(2011) 600-605.

48. S.T. Navale, D.K. Bandgar, S.R. Nalage, G.D. Khuspe, M.A. Chougule, Y.D. Kolekar, S. Sen and V.B. Patil, Synthesis of Fe_2O_3 nanoparticles for nitrogen dioxide gas sensing applications, Ceramics International 39 (2013), n. 6, 6453-6460.

49. J. Zaanen, G. A. Sawatzky and J. W. Allen, €Band Gaps and Electronic Structure of Transition-Metal Compounds,, Phys. Rev. Lett.55 418 (1985)

50. S. Mochizuki,Electrical conductivity of „Fe$_2O_3$ 1977 Phys. Status Solidi a 41,2 591-594

51. Y. Guo, S. J. Clark and J. Robertson, Electronic and magnetic properties of Ti_2O_3, Cr_2O_3, and Fe_2O_3 calculated by the screened exchange hybrid density functional, J. Phys.: Condens. Matter 24 (2012) 325504

52. S.K. Deb, Opportunities and challenges in science and technology of WO$_3$ for electrochromic and related applications, Solar Energy Materials and Solar Cells 92 (2008) 245-258.

53. R. Sivakumar, A. Moses Ezhil Raj, B. Subramanian, M. Jayachandran, D.C. Trivedi, C. Sanjeeviraja, Preparation and characterization of spray deposited n-type WO_3 thin films for electrochromic devices, Bulletin of Materials Science 39 (2004) 1479-1489.

54. J. Zhang,X.L. Wang, X.H. Xia, C.D. Gu, J.P. Tu, Electrochromic behavior of WO$_3$ nanotree films prepared by hydrothermal oxidation, Solar Energy Materials and Solar Cells 95 (2011) 2107-2112.

55. C. Chananonnawathorn, S. Pudwat, M. Horprathum, P. Eiamchai, P. Limnontakul, C. Salawan, K. Aiempanakit, Electrochromic property dependent on oxygen gas

flow rate and films thickness of sputtered WO_3 films, Procedia Engineering 32 (2012) 752–758.

56. K. Paipitak, C. Kahattha, W. Techitdheera, S. Porntheeraphat, W. Pecharap, Characterization of sol–gel derived Ti-doped tungsten oxide electrochromic thin films, Energy Procedia 9 (2011) 446–451.

57. W. Li, J. Li, X. Wang, S. Luo, J. Xiao, Q. Chen, Visible light photoelectrochemical responsiveness of self-organized nanoporous WO_3 films, Electrochimica Acta 56 (2010) 626–631.

58. W. Li, J. Li, X. Wang, J. Ma, Q. Chen, Photoelectrochemical and physical properties of WO_3 films obtained by the polymeric precursor method, International Journal of Hydrogen Energy 35 (2010) 13137–13145.

59. C. Zhang, A. Boudiba, C. Navio, C. Bittencourt, M.G. Olivier, R. Snyders, M. Debliquy, Highly sensitive hydrogen sensors based on sputtered platinumactivated tungsten oxide films, International Journal of Hydrogen Energy 36 (2011) 1107–1114.

60. C. Zhang, O. Van Overschelde, A. Boudiba, R. Snyders, M.G. Olivier, M. Debliquy, Improvement of sensing characteristics of radio-frequency sputtered tungsten oxide films through surface modification by laser irradiation, Materials Chemistry and Physics 133 (2012) 585–591.

61. C. Zhang, M. Debliquy, A. Boudiba, H. Liao, C. Coddet, Sensing properties of atmospheric plasma-sprayed WO_3 coating for sub-ppm NO_2 detection, Sensors and Actuators B 144 (2010) 282–288.

62. A. Boudiba, C. Zhang, C. Navio, C. Bittencourt, R. Snyders, M. Debliquy, Preparation of highly selective, sensitive and stable hydrogen sensors based on Pd doped tungsten trioxide, Procedia Engineering 5 (2010) 183–186.

63. C. Zhang, A. Boudiba, C. Navio, M.G. Olivier, R. Snyders, M. Debliquy, Study of electivity of NO_2 sensors composed of WO3 and MnO2 thin films grown by radio frequency sputtering, Sensors and Actuators B 161 (2012) 922–924.

64. R. Calavia, A. Mozalev, R. Vazquez, I. Gracia, C. Cané, R. Ionescu, E. Llobet, Fabrication of WO_3 nanodot-based microsensors highly sensitive to hydrogen, Sensors and Actuators B 149 (2010) 352-361.

65. S. Vallejos, T. Stoycheva, P. Umek, C. Navio, R. Snyders, C. Bittencourt, E. Llobet, C. Blackman, S. Moniz, X. Correig, Au nanoparticle-functionalised WO3 nanoneedles and their application in high sensitivity gas sensor devices, Chemical Communications 47 (2011) 565-567.

66. T.S. Kim, Y.B. Kim, K.S. Yoo, G.S. Sung, H.J. Jung, Sensing characteristics of dc reactive sputtered WO_3 thin films as an NOx gas sensor, Sensors and Actuators B 62 (2000) 102-108.

67. K. Aguir, C. Lemire, D.B.B. Lollman, Electrical properties of reactively sputtered WO_3 thin films as ozone gas sensor, Sensors and Actuators B 84 (2002) 1-5

68. A. Labidi, C. Jacolin, M. Bendahan, A. Abdelghani, J. Guérin, K. Aguir, M. Maaref, Impedance spectroscopy on WO_3 gas sensor, Sensors and Actuators B 106 (2005) 713-718.

69. F. Bender, C. Kim, T. Mlsna, J.F. Vetelino, Characterization of a WO3 thin film chlorine sensor, Sensors and Actuators B 77 (2001) 281-286.

70. M. Hübner, C.E. Simion, A. Haensch, N. Barsan, U. Weimar, CO sensing mechanism with WO_3 based gas, Sensors and Actuators B 151 (2010) 103-106.

71. J.K. Srivastava, P. Pandey, V.N. Mishra, R. Dwivedi, Sensing mechanism of Pd doped SnO_2 sensor for LPG detection, Solid State Sciences 11 (2009) 1600-1602.

72. N. Barsan, U. Weimar, Conduction model of metal oxide gas sensors, Journal of Electroceramics 7 (2001) 143-167.

73. D. Kohl, The role of noble metals in the chemistry of solid-state gas sensor, Sensors and Actuators B 1 (1990) 158-165.

74. P.P. Sahay, Zinc oxide thin film gas sensor for detection of acetone, Journal of Materials Science 40 (2005) 4383-4385.

75. I. Hafaiedh, S. Helali, K. Cherif, A. Abdelghani, G. Tournier, Characterization of tin dioxide film for chemical vapors sensor, Materials Science & Engineering C 28 (1) (2008) 584-587.

76. http://www.fhi-berlin.mpg.de/KHsoftware/Balsac/pictures.html

77. M.J. Verkerk, K. Keizer, A.J. Burggraaf, High oxygen ion conduction in sintered oxides of the Bi_2O_3-Er_2O_3 system, J. Electrochem. Soc. 10 (1980) 981-991

78. P. Shuk, H.D. Wiemhofer, U. Guth, W. Gopel, M. Greenblatt, Oxide ion conducting solid electrolytes based on Bi_2O_3, Solid State Ionics 89 (1996) 179-196.

79. A.M. Azad, S. Larose, S.A. Akbar, Bismuth oxide-based solid electrolytes for fuel cells: a review, J. Mat. Sci. 29 (1994) 4135-4151.

80. A. Cabot, A. Marsal, J. Arbiol, J.R. Morante, Bi_2O_3 as a selective sensing material for NO detection., Sens. Actuators B 99 (2004) 74-89.

81. H.W. Kim, J.W. Lee, S.H. Shim, Study of Bi_2O_3 nanorods grown using the MOCVD technique, Sens. Actuators B 126 (2007) 301-306.

82. L. Li, Y.W. Yang, G.H. Li, L.D. Zhang, Conversion of a Bi Nanowire Array to an Array of Bi†Bi_2O_3 Core†Shell Nanowires and Bi_2O_3 Nanotubes, Small 2 (2006) 548-553.

83. Y.F. Qiu, D.F. Liu, J.H. Yang, S.H. Yang, Controlled Synthesis of Bismuth Oxide Nanowires by an Oxidative Metal Vapor Transport Deposition Technique, Adv. Mater. 18 (2006) 2604-2608.

84. M. Miyayama, H. Yanagida, Oxygen Ion Conduction in γ-Bi_2O_3 Doped with Sb_2O_3, J. Mater. Sci. 21 (1986) 1233-1236.

85. P.S. Halasyamani, K.R. Poeppelmeier, Noncentrosymmetric Oxides, Chem. Mater. 10 (1998) 2753-2769.

86. K.R. Nemade, S.A. Waghuley, LPG sensing application of graphene/SnO_2/Bi quantum dots composites., Solid State Sciences 22 (2013) 27-32

87. D.K.; Nalage, S.R.; Khuspe, G.D.; Chougule, M.A.; Kolekar, Y.D.; Sen, S.; Patil, Synthesis of Bi_2O_3 nanoparticles for nitrogen dioxide gas sensing applications., Ceramics International 39 (2013) 6453-6460

88. G. Sberveglieri, Recent developments in semiconducting thin-film gas sensors, Sensors and Actuators B 23 (1995), pp. 103-109.

89. H. P. Huebner and S. Drost, Tin oxide gas sensors: an analytical comparison of gas sensitive and non-gas-sensitive tin films, Sensors and Actuators B 4 (1991), pp. 463-466.

90. C. Imawan, F. Solzbacher, H. Steffes and E. Obermeier, Gas sensing characteristics of modifies MoO3 thin films using Ti overlayers for NH3 gas sensors, Sensors and Actuators B 64 (2000), pp. 193-197.

91. P. K. Clifford and D. T. Tuma, Characteristics of semiconductor gas sensors I. Steady state gas response, Sensors and Actuators 3 (1983), pp. 233-254.

92. B. Timmer, W. Olthuis and A. van den Berg, Ammonia sensors and their applications-a review, Sensors and Actuators B 107 (2005), pp. 666-677.

93. C. N. Xu, N. Miura, Y. Ishida, K. Matuda and N. Yamazoe, Selective detection of NH3 over NO in combustion exhausts by using Au and MoO3 doubly promoted WO3 element, Sensors and Actuators B 65 (2000), pp. 163-165.

94. M. S. Wagh, G. H. Jain, D. R. Patil, S. A. Patil and L. A. Patil, Modified zinc oxide thick film resistors as NH3 gas sensor, Sensors and Actuators B 115 (2006), pp. 128-133.

95. D. R. Patil and L. A. Patil, Ammonia Sensing Resistors Based on Fe2O3 Modified ZnO Thick Films, IEEE Sensors Journal, Vol. 7, No. 3 (2007), pp. 434-439.

96. G. S. Trivikrama Rao and D. Tarakarama Rao, Gas sensitivity of ZnO based thick film sensor to NH3 at room temperature, Sensors and Actuators B 55 (1999), pp. 166-169.

97. C. Baroni, Phd Thesys of C. Baroni, Near room temperature NOX detection and soil humidity content determination by means of new doped hematite sensors, Ph.D Thesis, Politecnico di Torino, 2011.

98. Phd Thesys of A. Cavalieri, Room temperature ammonia sensors for food industry applicatons, Ph.D. Thesis, 2011.

Chapter 2

Food chemistry and state-of-art of instruments for foods' spoilage detection [1]

2.1 Introduction

Food spoilage is a metabolic process that causes foods to be undesirable or unacceptable for human consumption due to changes in sensory characteristics.
Growth of microorganisms in foods can cause spoilage by producing an unacceptable change in taste, odour, appearance, texture, and a combination of the above [2].
Food loss, from farm to fork, causes considerable environmental and economic effects. The USDA Economic Research Service estimated that more than sixty billion pounds of food in the U.S. were lost by retailers, foodservice and consumers in 1995. Fresh products and fluid milk each accounted for nearly 20% of this loss while lower percentages were accounted for grain products (15.2%), caloric sweeteners (12.4%), processed fruits and vegetables (8.6%), meat, poultry and fish (8.5%), and fat and oils (7.1%). Some of this food would have been considered still edible but was discarded because it was perishable, past its sell-by date, or in excess of needs. There are also environmental and resource costs associated with food spoilage and loss. If 20% of a crop is lost, then 20% of the fertilizer and irrigation water used to grow that crop is wasted.

The spoilage potential of a microorganism is the ability of a pure culture to produce the metabolites that are associated with the spoilage of a particular product. In general, several of the organisms isolated from a food product will be able to produce spoilage metabolites when allowed unlimited growth. It is crucial that quantitative considerations are introduced, since the spoilage activity of an organism lies in its quantitative ability to produce spoilage metabolites. These considerations in general, are the implementation of a careful combination of microbiology, sensory analysis and chemistry [3].

2.2 The nature of food spoilage

Spoilage can be microbial or mechanical in origin [4]. Microbial spoilage is by far the most common cause of spoilage of perishable foods and may manifest itself as visible growth (slime, colonies), as textural changes (degradation of polymers) or as off- and off-flavors. Despite chill chains, chemical preservatives and a much better understanding of microbial food spoilage, it has been estimated that 25% of all foods produced globally is lost post harvest or post slaughter due to microbial spoilage.

Physical and chemical characteristics of food and how it is stored, determine its degree of susceptibility to microbial attack. Although the total microbial flora may increase during storage, it is specific spoilage organisms which cause the chemical changes and the production of off-odors [5]. This is because the chemical properties of foods vary widely, and different foods are colonized by the indigenous spoilage organisms that are best able to use the nutrients available. Microbial growth in foods follows the standard pattern for a bacterial growth curve. It is only when the microbial population density reaches a substantial level that harmful spoilage effects are usually observed.

Off-odors or off-flavors can often be detected soon after 10^6 organisms per g or mL or per cm^2 of food surface have been produced. This level can be considered as a cut-off point between spoiled and unspoiled (level of incipient spoilage). Indeed, throughout much of the exponential phase of growth, population densities may be too low to observe any perceptible effect, but because of the nature of exponential growth, it is only the last doubling or two of the population that leads to observable spoilage.

2.3 The most important factors affecting the growth of food spoilage bacteria

2.3.1 Temperature

One of the most crucial factors affecting microbial growth in food is temperature. Growth is restricted to those temperatures at which an organism's cellular enzymes and membranes can function. As the temperature rises, chemical and enzymatic reactions in the cell proceed at more rapid rates, and growth becomes faster.

However, above a certain temperature, particular proteins may be irreversibly damaged. Thus, as the temperature is increased within a given range, growth and metabolic reactions increase up to a point where inactivation reactions set in. Every food spoilage bacteria has cardinal temperatures namely, a minimum temperature below which growth no longer occurs, an optimum temperature at which growth is most rapid, and a maximum temperature above which growth is not possible [6]. Since the first observation of bacterial growth at 0˜C, many terms were used for these organisms. The term •psychrotroph, was introduced by Eddy (1960) to replace the misnomer •psychrophilic,. The latter term indicates organisms that have a preference for growing at low temperatures, while psychrotrophs should rather be regarded as cold tolerant being able to grow at 7°C or less but having optimum temperatures of 25 to 35°C. In 1976 the International Dairy Federation (IDF) adopted the following definition: A psychrotroph is a microorganism which can grow at 7°C or less, irrespective of its optimum growth temperature.

Many psychrotrophic bacteria, when present in large numbers, can cause a variety of flavors as well as physical defects in foods. Raw foods held under refrigeration prior to processing, as well as nonsterile heat processed foods that rely on refrigeration for shelf life, are subject to quality loss and possible spoilage by psychrotrophic bacteria. Although psychrotrophic bacteria will not grow in frozen foods, they can grow and cause spoilage if the food is allowed to thaw partially, and is subsequently held at too high a temperature (i.e., unfrozen, but still refrigerated) [7].

Studies have revealed that the most common bacteria isolated on dairy equipment surfaces are Gram negative psychrotrophs (e.g. flavobacteria), which are responsible for growth and spoilage in milk at refrigeration temperatures [8]. Jooste investigated the role of flavobacteria as causative agents of the putrid butter defect and found that the optimum growth temperature for the six Flavobacterium strains from butter tested, was 25°C and that these strains were capable of multiplication in cream both at 6°C and 25°C [9].

2.3.2. pH

pH is one of the main factors affecting the growth and survival of microorganisms in culture media and in foods. All microorganisms have a pH range in which they can grow and an optimum pH at which they grow best.

Bacteria generally have a minimum pH for growth of around 4.5 and an optimum pH between 6.8 and 7.2, (that is, more or less neutral), and pH maxima between 8.0 and 9.0.

Organisms that thrive at low pH values are called acidophiles. Organisms that have high pH optima for growth, are known as alkaliphiles, which can produce hydrolytic enzymes, such as proteases and lipases.

The pH minimum for an organism is determined by the temperature of the environment (e.g. the incubation temperature in the laboratory), the nutrients that are available, the water activity and the presence or absence of inhibitors. Despite the pH requirements of a particular organism for growth, the optimal growth pH represents the pH of the extracellular environment only, the intracellular pH must remain near neutrality in order to prevent destruction of acid- or alkali-labile macromolecules in the cell. For the majority of microorganisms, whose pH optimum for growth is between 6 and 8 (referred to as neutrophiles), the cytoplasm remains neutral or very nearly so. When the microbial cell is subjected to extreme pH values, cell membranes become damaged. The pH minimum for an organism depends on the type of acid present. Generally, the minimum is higher if any organic acid is responsible for the environmental pH rather than an inorganic acid.

Foods are quite variable in terms of their pH values. Most are acidic, ranging from the very acidic to almost neutral in reaction. pH changes in foods due to the activity of micro organisms are common. Meat becomes more alkaline when spoilage is caused by Gram negative rods such as Pseudomonas spp.. The organism uses amino acids as its carbon source which leads to the production of ammonia, making the cell environment more alkaline. Shimomura found that the pH range of Chryseobacterium shigense for growth was 5-8 [10]. According to Park the pH range for growth of Chryseobacterium soldanellicola is pH 5-7 and that for optimal growth is pH 5.1 [11].

2.3.3 Water activity and Sodium chloride

Water availability not only depends on the water content of an environment, that is, how moist or dry a solid microbial habitat may be, but is also a function of the concentration of solutes such as salts, sugars, or other substances that are dissolved in water. This is because dissolved substances have an affinity for water, which makes the water associated with solutes unavailable to organisms. Water availability is generally expressed in physical terms such as water activity. The water content of a food may bear little relationship to its water activity (aw). Foods may have a low salt content but a low water activity. Each specific organism has its own range of water activity in which it will grow. Most

organisms have an optimum approaching 1.0, where the water activity is high but, where there is also sufficient dissolved nutrients to support rapid growth.

An added complication is the reaction that some organisms show towards sodium chloride (NaCl). Halophiles are organisms that require sodium ions in order to grow. Moderate halophiles are organisms that require NaCl but will grow only at moderate concentrations, i.e. between 1 and 10%. Sodium ions are believed to be involved with the transport mechanisms associated with the cell membrane and the uptake of materials from the environment. Extreme halophiles are organisms that will only grow at high sodium chloride concentrations and generally require 30% NaCl, depending on the species, for optimum growth. Halotolerant organisms can tolerate some reduction in the aw of their environment, but generally grow best in the absence of the added solute.

2.4 Spoilage caused by flavobacteria

Flavobacteria have been associated with spoilage of food, but information about the incidence and role of flavobacteria in food deterioration is difficult to obtain, mainly due to the history of faulty classification or reclassification of these organisms. They are, however, accepted as common contaminants of protein foods and under refrigerated storage, they are in competition with the pseudomonads [1-12].

Undesirable flavors and odors, possible slime production and/or toxic metabolic end products are detrimental and apart from an economical loss to industry and consumers, may also have a health impact on consumers.

Even if the spoilage bacteria are not pathogenic per se, changes in the biochemical status of stored food due to deterioration by such bacteria, may make conditions favorable for other bacteria, or even pathogens, to grow in. Studies on the proteolytic activity of flavobacteria have indicated that flavobacteria may possibly produce pasteurization resistant extracellular enzymes and that they may in this way contribute to the psychrotrophic spoilage of milk and dairy products. Although psychrotrophs secrete not enzymes with spoilage potential, e.g., glycosidases, the most important enzymes from the viewpoint of food spoilage are extracellular proteinases, lipases, and phospholipases on which this review will concentrate [11-16].

2.4.1 Proteolytic activity

All enzymes that catalyze hydrolysis of proteins to peptones, polypeptides, and amino acids, are called proteolytic enzymes. These enzymes hydrolytically cleave the peptide linkage with the formation of a free amino and carboxylic acid group. Animal pastes include such enzymes as pepsin, rennet, trypsin, chromotrypsin, and cathepsin [17]. Continued proteolysis results in putrid off-flavors associated with lower molecular weight degradation products such as ammonia, amines, and sulphides [18]. Bitter taste production by psychrotrophs is normally at a maximum in the late exponential or stationary phase of growth. Bitter peptides are normally characterized by large numbers of hydrophobic amino acids [19]. Proteases produced by psychrotrophs have been shown to hydrolyze casein, but whey proteins were more resistant against hydrolysis [20]. The optimum pH and temperature for protease production depends on the species and strain. The most common proteolytic activity in milk was reported as clotting.

Roussis found that Flavobacterium MTR3 proteinases were active at -2-22°C, and exhibited considerable activity at 7°C. The enzyme was active at pH 8.0, and exhibited considerable activity at pH 6.0 in the presence of 4% NaCl [21].

2.4.2 Lipolytic activity

Lipolytic enzymes can be defined as carboxylesterases that hydrolyze acylglycerols. Most bacterial lipases are extracellular and are produced during the late log and early stationary phases of growth [22]. True lipases act on insoluble substrates such as those in emulsion or surface monolayers [23].

Lipolysis is known to contribute both desirable and undesirable flavors to dairy products, initially through hydrolysis of milk triacylglycerols. Short-chain fatty acids, such as butyric acid (C4:0), caproic acid (C6:0) and caprylic acid (C8:0), impart sharp and tangy flavors. Medium-chain fatty acids, such as capric (C10:0) and lauric acid (C12:0) tend to impart a soapy taste, while long-chain fatty acids, such as myristic acid (C14:0), palmitic acid (C16:0) and stearic acid (C18:0), contribute little to flavor [24]. Unsaturated fatty acids released during lipolysis are susceptible to oxidation and the concomitant formation of

aldehydes and ketones, which give rise to flavors described as •oxidized cardboard, (tallowy), or metallic.

The lipases from many of the psychrotrophic bacteria are remarkably heat stable and may, therefore, contribute to lipolysis in dairy products, even when they are heat treated. The microbial lipases can attack intact fat globules and may cause lipolysis without any prior activation [25]. Other unpleasant flavors, such as ™€rancid, butyric, bitter, unclean, soapy and astringent€€ in milk and milk products, have also been attributed to lipolysis [26]. In general, flavobacteria are well-known for lipase production. However, significant lipase production by some Flavobacterium strains have been reported by some researchers. Optimal temperature for extracellular Gram negative bacterial lipases is found in the temperature range of 30 to 40°C. Bacterial lipases appear to be very stable at temperatures below 8°C. The optimum pH of most extracellular Gram negative bacterial lipases appears to be at neutral or alkaline pH values between seven and nine. It has been suggested that the optimum pH depends upon the nature of the substrate, the buffer solution, and other external conditions.

2.5 Microbial deterioration of food components

The type and extent of microbial colonization of a food only partly affects its ultimate deterioration, because the biochemical activities of the microbial community structure at the time of the onset of spoilage are also decisive [27]. Organoleptic deterioration may, however, occur before any marked chemical changes take place in the food. This is because some odiferous metabolites can be detected organoleptically at very low levels. Less than 1 ppm dimethyl sulphide or methyl mercaptan is sufficient to cause odour [28]. Even at the maximum cell concentration usually achieved (about 10^9 cfu mL^{-1}), metabolizing at the optimum rate would only produce about 2 $ml\ L^{-1}\ h^{-1}$ of carbon dioxide. At lower temperatures this rate would be much less. Conversely, high levels of microbes may be present in a food that shows no obvious organoleptic change.

The growth of microbes in foods inevitably causes chemical changes. Bacteria, the predominating organisms in the microbial ecology of most foods, are extremely small: a rod of 2 x 0.8 µm has a volume of about 10^{-12} cm^3. Although they have a high metabolic potential per cell, large numbers of bacteria are required before they can cause measurable chemical changes.

2.5.1 Microbial metabolites

Biological as well as fabricated food structures will possess receptors to which microorganisms can absorb. The resulting colonization of such structures may occur in a stratified way, leading to relatively high local concentrations of microbial metabolites [29 30]. The metabolites formed by a given spoilage association will once again depend on the prevailing intrinsic, extrinsic and implicit conditions.

These include the limiting factors influencing: (1) the type of spoilage, determined by the relative amounts of metabolites formed; and (2) the rate at which these metabolites are produced during storage and distribution of food. The latter is mostly expressed as the time to (onset of) spoilage, as detected by sensory evaluations of odor, color, structure and taste. The microbial metabolites depend not only on the storage conditions but also on other environmental factors such as aeration, glucose and lactate availability, and pH [31].

2.5.2 Carbohydrates

Carbohydrates, if available, usually are preferred by microorganisms to other energy-yielding foods. The carbohydrates are divided into monosaccharides, disaccharides, and polysaccharides. The monosaccharides are polyhydroxy aldehydes (aldoses), or polyhydroxy ketones (ketoses). For utilization, bacteria first need to break down complex carbohydrates such as starch into their constituent monosaccharides. The random splitting of glycosidic bonds results in softening and liquefaction [32]. Several bacteria possess an extracellular enzyme, diastase or amylase, which hydrolyses starch. Starch is then converted either directly to glucose or via intermediates such as maltose [33]

Although flavobacteria do not degrade lignin and cellulose, it is possible that these organisms are involved in the breakdown of various proteins and carbohydrates [34]. Glucose is the main carbohydrate used as a carbon and energy source. The breakdown of this monosaccharide can proceed by several pathways. In aerobic respiration the glucose metabolite, pyruvate is converted into carbon dioxide (CO_2) and water (H_2O) by means of the tricarboxylic acid (TCA) cycle, Krebs cycle, or citric acid cycle. To enter the system, the pyruvate is converted to acetate activated by coenzyme A. Only the aerobic and some facultatively anaerobic microorganisms possess an intact TCA cycle. The pyruvic acid can be decarboxylated to form acetaldehyde and CO_2. The acetaldehyde can remain or be reduced to ethyl alcohol, oxidized to acetic acid, or condensed to form acetoin or

acetylmethylcarbinol (AMC). The AMC can be oxidized to diacetyl, which has a butter flavor or reduced to 2,3-butanediol. Pyruvate can be aminated to form alanine. Boers observed that the glucose concentration had decreased to a low level at the first signs of spoilage. It has been concluded also that glucose limitations caused a switch from a saccharolytic to an amino acid degrading metabolism in at least some bacterial species [35]. Foods with high levels of carbohydrates are preferentially colonized by glycolytic organisms and tend to ferment rather than putrefy. This leads to the production of acids (mainly lactic and acetic) and is accompanied by a reduction in pH. The lactate occurring in flesh foods due to post mortem glycolysis can often be differentiated by its optical rotation from lactic acid formed by microorganisms; this increases its reliability as an index of spoilage [36]. However, in some instances lactic acid may be dissimilated and acetic acid may be a better indicator of microbial colonization and metabolism [37, 38].

2.5.3 Fats

The principle lipids in foods are fats. Fats are esters of glycerol and fatty acids and are called glycerides, in the ratio of one molecule of glycerol to three molecules of fatty acids. A pure fat is not attacked by microorganisms, since there must be a nutrient containing aqueous phase in which the organism can grow. Lipase, an enzyme that hydrolyzes fats to free fatty acids and glycerol, is present in many kinds of foods. Because milk contains an appreciable amount of this enzyme, milk fat often undergoes lipase-catalyzed hydrolysis with the production of free fatty acids, diglycerides, monoglycerides, and in extreme cases, free glycerol. Short-chain water-soluble fatty acids (butyric, caproic, and caprylic) cause obnoxious rancid flavors in milk. Lipolysis in foods followed by oxidation produce ketones, which always result in off-flavors. The oxidative deterioration of fats involves the reaction of unsaturated fatty acids with oxygen to yield hydroperoxides. The hydroperoxides are not flavor compounds, but readily decompose to carbonyl compounds resulting in off-flavors or -odors. The carbonyl compounds are mixtures of saturated and unsaturated aldehydes and produces ketones.

2.5.4 Proteins

Microorganisms, through their proteolytic enzymes, break down protein into simpler substances. The breakdown usually follows the following pattern: proteins → peptones →

polypeptides → peptides → amino acids → ammonia (NH_3) → elemental nitrogen (N).
Proteinases catalyze the hydrolysis of proteins to peptides, which may impart a bitter taste to foods. Peptidases catalyze the hydrolysis of polypeptides to simpler peptides and finally to amino acids. The latter impart flavors, desirable or undesirable, to some foods; e.g., amino acids contribute to the flavor of ripened cheeses [39]. The products that are formed depend upon (1) the type of microorganism; (2) the types of amino acids; (3) temperature; (4) the amount of available oxygen; and (5) the types of inhibitors that might be present. Decomposition of protein by aerobic organisms is called decay. Proteins containing amino acids with sulphur, such as cystine and methionine, can be broken down with no unpleasant odor because the end products are completely oxidized and stabilized. Sulphur compounds, however, are often associated with "putrid" odors.
The metabolites produced by microorganisms in proteinaceous foods such as meat include ammonia, ethanol, lactate, acetate, indole and acetoin, with smaller quantities of higher fatty acids, amines and ethyl esters of the lower fatty acids, sulphides, hydrogen sulphide and mercaptans [40]. Most of the esters, amines, ammonia and sulphur compounds are produced from amino acids. There is no significant degradation of protein proper until spoilage has progressed to obvious deterioration. Owing to production of amines and ammonia, the pH of proteinaceous foods tends to rise as spoilage progresses. An increase in the pH of a protein food indicates protein degradation, just as a decrease in pH results from the fermentation of carbohydrates.

2.6 Biogenic amines

Biogenic amines are basic nitrogenous compounds formed mainly by decarboxylation of amino acids or by amination and transamination of aldehydes and ketones. Biogenic amines in food and beverages are formed by the enzymes of raw material or are generated by microbial decarboxylation of amino acids, but it has been found that some of the aliphatic amines can be formed •in vivo, by amination from corresponding aldehydes [41]. Koessler proposed that biogenic amine formation is a protective mechanism for bacteria against acidic environments. The production of amines requires the availability of free amino acids and appropriate status of environmental factors such as pH and temperature [42-43]. The precursors of the main biogenic amines involved in food poisoning are: histidine → histamine, tyrosine → tyramine, hydroxytryptophane → serotonin,

tryptophaneðà tryptamine, lysineðà cadaverine, ornithineðà putrescine, arginineðà spermine, and arginineðà spermidine (Fig. 2.6.1).

The prerequisites for biogenic amine formation by microorganisms are: (1) availability of free amino acids, but not always leading to amine production; (2) presence of decarboxylase-positive microorganisms; and (3) conditions that allow bacterial growth, decarboxylase synthesis and decarboxylase activity.

Biogenic amines are present in a wide range of food products including fish products, meat products, dairy products, wine, beer, vegetables, fruits, nuts and chocolate. Virtually all foods that contain proteins or free amino acids and are subject to conditions enabling microbial or biochemical activity, are conducive to the production of biogenic amines. The total amount of the different amines formed strongly depends on the nature of the food and the microorganisms present [44]. Different biogenic amines (histamine, putrescine, cadaverine, tyramine, spermine, spermidine) have been detected in fish such as mackerel, herring, tuna, and sardines. Other amines, such as trimethylamine and dimethylamine are present in fish and fish products at levels depending on the fish freshness. Bacterial produced histamine has also been found in dairy products and vegetables [45]. Amines (e.g. histamine, tryptamine, tyramine) are also important because of their role in causing spoilage of dairy products by producing typical off-flavors and putrid odors [46]. Putrescine, cadaverine, histamine, tyramine, spermine and spermidine were found to be present in minced pork, beef and poultry stored at chill temperatures. Histamine has been recognized as the causative agent of scombroid poisoning (histamine intoxication), as well as nausea, vomiting, gastrointestinal distress and headache, whereas tyramine has been related to food-induced migraines and hypertensive crisis in patients under antidepressive treatment with monoamine oxidase inhibitor (MAOI) drugs. Secondary amines such as putrescine and cadaverine can react with nitrite to form heterocyclic carcinogenic nitrosamines, nitrosopyrolidine and nitrosopiperidine [47].

Figure 2.6.1. Chemical structures of some biogenic amines [49].

The levels reported for histamine and its potentiators in food would not be expected to pose any problem if normal amounts were consumed. Sandler [50] reported that 3 mg of phenylethylamine causes migraine headaches in susceptible individuals, while 6 mg total tyramine intake was reported to be a dangerous dose for patients receiving monoamine oxidase inhibitors [50,51]. The level of 1000 mg kg^{-1} (amine/food) is considered dangerous for health. This level is calculated on the basis of food borne histamine intoxications related to amine concentration in food [52].
The European Community has recently proposed that the average content of histamine should not exceed 200 mg/100 g of fish.

Biogenic amine content can be considered as a freshness marker or as a bad conservation marker [53]. Let us consider for example the case of the meats: red meat (adult bovine) and white meat (chicken) are particularly susceptible to protein degradation, which takes place

under appropriate conditions. So that the levels of biogenic amines in these two kinds of meat can be related to spoilage and sometimes to their protein degradation.

In reference [53], in order to find a correlation between the amines levels and the spoilage of the meat, an analytical study was carried out on red and white meat for determining quantitatively some biogenic amines. The amines considered were: tryptamine, putrescine, cadaverine, serotonin, tyramine, spermidine, spermine.

These biogenic amines were determined in red and white meats and their levels were controlled during storage time. The main aspect studied was the variation, as a function of time, of amine levels. The study was carried out on fresh meat samples, stored at T = 4 1°C for 36 days. The quantitative determination of biogenic amines was performed by HPLC (High-performance liquid chromatography).

In particular Fig. 2.6.2 shows histograms of the relative levels of each amine considered at the 5th, 15th and 30th day of storage, in the same samples. The experimental evidence showed that the great increase of cadaverine, in both kinds of meat, and of tyramine, for red meat, were an indicator of meat spoilage.

Figure 2.6.2. Histogram relative to the biogenic amine levels in red and white meats monitored at different days of storage at +4°.

The results showed that the biogenic amine levels were indicators of spoilage both in red and white meat. In particular the determination of cadaverine concentration could be used to monitor spoilage in both kinds of meats and also tyramine concentration appeared to be useful to control red meat storage.

2.7 State-of-art of the techniques used to detect biogenic amines

Spoilage is manifested by a variety of sensory cues such as slime, off-odors, softening of vegetables and fruits, and slime. However, even before it becomes obvious, microbes have begun the process of breaking down food molecules for their own metabolic needs. Sugars and easily digested carbohydrates are used first, plant pectins are degraded. Then proteins are attacked, producing volatile compounds with characteristic smells such as ammonia, amines, and sulfides. These odors start to develop in meat when there are about 10^7 cfu of bacteria/cm^2 (number of bacterial colonies on cm^2 of meat surface and are usually recognizable at populations of 10^8 cfu/cm^2 [54]. Early detection of spoilage would be advantageous in reducing food loss because there may be interventions that could halt or delay deterioration, and on the other hand food that had reached the end of its designated shelf life but was not spoiled could still be used. Numerous methods for detection of spoilage have been devised with the goals of determining concentrations of spoilage microbes or volatile compounds produced by these microbes.

2.7.1 Determination of biogenic amines

For determination of BA numbers of analytical methods were developed [55].
The analytical methods used for separation and quantification of BA are mainly based on chromatographic methods: gas chromatography (GC), thin layer chromatography (TLC), and high-performance liquid chromatography (HPLC) with precolumn or postcolumn derivatization techniques [56]. Aliphatic BA do not show pronounced absorption bands in the UV VIS region, so that usual spectrometric detectors cannot be used [57]. The direct analysis of BA without derivatization by means of ion-pair chromatography has been suggested using octylamine or heptanesulfonate as pair-ion reagents [58]. For the separation of ion pairs of the BA the usual reversed phase columns with C18 aliphatic chains phenyl residues bound to a silica core are suitable [59].

The HPLC procedures involve pre- or postcolumn derivatization step [60]. Different chemical reagents have been used for the BA analysis, for example ninhydrine and o-phthalaldehyde, as a postcolumn derivatisation agent, dansyl and dabsyl chloride, benzoyl chloride, fluoresceine, 9-fluorenylmethyl chloroformate with precolumn derivatization [61, 62, 63]. Dansyl chloride has been the most widely used reagent for derivatization of BA prior to HPLC. Light sensitivity and limited stability of dansyl chloride lead some authors to the use of different derivatisation agents. Benzoyl chloride is an inexpensive, stable, easily accessible chemical and its purity is less critical than that of dansyl chloride. Benzamides are not sensitive to light, reaction proceeds at room temperature in alkaline media and no buffers are required. For the detection fluorescence, UV, and electrochemical detectors are used. Electrochemical detector are based on the oxidation of amino groups.

TLC method is especially popular in plant biochemistry. The TLC procedure is of value for semiquantitative screening of food [64]. TLC with precolumn of sample and derivatization of BA can be used to detect chlorides, 3,5-dinitrobenzamides dansyl and fluorescein derivatives of BA [65]. Dansyl chloride reacts with primary and secondary amino groups and fluorescein reacts only with primary amino groups.

Dansylated BA emit the energy of absorbed long-wave UV light as fluorescent light, enabling the analyst to detect these compounds at low levels on the chromatogram. The natural fluorescence (under UV light) of the separated spots of dansylated BA from sample extract can be compared with that of standard spot by eye. The fluorescent dansyl derivative zones are visualized and marked with the aid of a suitable UV-light source (360 nm) [66]. TLC one dimensional developing techniques enable to give sufficient separation of BA, it is because other interfering compounds, such as amino acids also moved along with the analyzed BA. The multidimensional developing technique improved resolution of BA from each other and from interfering materials, and compact and intense spots were obtained. For visual detection of eluated BA, various systems of detecting agents such as ninhydrin, o-phthalaldehyde (for chloride of BA) solution of ethanol, and naphthylamine can be used.

GC is not so often applied for the determination of BA. Because of inherent tailing problems, derivatisation is also frequently used. The BA are determined in the form as trifluoroacetyl, trimethylsilyl or 2,4-dinitrophenyl derivatives. The columns used in the GC are capillary or filling. The capillary columns allowed better separation of BA. The

detectors for the determination of BA by GC are healthy conductivity, flame ionization, and electron capture detector.

Reports dealing with separation of BA by capillary electrophoresis (CE) are not numerous to data. There are three possible approaches to solve this task:

1. Aromatic or heterocyclic BA can be separated in selected buffer systems without derivatization.
2. Polyamines are determined either derivatized (usually in electrokinetic capillary chromatography
3. Their detection must be indirect

CE has several advantages: it is simple, rapid, cost effective, and reliable, making it a very useful tool for screening a large number of samples in a short period of time. Capillary isotachophoresis is used for quantification of histamine in fish [67] and different BA in the lactic acid-fermented vegetable juices [68].

Fluorometric methods are used owing to fluorescence of BA at some pH and reaction of BA with suitable agents to the fluorescence derivatives. The histamine can be determined by *o*-phthalaldehyde and tyramine by 2-naphthol.

Recently due to the commercial availability of enzymes like MAO and putrescine oxidase several groups tried to couple the enzymatic reactions with electrochemical sensors in order to obtain simple and reproducible biosensors. In some cases the BA have been coupled with oxygen sensors or hydrogen peroxide sensors. The biosensor procedure has advantages, such as low cost, short analysis time, simplicity of use and it can be used outside an organized laboratory. The biosensors show a low detection limit with a life estimated at one month with a 10–30% loss of sensitivity.

The principle of immunologic methods is an interaction between antigen and antibody, which leads to formation of a complex [69].

2.7.2 Colorimetric methods

With increasing consumer demand for minimally processed and mildly preserved ready-to-eat foods, safety is becoming more critical due to reduced product stability. Thus, there is a sustained interest from producers, retailers, consumers, and food safety agencies to accurately determine food product quality. To this end, intelligent packaging systems that

are capable of providing information on product quality, in real time, have been developed. One approach is to apply indicators to food packaging that changes color upon reacting with compounds which are associated with the deterioration reactions in food to provide visual cue on product freshness.

2.7.2.1 Indicator to monitor microbial activities

Many food-spoilage reactions result in changes in pH. Based on this phenomenon, a number of studies have leveraged the application of pH-sensitive dyes as quality indicators in intelligent packaging. For instance, Nopwinyuwong et al. [70] developed a colorimetric indicator to detect the spoilage of an intermediate-moisture dessert product, by using pH reagents which react with CO_2 produced by spoilage microorganisms. The indicator coating solution was comprised of methylcellulose binder, poly(ethylene glycol) 400 plasticizer, bromothylmol blue, and methyl red as pH indicators. The solution was cast onto nylon/LLDPE support film, allowed to dry and then followed by applying another cellulose-based topcoat. Placed within a glass jar that contained an intermediate moisture content dessert product, the indicator strip changed from light green to orange-red color, as the product underwent spoilage with concomitant release of CO_2 into the headspace (Figure 2.7.2.1.1). The reaction is based on the formation of carbonic acid that dissociated in water to give hydroxonium ions, which in turn reacted with the pH reagent. Accordingly, the indicator is suitable only for intermediate to high-moisture content products. Since the solubility of CO_2 in water decreases with increasing temperature, the color response of the detector is also expected to be temperature dependent. In uncontrolled environments, the reliability of such indicators may be problematic.

Figure 2.7.2.1.1 Changes in microbial counts of a dessert product (500 g), golden drop, packaged in 1000 ml glass jar. The right vertical axis is the corresponding CO_2 concentration in the headspace within the package during storage. Plots are recreated based on the original data from [71] .

2.7.2.2 Indicator for detecting meat spoilage

A similar quality indicator concept was adopted by Pacquit et al. [72, 73] for intelligent packaging of raw fish. Using pH indicating disposable labels, they monitored the release of alkaline volatile amines (e.g., trimethylamine, dimethylamine, and ammonia) as fish samples spoil. The label was prepared by entrapping within cellulose acetate matrix a bromocresol green pH-sensitive dye that changes color when it reacts with the volatile amines. A quarternary ammonium salt was added to prevent leaching of the dye. Indicator solutions were prepared in water and cast onto an optically clear polyethylene terephthalate) sheet and allowed to dry. The indicator labels were sandwiched between polytetrafluoroethylene gas permeable membranes to protect the indicator from water vapor condensates. The color response was correlated with changing microbial (total viable count and Pseudomonas spp.). The sensor thus can be used to track the increase in volatile amines in the package headspace (Figure 2.7.2.2.1). The response time of color change was found to be relative humidity dependent as the proton deprotonation of dye requires a proton transport medium between the acidic dye (proton donor) and basic ammonia (proton acceptor). Nevertheless, in sealed package for raw fish, this may not present a limitation since the humidity will remain relatively constant. Raw fish quality

indicators which are based on similar concept are already commercially available, such as FreshTag® from COX Technologies.

Smolander et al. [64] developed an innovative approach for monitoring the freshness of poultry meat. During spoilage of meat, H_2S is produced by microorganisms such as pseudomonas, psychrotrophic anaerobic clostridia, Enterobacter, and Alteromonas. By using myoglobin as a detector for H_2S, these investigators correlated the color change of the indicator with degree of spoilage in raw poultry samples packaged in modified atmosphere packages flushed with 40% O_2/60% N_2. In vitro testing, when exposed to H_2S, indicators with 0.5 mg/indicator resulted in most prominent color change from brown to green. When 2 mg/indicator concentration was used, the indicator first turned bright red and thereafter green. However, the total change of color, as measured by $\Delta E = (\Delta L^2 + \Delta a^2 + \Delta b^2)^{1/2}$ (where L, a, and b are HunterLab lightness, green–red, and blue–yellow tristimulus values, respectively), was highest when 4.0 mg/indicator concentration was used, indicating that higher myoglobin concentration may be more suitable if a indicator color change were measured using an instrument. During in vivo testing of packaged meat, MAP the color response was reportedly dependent on oxygen concentration. In packages where O_2 concentration was low at around 1%, the myoglobin turned brown to bright red as H_2S concentration increased. When the packages were punctured at the end of the experiment, the color of the indicator turned green due to the reaction with atmospheric oxygen to form sulphymyoglobin. The indicator may be useful to detect the onset of spoilage in raw poultry meat.

Figure 2.7.2.2.1 Correlation of bacterial growth and sensory quality indicator in whiting filet samples at 21 °C. Adapted from [73].

2.7.2.3 Ripeness indicator technologies for fruits

Although quality of food products usually deteriorates with the passage of time, others improve during storage and eventually become unacceptable. Many fruits belong to the latter category. For instance, pears are harvested before ripe and allowed to go under postharvest ripening, during which the product can exhibit various organoleptic properties, from crisp/sour to soft/juicy. Because this ripening process reveals little visual cue, the consumer tends to rely on pressing the fruit and/or sniffing for aroma to evaluate the state of ripeness. Such actions inevitably will result in product damage at the retail level.

To overcome this problem, various ripeness indicators have been developed. One patent application discloses a general process to employ a volatile indicator that reflects the maturity of maturing products, such as incorporating the indicator in a label and adhering to the maturing product. The indicator chemistries may be based on diffusion technology, oxidative reactions, silver salt redox reactions, enzymatic reactions, and/or electronic exposure indicator [75]. One such commercial sensor is known as ripeSense®, developed in New Zealand by Jenkins Group (self adhesive lebels supplier) and HortResearch (New Zealand Crop Research Institute). The indicator label is attached inside the lid of a transparent thermoformed clamshell packaging which holds four pears. A product label is printed with an indicator scale ranging from red (crisp), orange (firm), and yellow (juicy).

The proprietary reagent in the indicator reacts with the aroma compounds released by pear as it ripens. The sensor is initially red in color, but changes to orange and finally yellow as it reacts with the aroma compounds given off by the fruit. By visually evaluating the color of the indicator label, consumers can select fruits of various ripeness degrees that match their preference and be able to estimate the remaining product shelf-life. For instance, if the sensor is red, the fruit is at the beginning of its ripening process and has longer shelf life compared to those with yellow indicator. By knowing the degree the ripeness, the indicator also allows producer and consumer to decide when to slow down the ripening process by refrigeration once it has reached the desired degree of ripeness [76]. Similar indicators have been developed for kiwifruit, melon, mango, and avocado. In one patent application, a method was disclosed to apply ripeness indicator printed on small label that can be adhered to the skin of a fruit to better present condition of the produce and avoid possible adverse effects from local air convention currents [75]. Another patent application disclosed a similar approach based on ethylene detection involving color change of $KMnO_4$ and molybdenum chemistries. Here, ethylene is readily oxidized by $KMnO_4$ (purple) to form manganese oxide (brown) and ethylene glycol (i.e., Baeyer test to detect unsaturated hydrocarbons). Ethylene can also reduce ammonium molybdate ($(NH_4)_6MO_7O_{24}$) (yellow) catalyzed by palladium sulfate to MO_8O_{23} (blue) [77]. These color changes form the basis of ethylene detection, which is one of the vapors given off during the ripening of fruits [78].

2.8 Conclusion

In this chapter we focused on food chemistry, in order to know the products generated chemically during food spoilage.

The studied sensors are meant to be applied for food whom spoilage causes the formation of biogenic diamines. Recently, many works and patents can be found that deal with detection devices for biogenic amines; among these only a small part has been presented and described in this chapter , selecting the most interesting ones . Currently, the most widely used techniques for the detection of biogenic amines are chromatography, electrophoresis, mass spectroscopy and colorimetric techniques. However, in literature, few studies about ammonia ceramic sensors made with screen printing technique are present. They will be discussed in the experimental part.

This is the reason why the next chapter deals with simple, fast and cheap chemiresistors for the detection of ammonia at room temperature, since ammonia is the most simple amine compound taken as a reference.

Bibliography

1. Thesys of A. Mielmann Food Spoilage Characteristics of Chryseobacterium Species, Thesis, 2006.
2. Garbutt,J., Essentials of Food Microbiology. Arnold, London1997.
3. Gram, L., Ravn, L., Rasch, M., Bruhn, J.B., Christensen, A.B., Givskov, M., 2002. Food spoilage- interactions between food spoilage bacteria. International Journal of Food Microbiology 78, 79-97.
4. Ayres, J.C., Mundt, J.O., Sandine, W.E., 1980. Microbiology of Foods. W.H. Freeman and Company, San Fransisco.
5. Forsythe, S.J., 2000. The Microbiology of Safe Food. Blackwell Science, Oxford.
6. Madigan, M.T., Martinko, J.M., Parker, J., 2000. Brock Biology of Microorganisms, 9th edn. Prentice Hall International, New Jersey.
7. Gilliland, S.E., Michener, H.D., Kraft, A.A.,1976. Psychrotrophic microorganisms. In: Speck, L., (Ed.), Compendium of Methods for the Microbiological Examination of Foods. American Public Health Association, Washington D.C., pp. 173-174.
8. Koutzayiotis, C., Mostert, J.F., Jooste, P.J., Mc Donald, J.J., 1993. Growth and activity of Flavobacterium at solid-liquid interfaces. In: Jooste, P.J. (Ed.),Advances in the Taxonomy and Significance of Flavobacterium, Cytophaga and Related Bacteria, ICSB Subcommittee on Flavobacterium, Cytophaga and related bacteria, Proceedings of the 2nd International Symposium on Flavobacterium, Cytophaga and related bacteria. University Press, University of the Orange Free State, South Africa, pp. 103-109.
9. Jooste, P.J., Britz, T.J., 1986. The significance of flavobacteria as proteolytic psychrotrophs in milk. Milchwissenschaft 41, 616-621.
10. Shimomura K., Kaji, S., Hiraishi, A., 2005. Chryseobacterium shigense sp. nov., a yellow-pigmented, aerobic bacterium isolated from a lactic acid beverage. International Journal of Systematic and Evolutionary Microbiology 55, 1903-1906.
11. Park, M.S., Jung, S.R., Lee, K.H., Lee, S.M., Do, J.O., Kim, S.B., Bae, K.S., 2006. Chryseobacterium oncolanellicola sp. nov. Chryseobacterium taeanense sp. nov., isolated from roots from sand-dune plants. International Journal of Systematic and Evolutionary Microbiology 56, 433-438.

12. García-López, M.L., Santos, J.A., Otero, A., 1999. Flavobacterium. In: Robinson, R.K. (Ed.), Encyclopedia of Food Microbiology . Academic Press, San Diego, pp. 820-824.
13. De Beer, H., Hugo, C.J., Jooste, P.J., Willems, A., Vancanneyt, M., Coenye, T., Vandamme, P.A.R., 2005. Chryseobacterium vrystaatense sp. nov., isolated from raw chicken in a chicken-processing plant. International Journal of Systematic and Evolutionary Microbiology 55, 2149-2153.
14. Cousin, M.A., 1982. Presence and activity of psychrotrophic microorganisms in milk and dairy products: A review. Journal of Food Protection 45, 172-207.
15. Jooste, P.J., 1985. The taxonomy and significance of Flavobacterium-Cytophaga strains from dairy sources. Ph.D. thesis. University of the Orange Free State, Bloemfontein, South Africa.
16. Fox, P.F., Power, P., Cogan, T.M., 1989. Isolation and molecular characteristics. In: McKellar, R.C. (Ed.), Enzymes of Psychrotrophs in Raw Food. CRC Press, Florida, pp. 57-110.
17. Mountney, G.J., Gould, W.A., 1988. Practical Food Microbiology and Technology, 3rd edn. Van Nostrand Reinhold, New York.
18. Frank, J.F., 1997. Milk and Dairy Products. In: Doyle, M.P., Beuchat, L.R., Montville, T.J. (Eds.), Food Microbiology: Fundamentals and Frontiers. American Society for Microbiology, Washington, pp. 1-11.
19. Chen, L., Daniel, R.M., Coolbear, T., 2003. Detection and impact of protease and lipase activities in milk and milk powders. International Dairy Journal 13, 225-255.
20. Venter, H., 1997. Purification and characterization of a heat stable metalloprotease from a Chryseobacterium of dairy origin. M.Sc. thesis University of the Orange Free State, Bloemfontein, South Africa.
21. Roussis, I.G., Matselis, E., Papamichael, E.M., Sakaridis, I., Plakotis, M., Trianttafyllidou, M., 1999. Extracellular proteinases and lipases activity of Flavobacterium MTR3. Milchwissenschaft 54, 77-81.
22. Fox, P.F., Stepaniak, L., 1983. Isolation and some properties of extracellular heat stable lipases from Pseudomonas fluorescens strain AFT 36. Journal of Dairy Research 50, 77-89.
23. Stepaniak, L., Sorhaug, T., 1989. Biochemical classification. In: McKellar, R.C. (Ed.), Enzymes of Psychrotrophs in Raw Food. CRC Press, Florida, pp. 35-55.

24. Al-Shabibi, M.M.A., Langner, E.H., Tobias, J., Tuckey, S.L., 1964. Effect of added fatty acids on the flavor of milk. Journal of Dairy Science 47, 296-305.
25. Mottar, J.F., 1989. Effect on the quality of dairy products. In: McKellar, R.C. (Ed.), Enzymes of Psychrotrophs in Raw Food. CRC Press. Inc., Florida, pp. 227-243.
26. Deeth, H.C., Fitz-Gerald, C.H., 1994. Lipolytic enzymes and hydrolytic rancidity in milk and milk products. In: Fox, P.F. (Ed.), Advanced Dairy Chemistry, Vol. 2: Lipids. Chapman & Hall, London, pp. 247-308.
27. Mossel, D.A.A., Corry, J.E.L., Struijk, C.B., Baird, R.M., 1995. Essentials of the Microbiology of Foods, A textbook for advanced studies. John Wiley & Sons, Chichester.
28. Fields, M.L., Richmond, B.S., Baldwin, R.E., 1968. Food quality as determined by metabolic by-products of microorganisms. Advances in Food Research 16, 161-229.
29. Marshall, K.C., 1985. Bacterial adhesion in oligotrophic habitats. Microbiological Sciences 2, 321-326.
30. Delaquis, P.J., Caldwell, D.E., McCurdy, A.R., 1988. The effect of salt on growth of attached and unattached cells of Lactobacillus viridescens. Canadian Institute of Food Science and Technology Journal 21, 103-106. Dugas, J.E., Zurek, L., Paster, B.J., Keddie, B.A., Leadbetter, E.R., 2001.
31. Dainty, R.H., Edwards, R.A., Hibbard, C.M., 1985. Time course of volatile compound formation during refrigerated storage of naturally contaminated beef in air. Journal of Applied Bacteriology 59, 303-309.
32. Chesson, A., 1980. Maceration in relation to the post-harvest handling and processing of plant material. Journal of Applied Bacteriology 48, 1-15.
33. Banwart, G.J., 1989. Basic Food Microbiology, 2nd edn. Van Nostrand Reinhold, New York.
34. Shewan, J.M., McMeekin, T.A., 1983. Taxonomy and ecology of Flavobacterium and related genera. Annual Review of Microbiology 37, 233-252.
35. Borch, E., Berg, H., Holst, O., 1991. Heterolactic fermentation by a homofermentative Lactobacillus sp. during glucose limitation in anaerobic continuous culture with complete cell recycle. Journal of Applied Bacteriology 71, 265-269.

36. Nychas, G.-J.E., Drosinos, E.H., Board, R.G., 1998. Chemical changes in stored meat. In: Davies, A., Board, R. (Eds.), The Microbiology of Meat and Poultry. Blackie Academic & Professional, London, pp. 288-326.

37. Kakouri, A., Nychas, G.J.E., 1994. Storage of poultry meat under modified atmospheres or vacuum packs: possible role of microbial metabolites as indicators of spoilage. Journal of Applied Bacteriology 76, 163-172.

38. Boers, R.H., Dijkmann, K.E., Wijngaards, G., 1994. Shelf-life of vacuum packaged wild boar meat in relation to that of vacuum-packaged pork: relevance of intrinsic factors. Meat Science 37, 91-102.

39. Frazier, W.C., 1988. Part 1: Foods and Microorganisms. In: Dallinger, E. (Ed.), Food Microbiology. McGraw-Hill, New York, pp. 76-79.

40. Edwards, R.A., Dainty, R.H., 1987. Volatile compounds associated with spoilage of normal and high pH vacuum-packed pork. Journal of the Science of Food Agriculture 38, 57-66.

41. Santos, M.H.S. 1996. Biogenic amines: their importance in foods. International Journal of Food Microbiology 2 9, 213-231.

42. Koessler, K.K., Hanke, M.T., Sheppard, M.S., 1928. Production of histamine, tyramine, bronchospastic and arteriospastic substances in blood Broth by pure cultures of microorganisms. Journal of Infectious Diseases 43, 367-373

43. Maijala, R.L., Eerola, S.H., Aho, M.A., Hirn, J.A., 1993. The effect of GDL-induced pH decrease on the formation of biogenic amines in meat. Journal of Food Protection 56, 125-129.

44. Brink, B., Damink, C., Joosten, H.M.L.J., Huis in't Veld, J.H.J., 1990. Occurrence and formation of biologically active amines in foods. International Journal of Food Microbiology 11, 73-84.

45. Actis, L.A., Smoot, J.C., Barancin, C.E., Findlay, R.H., 1999. Comparison of differential plating media and two chromatography techniques for the detection of histamine production in bacteria. Journal of Microbiological Methods 39, 79-90.

46. Chander, H., Batish, V.K., Babu, S., Singh, R.S., 1989. Factors affec ting amine production by a selected strain of Lactobacillus bulgaricus . Journal of Food Science 54, 940-942.

47. Ienistea, C., 1973. Significance and detection of histamine in food. In: Hobbs, B.C., Christian, J.H.B., (Eds.), The Microbiological Safety of Food. Academic Press , London, pp. 327-343.

48. Niven C.F., Jeffrey, M.B., Corlett, D.A., 1981. Differential plating medium for quantitative detection of histamine-producing bacteria. Applied and Environmental Microbiology 41, 321-322.
49. A. Önal, A review: Current analytical methods for the determination of biogenic amines in foods, Food Chemistry 103 (2007), pp. 1475-1486.
50. Sandler, M., Youdin, M.B.H., Hanington, E., 1974. A phenylethylamine oxidizing defect in migraine. Nature 250, 335-336.
51. Shalaby, A.R., 1993. Survey on biogenic amines in Egyptian food: sausage. Journal of the Science of Food Agriculture 62, 291-293.
52. Taylor, S.L., 1985. Histamine poisoning associated with fish, cheese and other foods. World Health Organization. WPH/FOS/85.7, 1-7.
53. G. Vinci and M. L. Antonelli, Biogenic amines: quality index of freshness in red and white meat, Food Control 13 (2002), pp. 519-524.
54. Ellis DI and Goodacre R. 2006. Quantitative detection and identification methods for microbial spoilage, p. 1-27. In Balakburn C deW (ed.), Food poilage Microorganisms. CRC Press LLC, Boca Raton FL.
55. Silla-Santos, M. H., Biogenic amines: their importance in foods, Int. J. Food Microbiol. 29, 213 (1996).
56. Casella, I. G., Gatta, M., and Desimoni, E., Determination of histamine by high pH anionexchange chromatography with electrochemical detection Food Chem. 73, 372 (2001).
57. Seiler, N., Polyamines, J. Chromatogr. 379, 176 (1986).
58. Cobo, M. and Silva, M., J., Continuous solid-phase extraction and dansylation of low-molecular-mass amines coupled on-line with liquid chromatography and peroxyoxalate chemiluminescence-based detection, Chromatogr. A 848, 115 (1999).
59. Bockhardt, A., Krause, I., and Klostermeyer, K., Z. Lebensm. Unters, Determination of biogenic amines by RP-HPLC of the dabsyl derivates, Forsch. 203, 70 (1996).
60. Pacheco-Aguilar, R., Lugo-Sánchez, M.E., Villegas-Osuna, R.E., and Robles-Burgueño, R., 1998., Histamine formation in muscle of sardine and its quantification in canned products from Northwestern Mexico. J. Food Comp. and Anal. 11:188-195.

61. Greif, G., Greifová, M., and Drdák, M., Stanovenie biogénnych amínov v potravinšch ›ivoc•žneho pôvodu metódou HPLC (HPLC method for determination of biogenic amines in foods of animal origin), Potrav. V dy 15, 129 (1997).
62. Wei, C., Chen, C. M., Koburger, J. A., Otwell, W. S. and Marshall, M. R. 1990. Bacterial growth and histamine production on vacuum-packaged tuna. Journal of Food Science 55: 56-63.
63. Beljaars, P. R., J, Liquid chromatographic determination of histamine in fish. AOAC Int. 81, 998 (1998).
64. Shalaby, A. R., Multidetection semiquantitative method for determining biogenic amines in food, Food Chem. 52, 372 (1995).
65. Ascar, A. and Treptow, H., Biogene Amine in Lebensmitteln, Ulmer, Stuttgart, 1986.
66. Shalaby, A. R., Separation, identification and estimation of biogenic amines in foods by thin-layer chromatography, Food Chem. 49, 310 (1994).
67. Vold¡ich, M., Hrdlicœka, J., and Opatovš, M., Potrav. V dy 6, 103 (1988).
68. Karovicœovš, J., Kohajdovš, Z., and Lukšcœovš, Porovnanie fermentšci• zeleninovœch žtiav (comparison of fermentations vegetable juices) D., Bull. PV 41, 195 (2002).
69. Rauch, P., Potrav. V dy 9, 16 (1991).
70. Nopwinyuwong A., Trevanich S., and Suppakul P., Development of a novel colorimetric indicator label for monitoring freshness of intermediate moisture dessert spoilage. Talanta 81: 1126-1132 (2010).
71. Nopwinyuwong A., Trevanich S., and Suppakul P., Development of a novel colorimetric indicator label for monitoring freshness of intermediate moisture dessert spoilage. Talanta 81: 1126-1132 (2010).
72. Pacquit A., Frisby J., Diamond D., et al., Development of a smart packaging for the monitoring of fish spoilage. Food Chemistry 102: 466-470 (2007).
73. Pacquit A., Lau K.T., McLaughlin H., et al., Development of a volatile amine sensor for the monitoring of fish spoilage. Talanta 69: 515-520 (2006).
74. Smolander M., Hurme E., Latva-Kala K., et al., Myoglobin-based indicators for the evaluation of freshness of unmarinated broiler cuts. Innovative Food Science and Emerging Technologies 3: 27-38 (2002).

75. Prusik T., Martin J.P., and Gozlan S.P., Method of Marketing Maturing Consumable Products and Products Used Therein. US Patent Application 2006/0247967A1 (2006).
76. http://www.ripesense.com
77. Klein R.A., Ridley M.R., DeCianne D.M., and Srinavakul N., Non-Invasive Colorimetric Ripeness Indicator. US Patent Application 2006/0127543A1 (2006).
78. Lim. L.T., Active and Intelligent Packaging Materials, Intergration of Biotechnologies 629-644 (2011)

Part III

Experimental chapter

Chapter 3

Electrical characterizations of ceramic sensors through screen-printing technique

3.1 Introduction

Screen printing technique was introduced in the later part of the 1950€s to produce compact, robust and relatively inexpensive hybrid circuit for many purposes. Later on thick film technique has been attracted by the sensor field [1].
Only from the 1970€s screen-printing reached the full maturity and from this period it has been employing for the realization of miniaturized devices, such as circuits, conductors, insulators, resistors, capacitors and humidity and gas sensors. Screen printing is a viable and economical method to produce thick films of various materials [2-3].
In this chapter a more detailed presentation of screen-printing is made, then the ceramic sensors entirely prepared by means of this technique during my Ph.D. work are described. The synthesis of the sensing materials, as well as their microstructural characterization, by means of laser granulometry, XRD and SEM observations and their electrical characteristics in presence of water and of ammonia are also described.

3.2 Screen printing technique

3.2.1 Generalities of the process

Screen-printing process is a simple method that allows the production of low cost and robust oxide thick films sensors with good reproducibility provided that the starting materials are well controlled.
Screen-printing is a technique of controlling fluid flow. In this process, the ink is submitted to different forces, squeegee pressure, force of surface tension at the screen/substrate

interface and gravity (Fig. 3.2.1.1). The mesh is coated with a ultra-violet (UV) sensitive emulsion onto which the circuit pattern can be formed photographically. The most common type of screen comprises a frame, normally cast aluminium or stainless steel, onto which a finely woven mesh is stretched. The mesh itself is usually based on a plain weave pattern, as depicted in Fig. 3.2.1.2. During printing process, the squeegee pushes the ink ahead on the screen and wherever there is opening in the screen mesh, the downward force of the squeegee causes the ink to flow through the mesh onto the substrate.

It is possible to quantify the percentage of mesh open area through which the ink is able to pass:

$$\text{Percentage} = 100 A^2 / (A + D)^2 \qquad (3.2.1.1)$$

where A is the mesh aperture and D is the filament diameter.

A cross-section of a mesh and many definitions and terms used are shown in Fig. 3.2.1.3.

After the passage of the squeegee and snap off of the screen, the printed ink pattern is in the free standing state. At this stage, the final shape of the pattern is decided by the balance between forces of gravity and surface tension and the viscosity of the ink. Thus, for best printing, the viscosity of the ink should be low during printing to allow free flow within the pattern and fill voids created while printing. But at the same time after printing, the viscosity should increase so as to prevent spreading of the ink. This implies that the paste should exhibit thixotropic property i.e. on application of pressure, the viscosity should be low for easy flow and after removal of pressure it should regain its original viscosity.

Semi-automatic screen-printing machine used in the laboratory to realize sensors is shown in Fig. 3.2.1.4, while the masks used to deposit the components of the sensors are presented in Fig. 3.2.1.5: in particular the screen's patterns can be different depending on what it is deposited, for example in laboratory two screens were used, the former to print the electrodes (Fig. 3.2.1.5a), the latter to deposit the sensing layer (Fig. 3.2.1.5b).

Figure 3.2.1.1. The basic screen printing process.

Figure3.2.1.2. A plain weave pattern for a typical thick film screen.

The screens used were all made of stainless steel and their apertures were 270 mesh, corresponding to 53 Šm [4].

Figure 3.2.1.3. Cross section of a screen mesh.

Figure 3.2.1.4. Screen printer used for sensors assembly.

Figure 3.2.1.5. Patterns of the screens used to deposit a) the electrodes and b) the rectangular sensing films.

3.2.2 The squeegee

The squeegee is a flexible blade whose function is to transfer the ink or the paste through the screen onto the substrate. During printing, the squeegee forces the ink to pass through the open areas of the mesh and, by virtue of the substrate tension between the film and the substrate, the required pattern is then transferred to the substrate as the screen and substrate separate. The squeegee must be resistant to the solvents and ink. Common materials used are polyurethane and neoprene.

3.2.3 Screen printing inks

The range of materials available for thick film technology is determined by the capacity to be both printed and fired. Each paste for producing thick films contains three components: the basic component, the flux and the binding phase [5].

(i) Sensing material: metals or metal oxides which determine electrical resistivity, solderability etc. The basic components taken into consideration for humidity and ammonia detection at room temperature were ZnO, WO_3 and Bi_2O_3 powders.

(ii) Temporary binder poly-(vinyl butyral-co-vinyl alcohol-co-vinyl acetate) (PVB, Aldrich, USA), which created the paste plasticity and ensured the necessary adhesion of the film to the substrate before the paste was fired.

(iii) Organic vehicle used for making the paste and for controlling the viscosity and rheological properties of the paste. The vehicle is a temporary, sacrificial ingredient, which should be removed completely in the following steps of the process, during which the microstructure of the deposits is formed. In our case, a blend of terpineol type solvent, namely ethyleneglycolmonobutylether (Emflow, Emca Remex, USA), was used.

It is possible to remove the sacrificial ingredients by considering two steps: the drying and the firing processes. In general these two steps are necessary for sensors realization: after screen printing, the film or electrodes should stand in air for few minutes, in order for the ink to level off and settle. The aim of the drying stage is to remove the organic solvents and make the printed film adherent to the substrate and relatively immune to smudging. The firing process is a phase in which the printed films or electrodes are heat treated at higher temperatures: the thermal treament is specifically studied for every sample. At this step, the ink€s components are thermally decomposed, leading to an evident shrinkage of the deposit (Fig. 3.2.3.1).

Figure 3.2.3.1. Shrinkage of the thick film from the wet to the dried phase, followed by the firing stage.

In particular, for all the pastes realized in this Ph.D. work, 0.05 g of PVB and 1.2 cc of Emflow were used: these components were mixed 30 minutes in an ultrasonic bath, in order to obtain a homogeneous viscous liquid, then 2 g of the basic components were added and mixed to the liquid, thus obtaining a dense paste, to be screen printed onto the substrate.

Two different kinds of screen printed devices were prepared:

1. the interdigitated electrodes were either deposited on Al_2O_3 planar substrates (Coors Tek, USA, ADS-96 R, 96% alumina, 0.85 cm × 5 cm, 2 mm),
2. and then on top of them, the sensing materials were screen printed (Figure 3.2.3.2), or were screen printed onto the sensing layer directly deposited onto the alumina substrates.

Figure 3.2.3.2. Steps for the classical sensors assembly: the alumina substrate (a), onto which gold interdigitated electrodes are screen printed (b). Subsequently, after firing, the sensing layer is screen printed (c). The final step concerns sintering of the sensing layer.

For interdigitated gold electrodes screen printing, a commercial ink was used (ESL EUROPE 8835 (520C)). After drying overnight, the electrodes were fired at 520°C for 18 minutes with a 2°C/min heating ramp to optimize their electrical conductivity, according to the ink€s manufacturer recommendations.

3.3 Synthesis of the sensing materials

3.3.1 Hydrothermal synthesis

ZnO, WO_3, Fe_2O_3 and Bi_2WO_6 powders were prepared in different containers:

1. a teflon bottle with autoclavable screw cap;
2. a glass bottle with autoclavable cap;
3. a beaker

Containers were heated in the range 90-160°C and kept for the desired times (2-24 hours) in an ordinary laboratory oven. Subsequently the bottle was cooled down to room temperature naturally (~2 hours).

Below, the ZnO hydrothermal synthesis is reported, according to refs. [67].

The formation of tubular ZnO occurs in two steps, as can be seen in Figure 9: through hydrothermal synthesis, starting from ZnCl2 dissolved in water and ammonia solution:

- Formation of ZnO nanorods at a temperature of 95° C,
- Dissolution of ZnO at temperatures <75°C.

Dissolution leads to the formation of ZnO nanorods.

Figure 9 Growth mechanisms of ZnO nanotubes

The chemical reactions involved are the following ones:

$$ZnCl_2 \rightarrow Zn^{2+} + 2Cl^- \quad (3.3.1.1)$$

$$NH_3 \cdot H_2O \rightarrow NH_4^+ + OH^- \quad (3.3.1.2)$$

$$Zn^{2+} + NH_3 \cdot H_2O \rightarrow Zn(NH_3)_4^{2+} + OH^- \rightarrow ZnO + NH_3 + H_2O \quad (3.3.1.2)$$

During the first step, at the temperature of 95°C, $Zn(NH_3)_4^{2+}$ reacts with OH^- to form ZnO. Until the concentration of $Zn(NH_3)_4^{2+}$ is high, this reaction is dominant. When the concentration of $Zn(NH_3)_4^{2+}$ decreases, dissolution becomes the main phenomenon that leads to the formation of nanorods. When the temperature reaches a temperature below 75°C, the equilibrium shifts to the left and the dissolution leads to the formation of nanotubes

We report hereafter the experimental synthesis process used in this work.

ZnO synthesis was performed in different containers. A $ZnCl_2$ solution 0.1M was brought at pH 10 with NH_4OH. Before putting the solution in the oven, a piece of metallic copper was introduced into it, to act as a catalyst.

The solution was put in the oven at different times and temperatures and then was cooled at room temperature [8]. Table 3.3.1.1 reports the different investigated parameters of ZnO hydrothermal synthesis.

Name	Containers	Temperature [°C]	Time [h]	Cooling time [h]
Beaker 1.5-5	Beaker	90	1.5	5
Beaker 1,5-5	Beaker	90	1.5	5
Becker 7-0	Beaker	90	7	0
Glass1.5-5	Glass autoclave	90	1.5	5
Glass1,5-5 Cubefore	Glass autoclave	90	1.5	5
Vetro 3-3	Glassautoclave	90	3	3
Teflon 4-2	Teflon autoclave	120	4	2
Teflon 4-3	Teflon autoclave	120	4	3
Teflon 4-4	Teflon autoclave	120	4	4
Teflon 4-3 0,2M	Teflon autoclave	120	4	3
Teflon 4-4 0,2M	Teflon autoclave	120	4	4
Teflon 4-2 40°C	Teflon autoclave	120	4	2
Teflon 4-2 50°C	Teflon autoclave	120	4	2
Teflon 4-2 60°C	Teflon autoclave	120	4	2
Teflon 4-2 rt	Teflon autoclave	120	4	2
Teflon 4-2 open	Teflon autoclave	120	4	0
Teflon 4-2 <75°C	Teflon autoclave	120	4	2
Teflon 4-2 <75°C + ZnO	Teflon autoclave	120		
Teflon 5-2	Teflon autoclave	120	5	2
Teflon 5-2 Li	Teflon autoclave	120	5	2
Teflon 5-2 Al	Teflon autoclave	120	5	2
Teflon 5-2 Nb	Teflon autoclave	120	5	2
Teflon 5-2 Pb	Teflon autoclave	120	5	2
Teflon 5-2 Y	Teflon autoclave	120	5	2
Teflon 5-2 W	Teflon autoclave	120	5	2
Teflon 5-2 Pd	Teflon autoclave	120	5	2
Teflon 6-2	Teflon autoclave	120	6	2

Table 3.3.1.1. Hydrothermal synthesis performed with ZnO

In Table 3.3.1.1 are also presented some hydrothermal synthesis, in which we tried to verify if the introduction of some metal ions could affect the sensor response towards ammonia. The sensors responses are reported in section 3.6.5.

In the hydrothermal synthesis of ferric oxide nanopowders we started from a solution of ferric chloride 1.5 M; the solution was brought to pH 3.5 with ammonium hydroxide and put in the oven at 100°C for 14 hours. Afterwards it was put in the furnace at 600°C for 2 hours. [9]

In the hydrothermal synthesis of WO_3 nanopowders, we started from a solution of 0.4M WCl_6, to which was added a solution of CTAB 0.08 M and subsequently 10 mL of ammonium hydroxide at 25% We was left stirring the solution for 4 hours. When the solubilization was completed, the solution was put in the oven for 4 days at 200°C. After washing with water and ethanol, we put the powder in furnace at 500° C for 2 hours [10].

Table 3.3.1.2 reports hydrothermal synthesis performed with substances different from zinc oxide

Name	Containers	Temperature [°C]	Time [h]	Cooling time [h]
Fe_2O_3 teflon	Teflon autoclave	100	14	2
Fe_2O_3 glass	Glass autoclave	100	14	2
Fe_2O_3 Glass + Cu	Glass autoclave	100	14	2
WO_3	Teflon autoclave	160	16	2
Bi_2WO_6	Teflon autoclave	160	24	

Table 3.3.1.2. Hydrothermal synthesis performed with Fe_2O_3, WO_3 and Bi_2WO_6.

In paragraph 3.6.5 the electrical responses to some of the sensors reported in the previous two tables, are shown.

In paragraph 3.5.2 SEM images of most of the hydrothermal synthesis reported in the two tables above, are reported.

3.3.2 Glass Ceramic

The first step to obtain glass ceramic was to prepare the glass from B_2O_3, WO_3 and ZnO powders. We used a defined nominal composition (Figure 3.3.2.1) by melt quenching technique at 1300°C for 10 min in a Pt crucible.
The second step was a thermal treatment at 500°C for 15 hours to make the powder crystallize.

Figure 3.3.2.1. Triangle of glass ceramic

3.3.3 Zinc Oleate

The zinc oleate was synthesized after the aging tests of ZnO samples functionalized with carboxylic acids, which have shown deterioration of the sensors' performances with time (Figure 3.6.2.2.15-3.6.2.2.16).
To resolve this problem, we thought to use the zinc oleate, a compound deriving from oleic acid, that gave good responses to ammonia (Figures 4 and 5). The zinc oleate was tested to evaluate if it was more resistant to ageing.
The zinc oleate is synthesized starting from the alcoholic solution of oleic acid, which is neutralized with NaOH. Afterward the solution is put in the oven to allow the evaporation of ethanol. Amber-yellow crystals are obtained which are then dissolved in water. To this solution zinc chloride is added under strong stirring. Finally the product is washed with water and ethanol and left drying in the oven for one night at 60°C.

The reaction performed to obtain Zinc oleate was the following one:

Oleic acid + Zinc hydroxide → zinc oleate (3.3.3.1)

Figure 3.3.3.1 Chemical formula of zinc oleate

We used 2.6 g of oleic acid in 30 mL of ethanol, that were neutralized with $Zn(OH)_2$ until pH 7 and afterwards were put in an oven at 70°C for 1 day. [11]

3.4 Functionalization

3.4.1 Fluorides

We functionalized ZnO sensors fired at 900°C with fluorides group in fluorhydric acid solution at $5x10^{-5}$ M for different functionalization times (Figure 3.6.2.1) according to ref. [12]. It was not possible to use higher concentrations of acids because it would damage sensors, due to the dissolution of ZnO.

3.4.2 Carboxylic acids

Since the aim of the work is to find a material able to detect low concentrations of NH_3 and to produce a sensor having a high SR, over 10%, and on the basis of ref. [13], we functionalized ZnO sensors fired at 900°C with carboxylic group in different carboxylic acid solution by pretreatment with NH_4Cl.

The use of functionalized zinc oxide with suitable chemical groups in sensor assembly can enhance the electrical response of the devices under ammonia atmosphere. For example it is known that the carboxylic (COOH) groups let NH_3 to chemisorb onto them by transferring a hydrogen ion to the lone pair on the nitrogen of NH_3, forming an ammonium (NH_4^+) ion [14]:

$$RCOOH + NH_3 \rightarrow RCOONH_4 \quad (3.4.2.1)$$

The functionalization of the sample was done in two different ways. In the first way we functionalized the ZnO sensor heat treated at 900°C while in the second way we first functionalized the ZnO powder that was then used for the ink preparation before screen printing the sensors.

In the first case, the ZnO powder was heat treated at 900°C, in the second case the ZnO powder was used without any heat treatment.

The functionalization of the heat treated sensor was performed according two different techniques. In the first technique, the sample was immersed in the acid solution for two days, in the second case it was treated with plasma. The plasma functionalization allows to reduce the pretreatment time with NH_4OH and with carboxylic acid; pretreatment with NH_4OH lasts only 30 seconds, while pretreatment with carboxylic acid takes only 2 minutes.

3.5 Characterization

3.5.1 SEM observations on ZnO powders from hydrothermal synthesis

In Figure 3.5.1.1 and 3.5.1.2 we can observe the samples obtained in a beaker at 95°C for 90 minutes. In the second experiment (Figure 3.5.1.2) we put metallic copper in the solution after NH_4OH addition, while in the first experiment (Figure 3.5.1.1) we put it before. It can be observed how the introduction of copper at acid or basic pH, influences the size of the powders obtained.

Figure 3.5.1.1SEM analysis of ZnO nanopowder from hydrothermal synthesis in becker at 95°C for 90 minutes.

Figure 3.5.1.2. SEM analysis of ZnO nanopowder from hydrothermal synthesis in becker at 95°C for 90 minutes.

Figure 3.5.1.3. SEM analysis of ZnO nanopowder from hydrothermal synthesis in a beaker at 95°C for 7 hours.

Figure 3.5.1.4. SEM analysis of ZnO nanopowder from hydrothermal synthesis in beaker at 95°C for 90 minutes.

Figure 3.5.1.5. SEM analysis of ZnO nanopowder from hydrothermal synthesis in Teflon autoclave at 120°C for 4 hours and 2 hours of cooling.

Figure 3.5.1.6. SEM analysis of ZnO nanopowder from hydrothermal synthesis with a 0.2 M $ZnCl_2$ in Teflon autoclave at 120°C for 4 hours and 2 hours of cooling.

We observe in Figure 3.5.1.6 that the increase of the $ZnCl_2$ concentration , did not lead to ZnO nanopowders.

Figure 3.5.1.7. SEM analysis of ZnO nanopowder from hydrothermal synthesis in Teflon autoclave at 120°C for 4 hours and 4 hours of cooling.

In Figure 3.5.1.7 we can observe that longer cooling times lead to the formation of flowers.

Figure 3.5.1.8. SEM analysis of ZnO nanopowder from hydrothermal synthesis with ZnCl2 at 0.2M in Teflon autoclave at 120°C for 4 hours and 4 hours of cooling.

Even in this case, in figure 3.5.1.8, a greater concentration does not favor the formation of nanopowders.

Figure 3.5.1.9. SEM analysis of ZnO nanopowder from hydrothermal synthesis in Teflon autoclave at 120°C for 5 hours and 2 hours of cooling.

We can see in figure 3.5.1.9 that longer times in the oven lead to the formation of flowers. Comparing the -2 (Figure 3.5.19) and -4 (Figure 3.5.1.10) synthesis the size of the powders results lower in the 4 synthesis.

Figure 3.5.1.10. SEM analysis of ZnO nanopowder from hydrothermal synthesis in Teflon autoclave at 120°C for 4 hours and 4 hours of cooling.

An hour more in 5-2 synthesis (Figure 3.5.1.9) in the oven doesn't lead to great differences if compared to 4-4 synthesis (Figure 3.5.1.10).

Figure 3.5.1.11. SEM analysis of ZnO nanopowder from hydrothermal synthesis in glass autoclave at 90°C for 1.5 hours and 5 hours of cooling.

Using the glass autoclave (Figure 3.5.1.11) it is not possible to obtain nanorods even if the dimensions are smaller.

Figure 3.5.1.12. SEM analysis of ZnO nanopowder from hydrothermal synthesis in glass autoclave at 90°C for 3 hours and 3 hours of cooling.

Figure 3.5.1.13. SEM analysis of ZnO nanopowder from hydrothermal synthesis in Teflon autoclave at 120°C for 4 hours and 2 hours of isotherm at 40°C.

Figure 3.5.1.14. SEM analysis of ZnO nanopowder from hydrothermal synthesis in Teflon autoclave at 120°C for 4 hours and 2 hours of isotherm at 50°C.

Figure 3.5.1.15. SEM analysis of ZnO nanopowder from hydrothermal synthesis in Teflon autoclave at 120°C for 4 hours and 2 hours of isotherm at 60°C.

By decreasing the isotherm temperature (Figure 3.5.1.13 - 3.5.1.15), there is a gradual reduction of dust and an appearance of flowers.

3.5.2. XRD pattern of powder from hydrothermal synthesis

We characterized the powders prepared from hydrothermal synthesis by XRD analysis. The diffractogram in Figure 3.5.2.1 indicates that the powder is ZnO

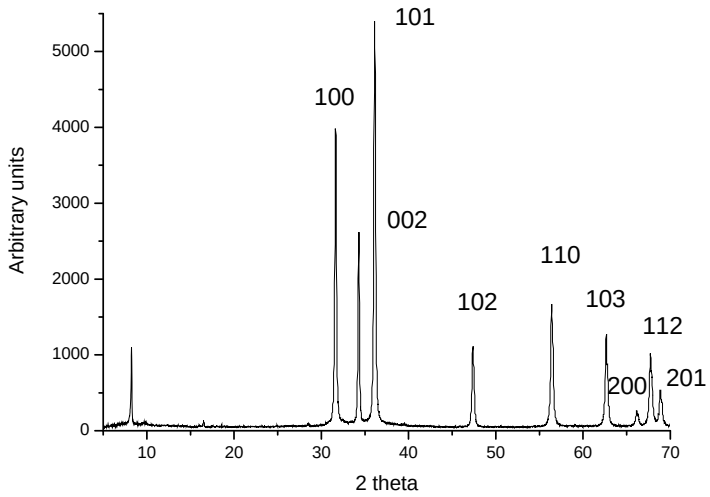

Figure 3.5.2.1. XRD pattern of ZnO nanopowder from hydrothermal synthesis in Teflon autoclave at 120°C for 4 hours and 2 hours of isotherm at 40°C.

ZnO JCPDS file 36-1451		
hkl	2 theta	Intensity
100	31.76	57
002	34.42	44
101	36.25	100
102	47.53	23
110	56.60	32
103	62.86	29
200	66.37	4
112	67.96	23
201	69.09	11

Table 3.5.2.1. ZnO JCPDS file 36-1451

Figure 3.5.2.2. XRD pattern of Bi_2WO_6 nanopowder from hydrothermal synthesis in Teflon autoclave.

In the Figure 3.5.2.2 all the diffraction peaks can be indexed to orthorhombic Bi_2WO_6 according to the JCPDS card n. 39-0256.

Figure 3.5.2.3. XRD pattern of Fe_2O_3 nanopowder from hydrothermal synthesis in Teflon autoclave.

In the Figure 3.5.2.3 all peaks marked with indices are matched with hematite reference JCPDS 86-0550.

3.5.3 FTIR of glass ceramic

Figure 3.5.2.1 FTIR analysis of glass ceramic functionalized via plasma with camphorquinone and benzophenone (red line), only with camphorquinone (purple line) and only with benzophenone (blue line).

When we functionalized the sample with CQ and BP simultaneously, it was possible to observe two new peaks at 1699 and 1404 cm^{-1} in the IR spectrum.
The same phenomenon was not observed in the case of functionalization with BP and CQ taken individually.
It can be assumed that the peak at 1699 cm^{-1} is due to a C = O group while the peak at 1404 cm^{-1} is attributable to the formation of new aliphatic chains.

3.6 Electrical characterization of the sensors

All the humidity and ammonia (NH_3) tests (in all the characterizations, the ammonia was used insolution as NH_4OH diluted into water) of the sensors were carried out by using a laboratory apparatus in which relative humidity (RH) could be varied by steps between 0 and 96% and NH_3 concentration between 0 and about 1500 ppm.

3.6.1 Electrical responses of pure ZnO sensor

We started by evaluating the electrical response of the sensors made from commercial ZnO (ZnO Advanced Nanomaterials VP AdNano 20, Degussa, Germany). The mean diameter of the Degussa ZnO powder (d50) was about 9.70 Šm and the diameters corresponding to 10% (d10) and 90% (d90) of the particle size distributions were, respectively, 1.80 and 21.00 Šm. The particle size of ZnO was estimated, that can be observed in figure 3.6.1.1.

Figure 3.6.1.1 Particle size distributions of Degussa commercial ZnO powders.

ZnO sensors were tested under ammonia atmosphere and their sensor response (SR) was evaluated with respect to NH_3 concentration (Fig. 3.6.1.1). We observed that electrical response of zinc oxide wasn€t good to ammonia gas.

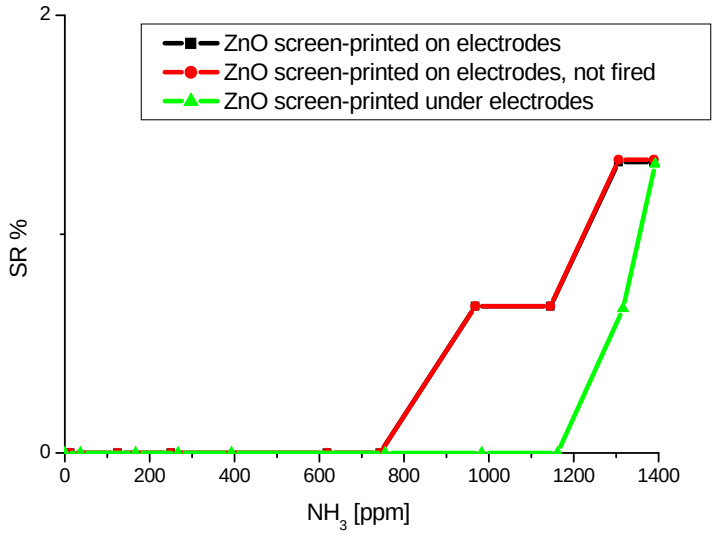

Figure 3.6.1.1. Electrical responses of the sensor based on commercial pure ZnO in function of NH_3 concentration. ZnO screen-printed on electrode and fired at 900°C (black line), ZnO screen-printed on electrode and not fired (red line) and ZnO screen-printed below electrode and fired at 900°C (green line).

We tried to improve the sensor's response in two ways: through the functionalization of ZnO with fluorides orcarboxylic groups and by hydrothermal synthesis of zinc oxide nanopowders.

3.6.2 Electrical characterization of functionalized ZnO

3.6.2.1 Fluoride groups

We functionalized ZnO sensors fired at 900°C with fluorides group in hydrofluoric acid solution at $5x10^{-5}$M (Figure 3.6.2.1.1).

From these first tests it is possible to note that the sintered device had a limited variation of SR. We observe that the electrical response increases until six days of functionalization in acid solution; it is also possible to observe that the sensor immersed in solution for 15 days gives a response for lower concentration of ammonia. However, there is only a slight improvement of the sensor response with respect to the screen printed film as such.

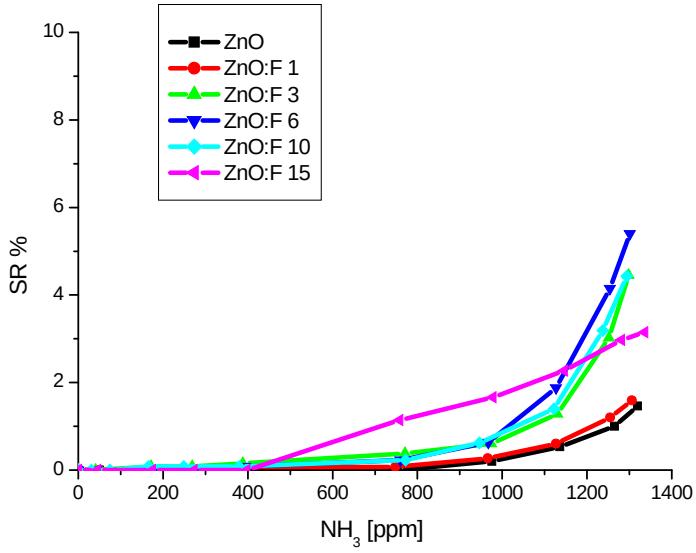

Figure 3.6.2.1.1. Electrical responses of the ZnO sensor functionalized for different days with fluorides groups in function of NH_3 concentration.

3.6.2.2 Carboxylic acid group

To improve the electrical response of the sensors we functionalized sensors with carboxyl groups.

In this section we can observe the electrical response of several sensors functionalized with carboxylic group after a pretreatment with NH_4OH at different concentration (reported in the list below).

The following carboxylic acids were used:

- Acetic acid
- Propionic acid
- 3-phosphopropionic acid
- Formic acid
- Maleic acid
- Oleic acid
- Salicylic acid

· Oxalic acid

In the first three figures (Figures 7.5.2.1-7.5.2.3) it is possible to observe the sensor response under ammonia of ZnO films functionalized with different carboxylic acids for different times. In these cases the sensors were immersed in a NH_4Cl solution at 15% for 90 minutes and afterwards there were immersed in a carboxylic acid solution for 24 hours.

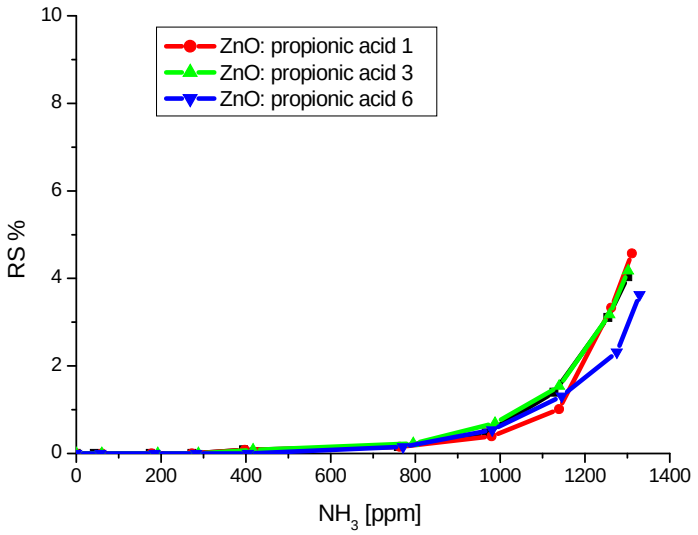

Figure 3.6.2.2.1. Electrical responses of the ZnO sensor functionalized dipping samples in a propionic acid solution for different times (1, 3 and 6 days) in function of NH_3 concentration.

In Figure 3.6.2.2.1 SR% was comprised between 0% and 5%: it is possible to conclude that this kind of device was not so sensitive to NH_3.

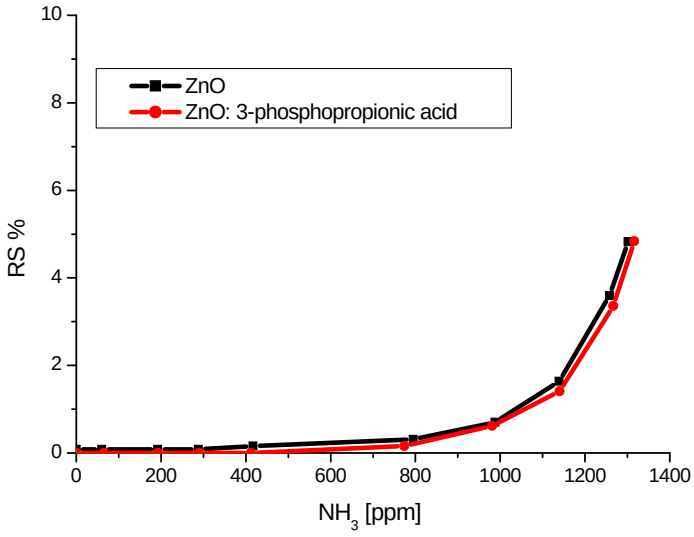

Figure 3.6.2.2.2. Electrical responses of the ZnO sensor functionalized for one day with 3-phosphopropionic acid in function of NH_3 concentration.

In Figure 3.6.2.2.2 it is possible to note that the sintered device gave the same response under NH_3 atmosphere while in Figure 3.6.2.2.3 the electrical response was better under NH_3 without functionalization.

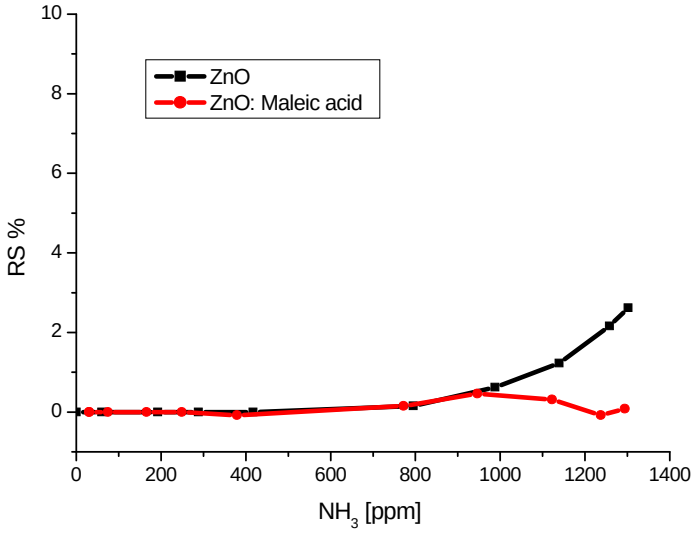

Figure 3.6.2.2.3. Electrical responses of the ZnO sensor functionalized for one day with maleic acid in function of NH_3 concentration.

Electrical response under ammonia gas of the ZnO sensor functionalized with propionic acid, 3-phosphopropionic acid and maleic acid were not good, so the concentration of carboxylic acids was increased.

In Figure 3.6.2.2.4 - 3.6.2.2.5 it is possible to observe the electrical response under ammonia for the ZnO sensor functionalized with carboxylic acids at 5×10^{-4} M.

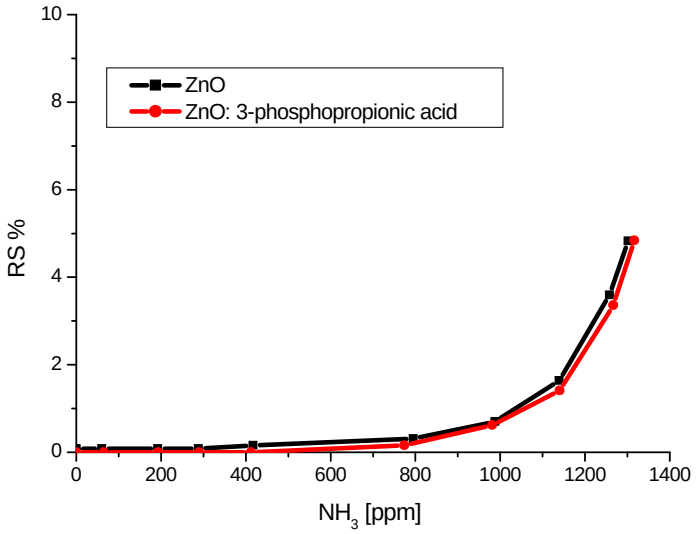

Figure 3.6.2.2.4 - Electrical responses of the ZnO sensor functionalized for one day with 3-phosphopropionic acid in function of NH_3 concentration.

The carboxylic acid increased concentration doesn't give a better response, therefore it was decided to functionalize directly the ZnO powder.

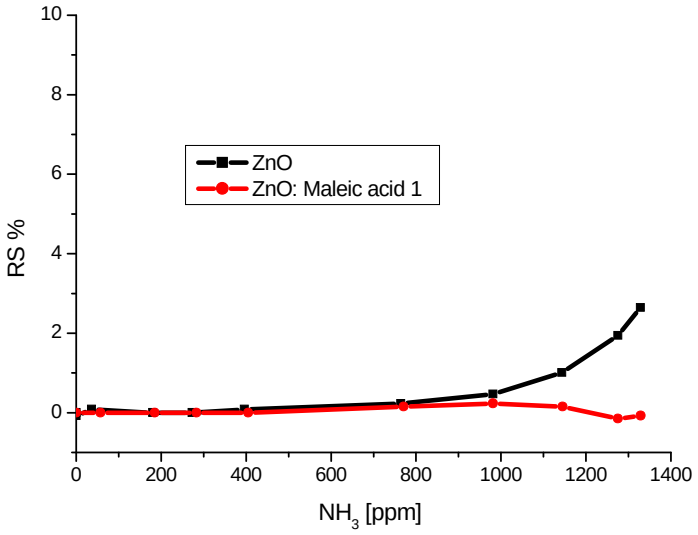

Figure 3.6.2.2.5 Electrical responses of the ZnO sensor functionalized for different days with maleic acid in function of NH_3 concentration.

We then functionalized ZnO with the oxalic acids in two different ways: first we functionalized directly the ZnO sensors screen-printed on electrodes (Figure 3.6.2.2.6-3.6.2.2.11), afterwards we functionalized ZnO powder and then screen-printed the electrodes (Figure 3.6.2.2.12-3.6.2.2.15).

For the first time it is possible to observe a variation reaching 16% under NH_3 atmosphere, and a sensor starting to respond over 1100 ppm, which was at the same time quite insensitive to humidity.

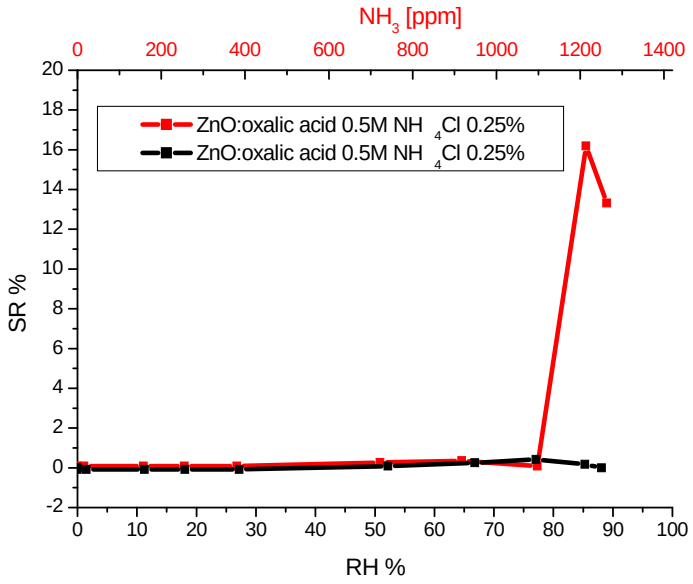

Figure 3.6.2.2.6. Electrical responses of the ZnO sensor functionalized with oxalic acid (0.5 M) and NH_4Cl 0.25% in function of NH_3 (red curve) and of humidity (black curve).

Our aim is now to obtain an electrical response for lower ammonia concentrations. We changed the concentrations of carboxylic acids and ammonia chloride solutions.

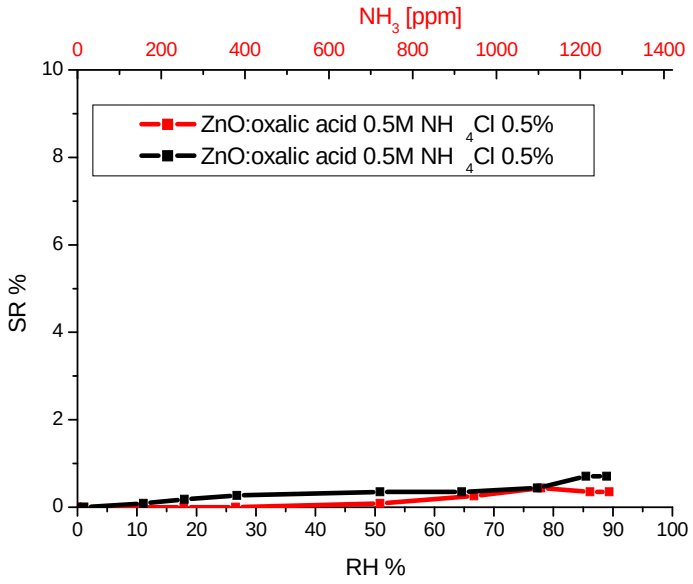

Figure 3.6.2.2.7. Electrical responses of the ZnO sensor functionalized with oxalic acid at 0.5 M and NH_4Cl 0.5% in function of NH_3 (red curve) and of humidity (black curve).

The sensor in Figure 3.6.2.2.7 didn't respond under ammonia and humidity while the sensor in Figure 3.6.2.2.8 respond under both gases. In this latter functionalization we decreased the acid concentrations but we increased the concentration of the pretreat solution.

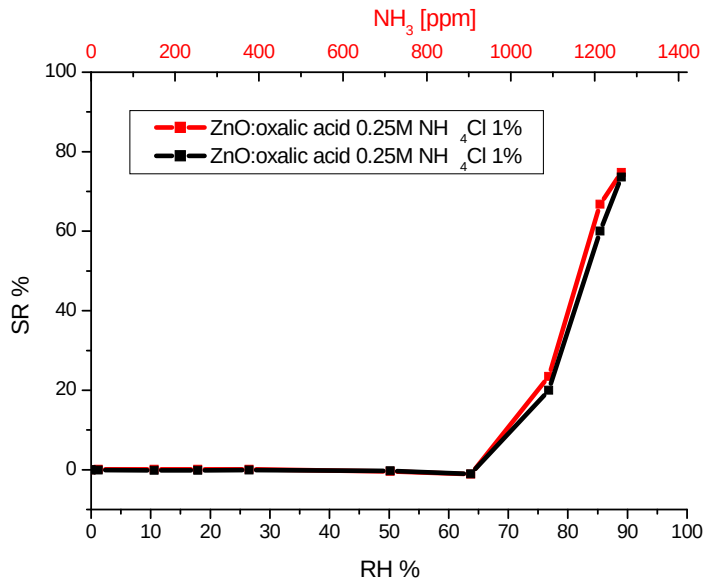

Figure 3.6.2.2.8. Electrical responses of the ZnO sensor functionalized with oxalic acid (0.25 M) and NH_4Cl 1% in function of NH_3 and of humidity.

In Figure 3.6.2.2.9 it is possible to observe a good electrical response under NH_3. SR% reached 65% and only 15% under water. However, the sensor starts to respond only from 900 ppm of ammonia.

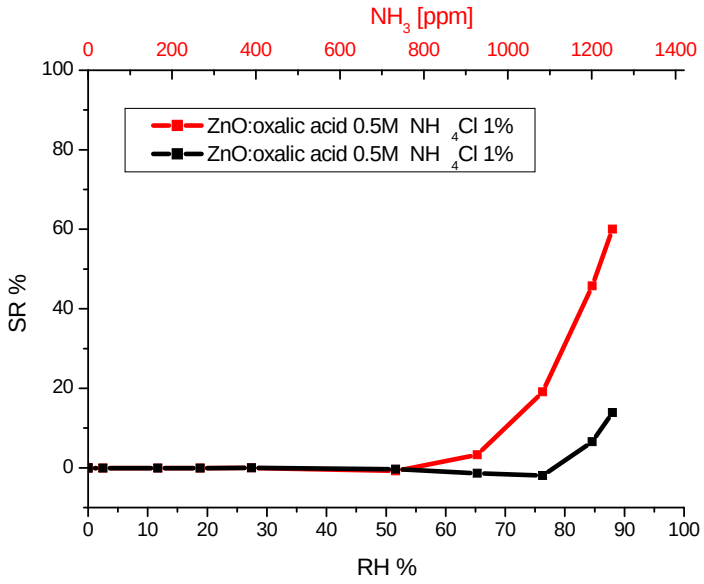

Figure 3.6.2.2.9. Electrical responses of the ZnO sensor functionalized with oxalic acid (0.5 M) and NH_4Cl 1% in function of NH_3 and of humidity.

Afterwards the same sensor was tested after two weeks and we observed that it didn€t respond anymore (Figure 3.6.2.2.10). This has allowed us to understand that this kind of functionalization does not last over time.

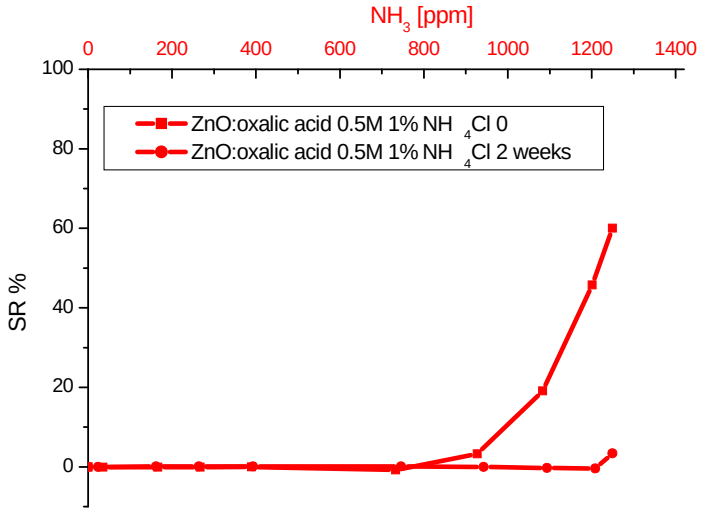

Figure 3.6.2.2.10. Electrical responses of the ZnO sensor functionalized with oxalic acid (0.5 M) and NH_4Cl 1% in function of NH_3 and of humidity.

In Figure 3.6.2.2.11, the carboxylic acid concentration was varied from 0.5 to 0.1 M but the electrical response didn€t change significantly.

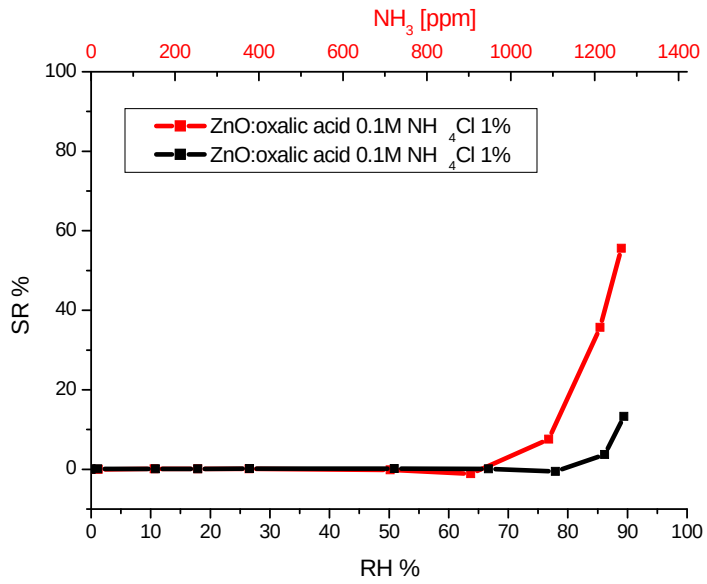

Figure 3.6.2.2.11. Electrical responses of the ZnO sensor functionalized with oxalic acid (0.1 M) and NH_4Cl 1% in function of NH_3 and of humidity.

The sensor in Figure 3.6.2.2.12 wasn€t good too because it responded very well under humidity, while the sensor in Figure 3.6.2.2.13 responded at high concentrations of humidity and at low concentration of ammonia.

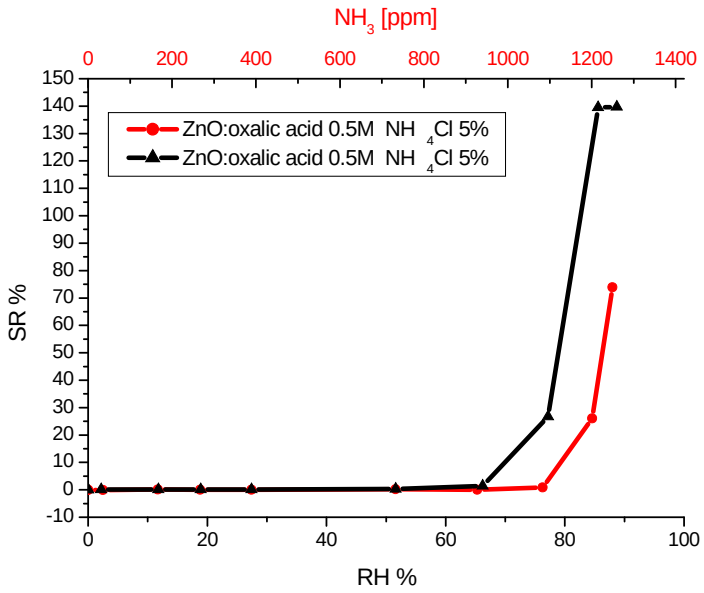

Figure3.6.2.2.12. Electrical responses of the ZnO sensor functionalized with oxalic acid (0.5 M) and NH_4Cl 5% in function of NH_3 and of humidity.

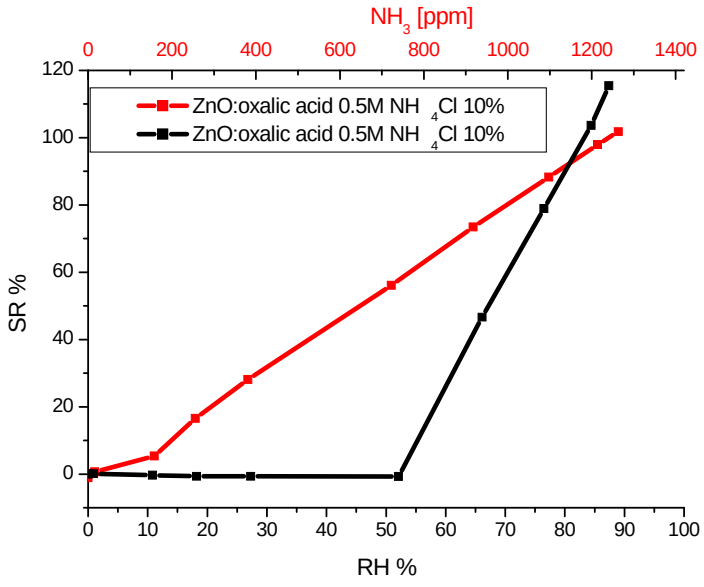

Figure 3.6.2.2.13. Electrical responses of the ZnO sensor functionalized with oxalic acid (0.5 M) and NH_4Cl 10% in function of NH_3 and of humidity.

In Figure 3.6.2.2.13 we observe a good electrical response starting from near 100 ppm of NH_3 but we have also a response under water vapor above 50%, so we can€t use this sensor

at high watervapor concentrations. In Figure 3.6.2.2.14 we observe how the response to humidity is greater than the one to ammonia.

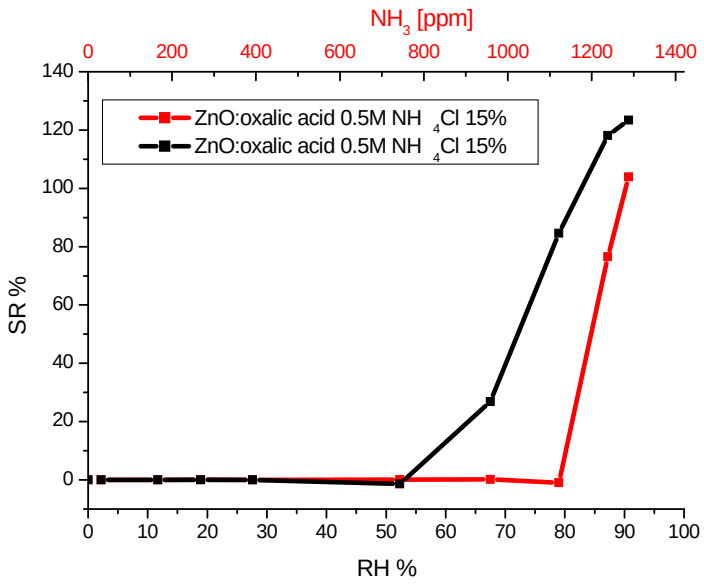

Figure 3.6.2.2.14. Electrical responses of the ZnO sensor functionalized with oxalic acid (0.5M) and NH_4Cl 15% in function of NH_3 and of humidity.

We obtained the best response with the treatment in 0.1 M oxalic acid and 15% of NH_4Cl (Figure 3.6.2.2.15).

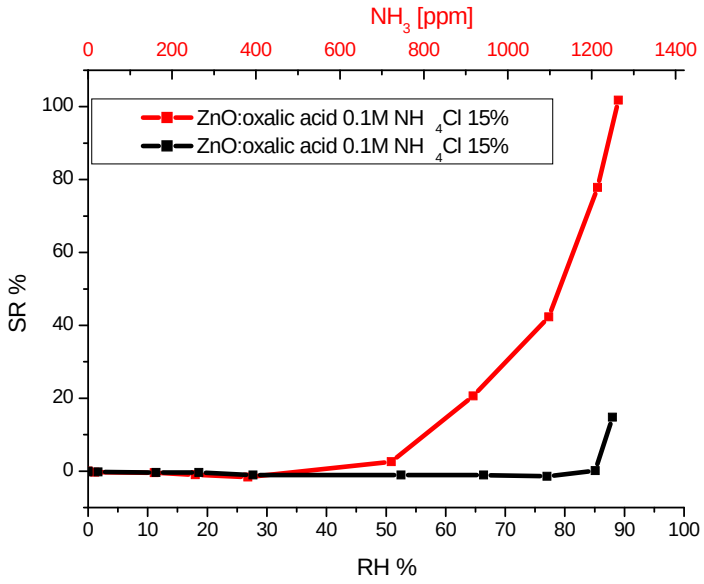

Figure 3.6.2.2.15. Electrical responses of the ZnO sensor functionalized with oxalic acid (0.1 M) and NH_4Cl 15% in function of NH_3 and of humidity.

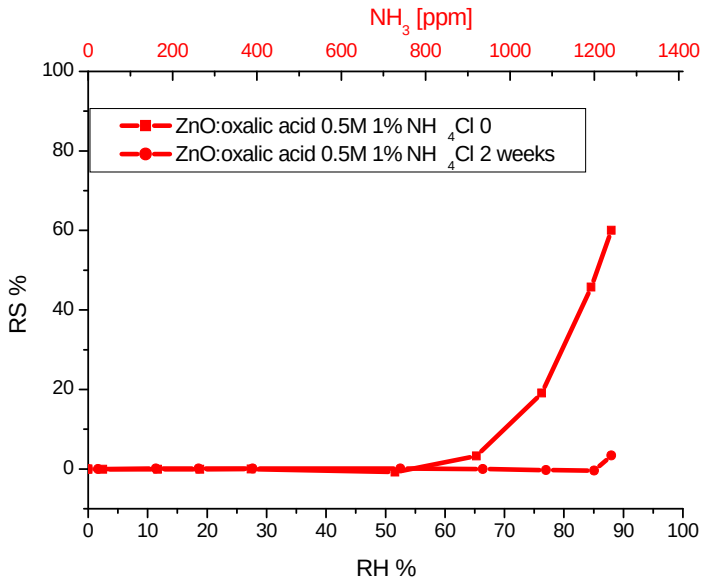

Figure 18, electrical response to ammonia of ZnO functionalized with oxalic acid 0.1 M at time 0 and after two weeks.

We functionalized ZnO powder with other carboxylic acids (Figure 3.6.2.2.16-3.6.2.2.26). When we used salicylic acid, we observed that the sensor responded to ammonia and to

humidity (Figure 3.6.2.2.16). The device was the same of that presented in Figure 3.6.2.2.13 because answers at low concentration of ammonia and air humidity.

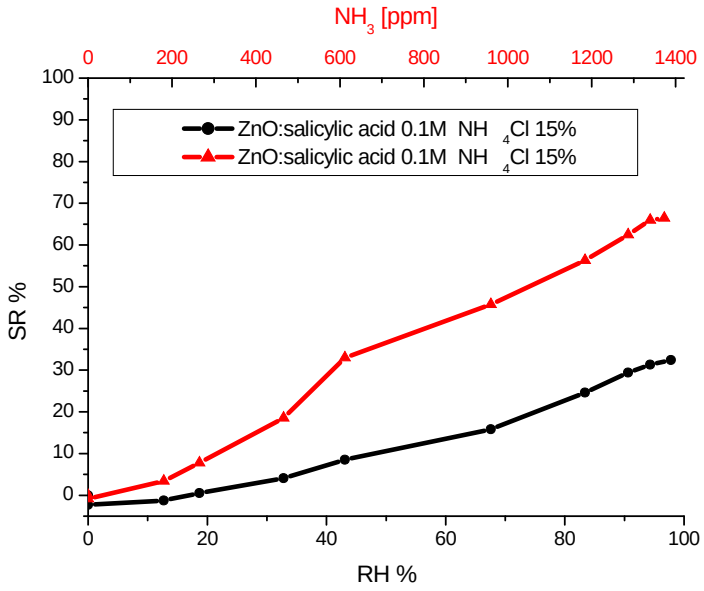

Figure 3.6.2.2.16. Electrical responses of the ZnO sensor functionalized with salicylic acid (0.1 M) and NH_4Cl 15% in function of NH_3 and of humidity.

We observed that the functionalization of ZnO sensors with short chain carboxylic acid wasn't good as with formic, acetic and maleic acids (Figure 3.6.2.2.17-3.6.2.2.25).

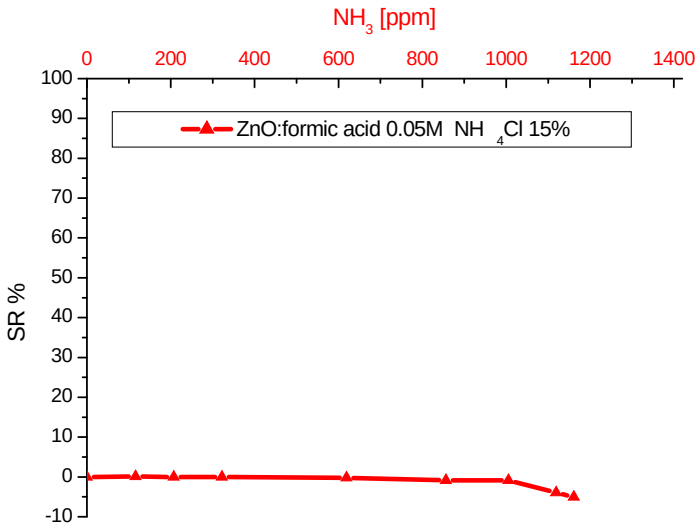

Figure 3.6.2.2.17. Electrical responses of the ZnO sensor functionalized with formic acid (0.05 M) and NH_4Cl 15% in function of NH_3.

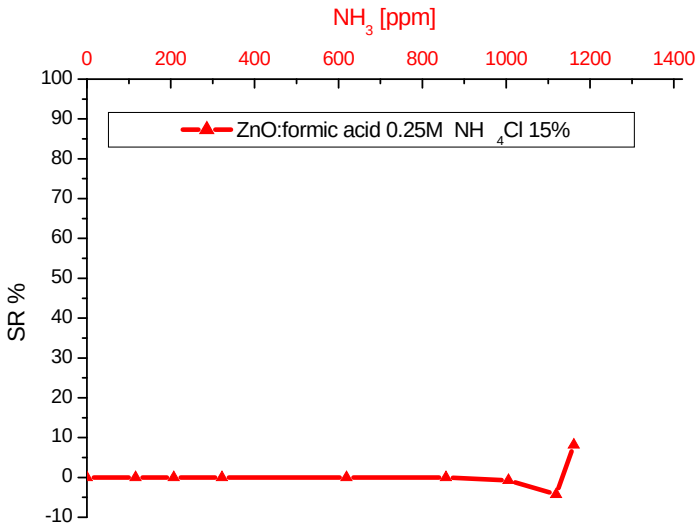

Figure 3.6.2.2.18. Electrical responses of the ZnO sensor functionalized with formic acid (0.25 M) and NH_4Cl 15% in function of NH_3.

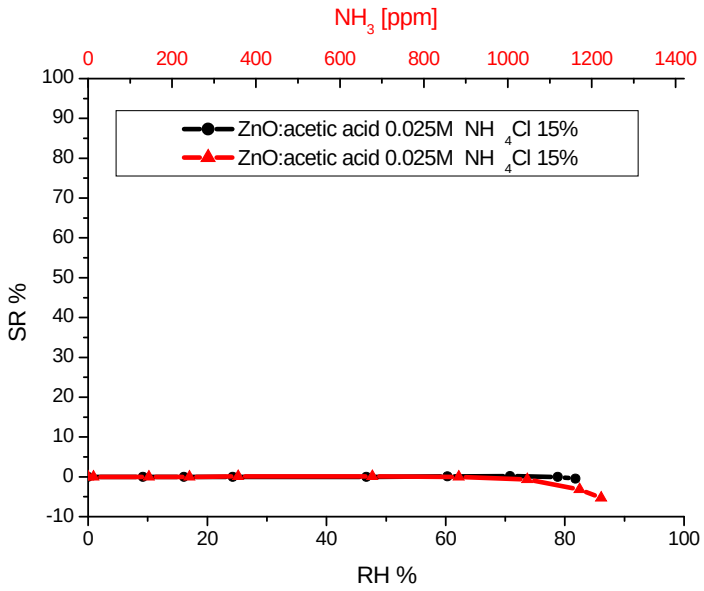

Figure 3.6.2.2.19. Electrical responses of the ZnO sensor functionalized with acetic acid (0.025 M) and NH_4Cl 15% in function of NH_3 (red line) and of humidity (black line).

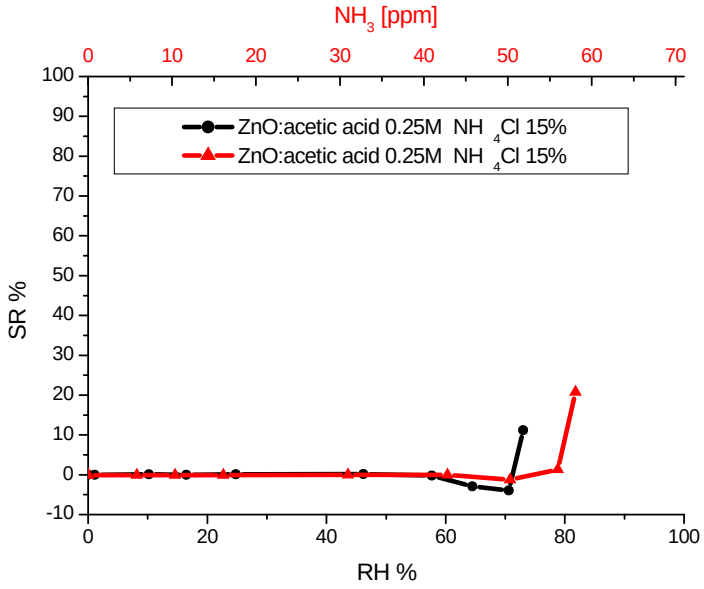

Figure 3.6.2.2.20. Electrical responses of the ZnO sensor functionalized with acetic acid (0.25 M) and NH_4Cl 15% in function of NH_3 (red line) and of humidity (black line).

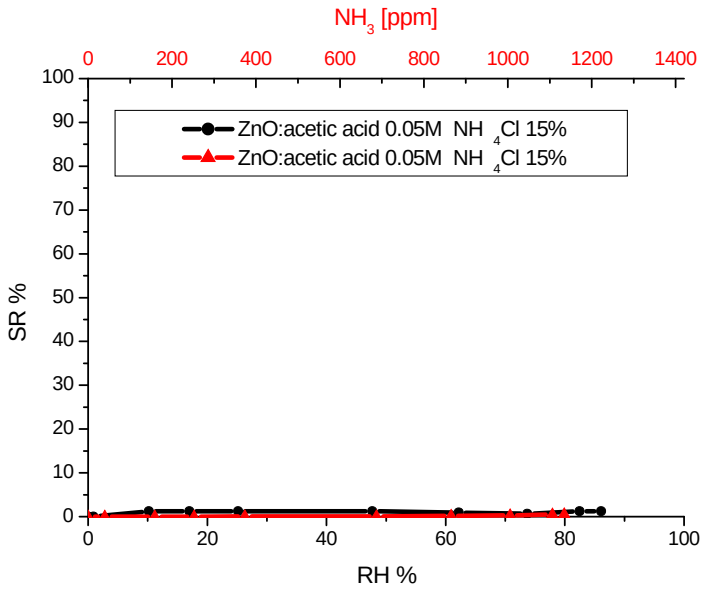

Figure 3.6.2.2.21. Electrical responses of the ZnO sensor functionalized with acetic acid (0.05 M) and NH_4Cl 15% in function of NH_3 (red line) and of humidity (black line).

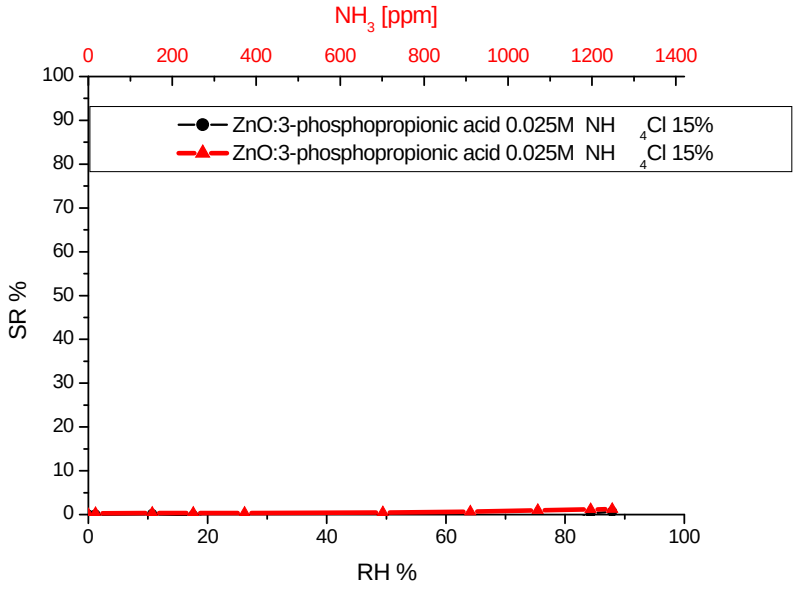

Figure 3.6.2.2.22. Electrical responses of the ZnO sensor functionalized with 3-phosphopropionic acid (0.025 M) and NH_4Cl 15% in function of NH_3 (red line) and of humidity (black line).

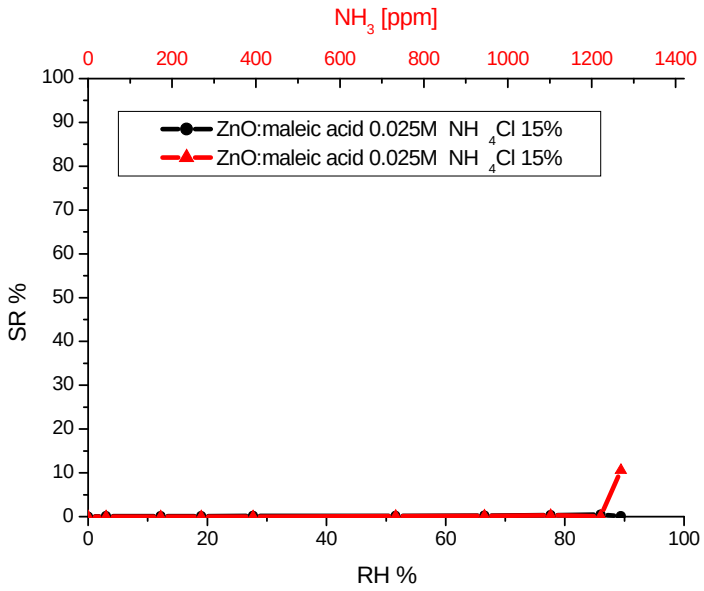

Figure 3.6.2.2.23. Electrical responses of the ZnO sensor functionalized with maleic acid (0.025M) and NH_4Cl 15% in function of NH_3 (red line) and of humidity (black line).

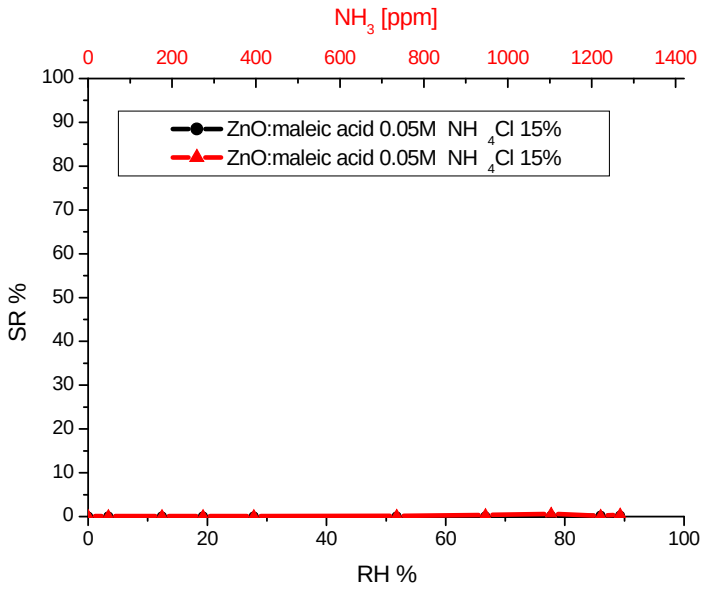

Figure 3.6.2.2.24. Electrical responses of the ZnO sensor functionalized with maleic acid (0.05 M) and NH_4Cl 15% in function of NH_3 (red line) and of humidity (black line).

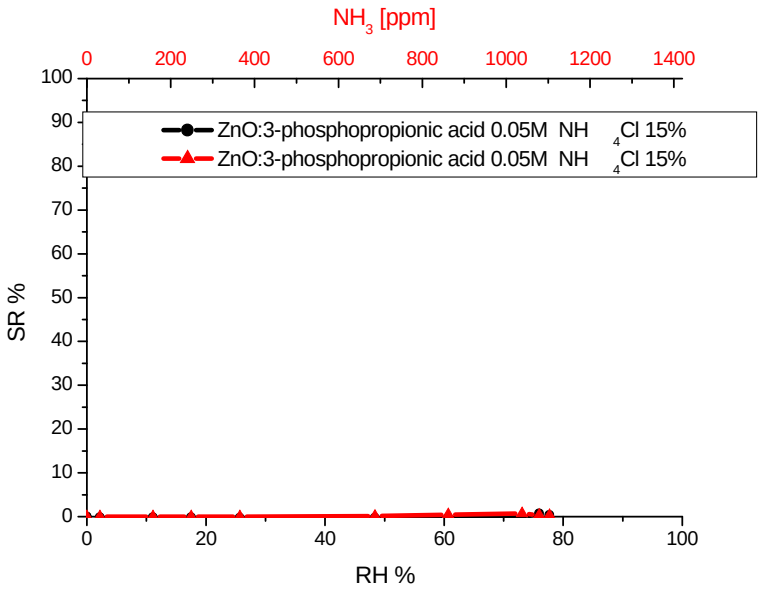

Figure 3.6.2.2.25. Electrical responses of the ZnO sensor functionalized with 3-phosphopropionic acid (0.05 M) and NH_4Cl 15% in function of NH_3 (red line) and of humidity (black line).

The ZnO sensor functionalized with oleic acid gave a response reaching 40% under NH_3 atmosphere (Figure 3.6.2.2.26), starting from 400 ppm, which was less sensitive to humidity.

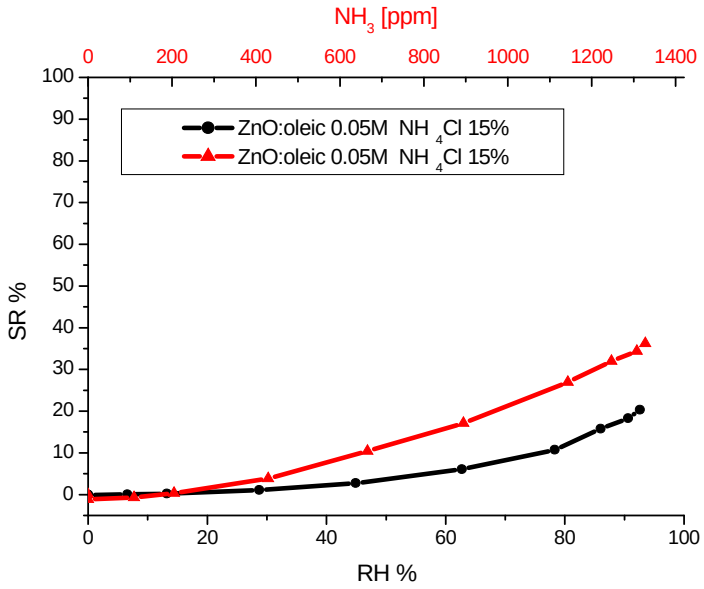

Figure 3.6.2.2.26. Electrical responses of the ZnO sensor functionalized with oleic acid (0.05 M) and NH_4Cl 15% in function of NH_3 (red line) and of humidity (black line).

We tested the ZnO sensor functionalized with zinc oleate under ammonia and humidity and we obtained a good electrical response (Figure 3.6.2.2.27) from 700 ppm of NH_3 while it was insensitive to air humidity.

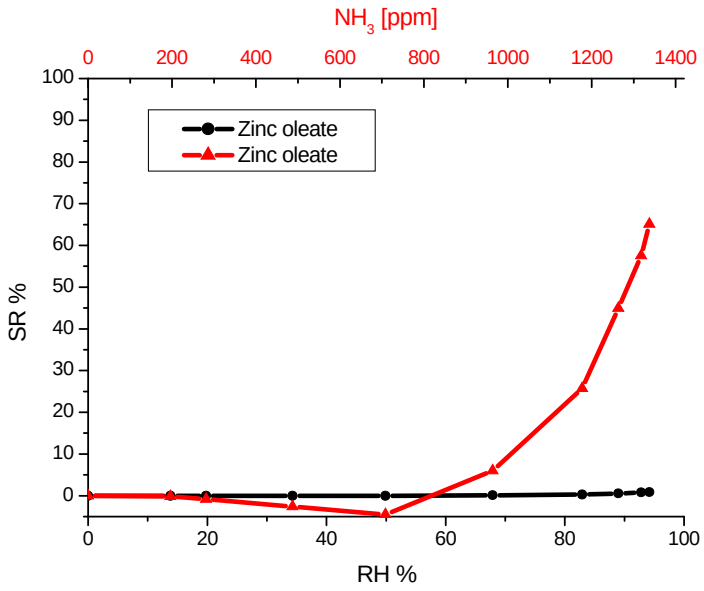

Figure 3.6.2.2.27. Electrical responses of the zinc oleate sensor in function of NH_3 (red line) and of humidity (black line).

We tried to functionalize ZnO with amino acids such as lysine, glutamic acid and glycine; it is possible to observe in Figure 3.6.2.2.29 and 3.6.2.2.30 that these sensors responded only at high concentrations of ammonia.

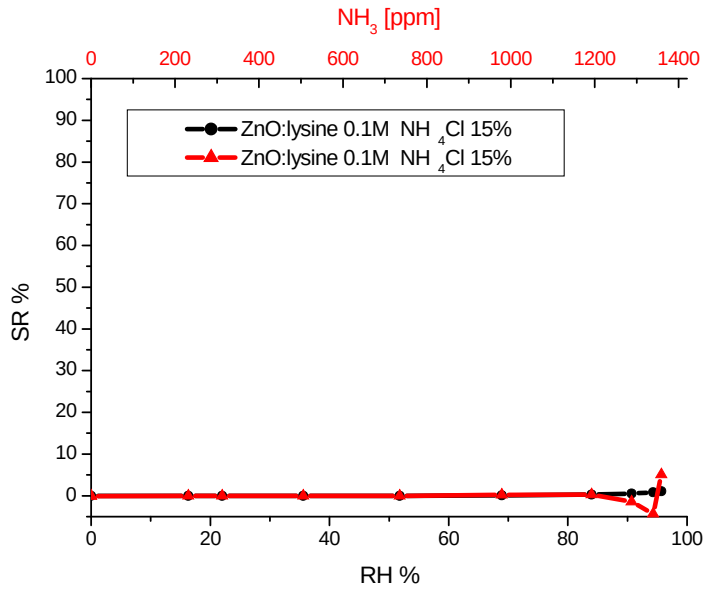

Figure 3.6.2.2.28. Electrical responses of the ZnO sensor functionalized with lysine (0.1 M) and NH_4Cl 15% in function of NH_3 (red line) and of humidity (black line).

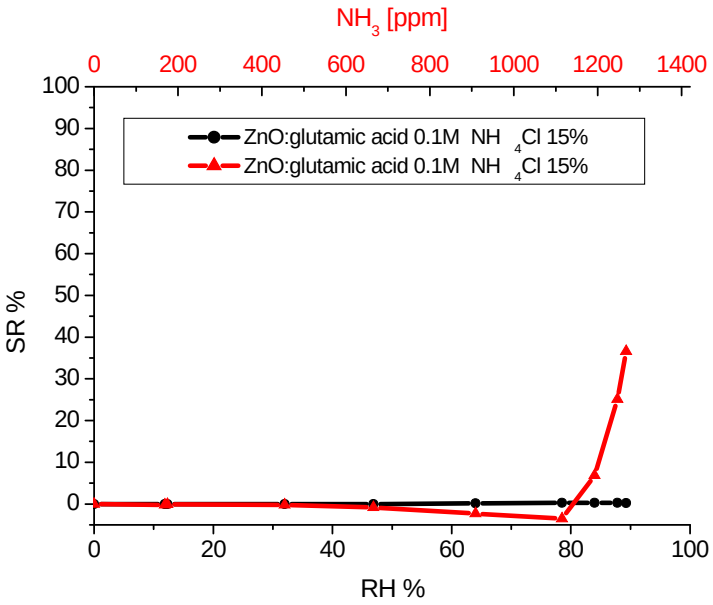

Figure 3.6.2.2.29. Electrical responses of the ZnO sensor functionalized with glutamic acid (0.1 M) and NH_4Cl 15% in function of NH_3 (red line) and of humidity (black line).

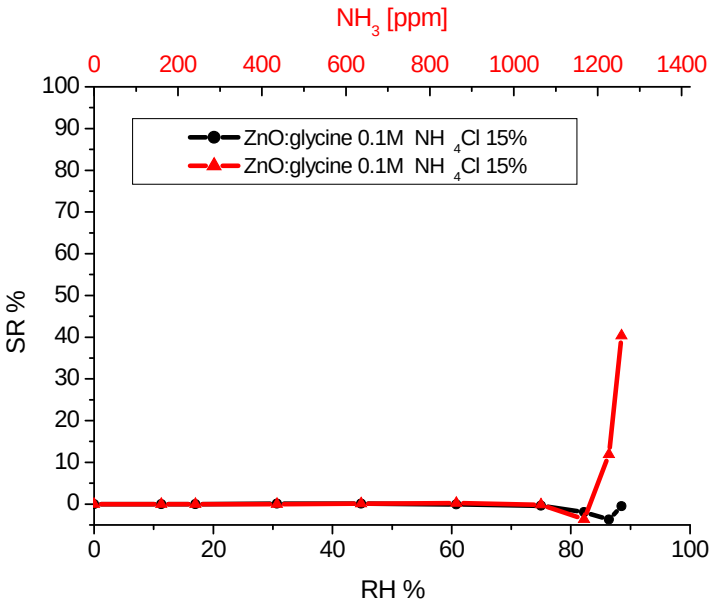

Figure 3.6.2.2.30. Electrical responses of the ZnO sensor functionalized with glycine (0.1 M) and NH_4Cl 15% in function of NH_3 (red line) and of humidity (black line).

3.6.3 Electrical characterization of sensors functionalized via plasma

We functionalized ZnO sensors with oleic acid via plasma at different concentrations of acid and after pretreatment with NH_4Cl at different concentrations. Usually, we put some drops of NH_4Cl on sensors and then we put them in the plasma chamber for 30 seconds. Afterwards we put some drops of acid on sensors and we placed them in the plasma chamber for 2 minutes [155,156]. The corresponding electrical responses are described in Figure 2.6.3.1-2.6.3.3.

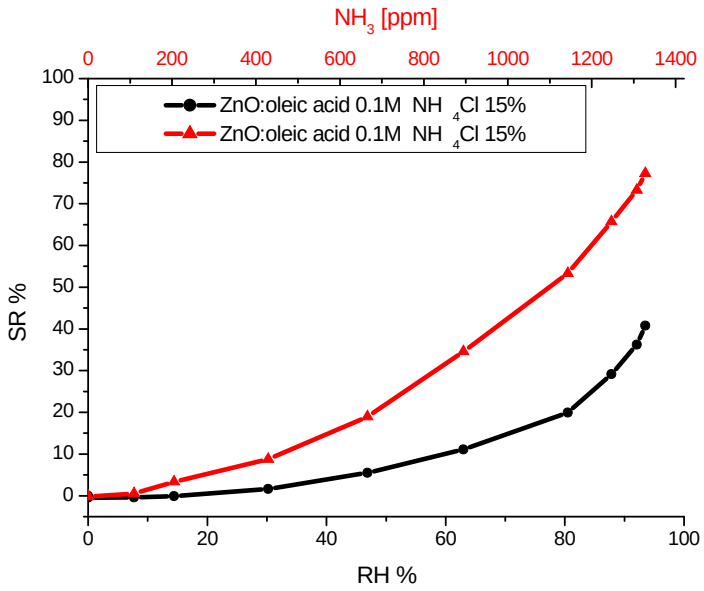

Figure 3.6.3.1. Electrical responses of the ZnO sensor functionalized with oleic acid (0.1 M) and NH_4Cl 15% via plasma with 50 W power in function of NH_3 (red line) and of humidity (black line).

It is possible to observe a response reaching 80% under NH_3 atmosphere, starting from 100 ppm. However, this device was also sensitive to humidity.

If we increase the carboxylic acid concentration during functionalization, the sensor becomes insensitive to humidity but starts to respond from 800 ppm of NH_3.

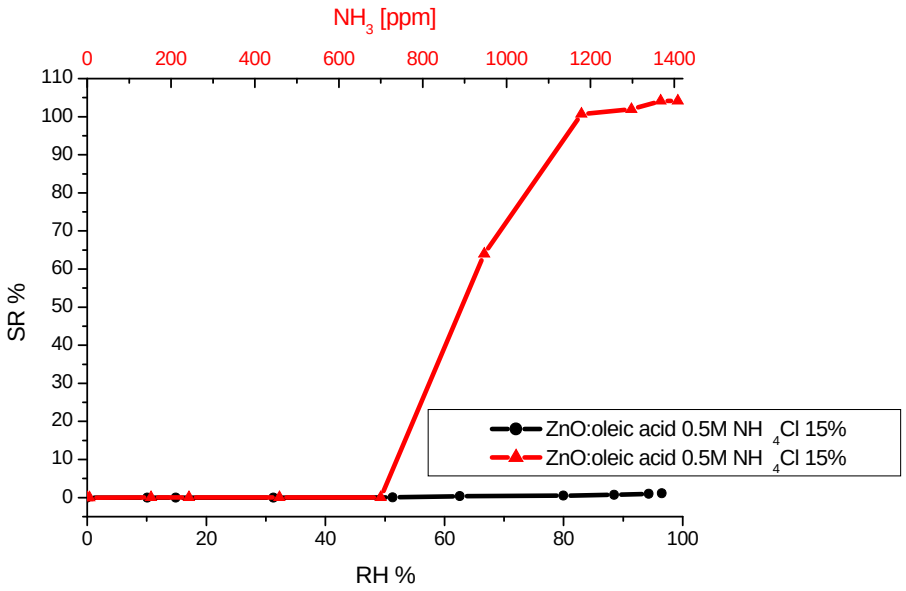

Figure 3.6.3.2. Electrical responses of the ZnO sensor functionalized with oleic acid (0.05 M) and NH_4Cl 15% via plasma with 50 W power in function of NH_3 (red line) and of humidity (black line).

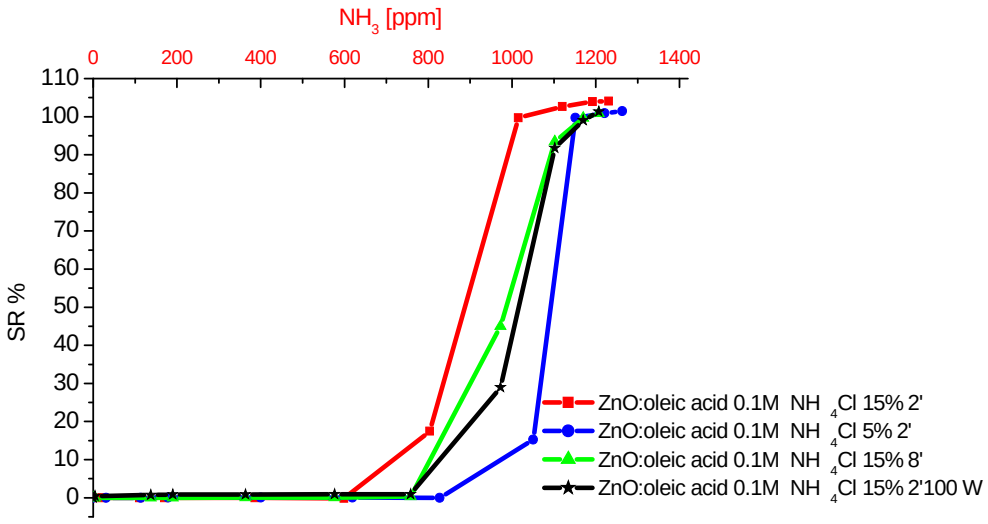

Figure3.6.3.3. Electrical responses of the ZnO sensor functionalized with oleic acid (0.1 M) and NH_4Cl 15% via plasma with 50 W and 100 W power in function of NH_3

In Figure 3.6.3.3 we changed the conditions of functionalization but we didn€t were able to increase the electrical response of the sensors to lower ammonia concentrations.

3.6.4 Electrical characterization of glass ceramic

To obtain an electrical response to low concentrations of ammonia we thought to functionalize our sensors with two different photoinitiators. This idea came from the work of M. Atilla Tasdelen et Al. [17] where this author explains how CQ is able to extract H^+ ions in the presence of UV radiation [18].

For this functionalization the glass ceramic has been used as the sensing material (Section 3.3.2).

We prepared glass ceramic with ZnO, WO_3 and Bi_2O_3. We used B_2O_3 for decreasing the melting temperature. The material is composed by 58% of ZnO, 4% of WO_3, 4% of Bi_2O_3 and 33,3% of B_2O_3.

In the first step we melt the mixture of oxide powders for 10 minutes at 1300°C and afterwards the glass was subjected to a 500°C treatment for 15 hours.

It is known in the literature that UV radiations are able to excite semiconductors and to make them more sensitive to ammonia [19].

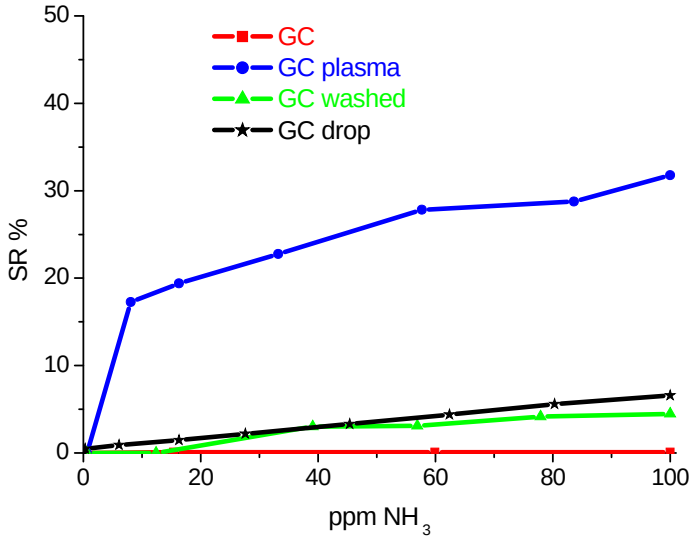

Figure 3.6.4.1 Electrical responses of glass ceramic sensors: pristine (red line), functionalized with camphorquinone and benzophenone via plasma (blue line), washed with methanol (green line) and functionalized with one drop of 0.1 M solution of camphorquinone and benzophenone (black line).

In Figure 3.6.4.1 it is possible to observe that the GC sensor functionalized with CQ and BP gives response under low concentrations of ammonia gas while in the absence of functionalization the sensors doesn't give any response to ammonia.
We observed that the washing with methanol worsens the sensor response.

3.6.5 Electrical characterization of nanopowder

In Figure 3.6.5.1 and 3.6.5.2 we worked in a beaker at 95°C for 90 minutes. In the first experiment we put a copper ribbon in the solution after NH_4OH addition, while in the second experiment it was put before ammonium hydroxide addition.

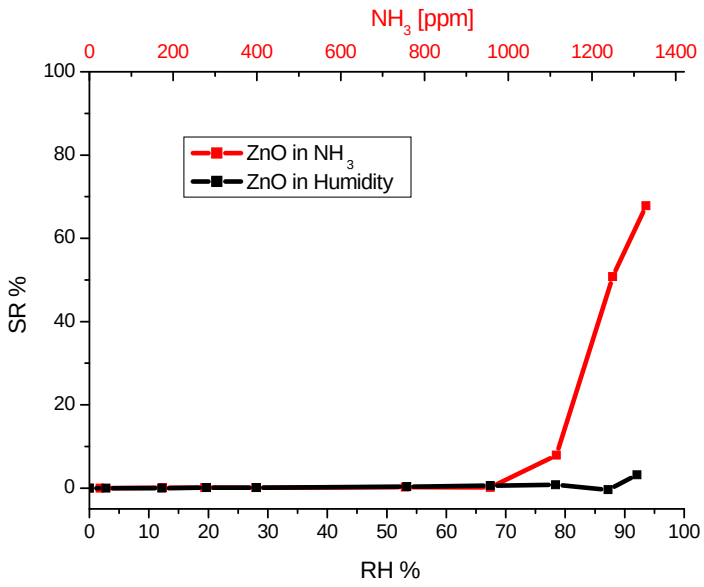

Figure 3.6.5.1. Electrical responses of the sensor based on ZnO prepared by hydrothermal synthesis in function of RH (black line) and of NH_3 concentration (red line).

In Figure 3.6.5.1 and 3.6.5.2 it is possible to observe that sensors responded only to high ammonia concentrations.

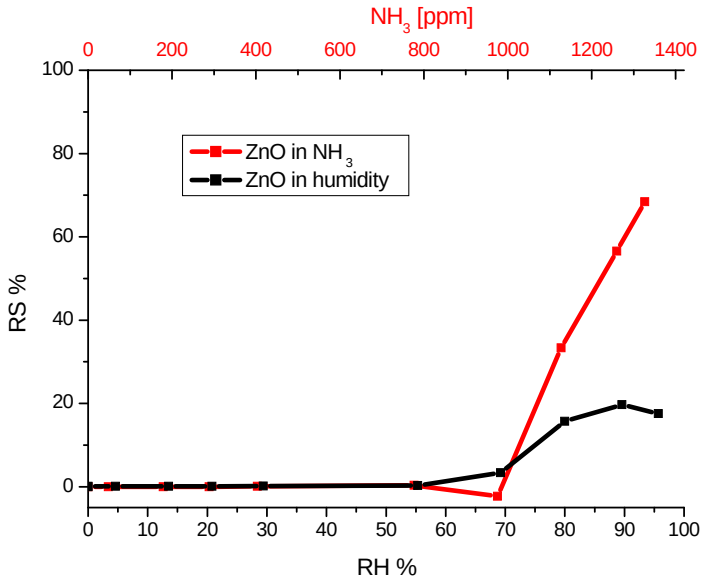

Figure 3.6.5.2. Electrical responses of the sensor based on ZnO prepared by hydrothermal synthesis in function of RH (black line) and of NH_3 concentration (red line).

In Figure 3.6.5.3 we worked in a beaker at 95°C for 7 hours. This sensor responded to ammonia but to humidity too.

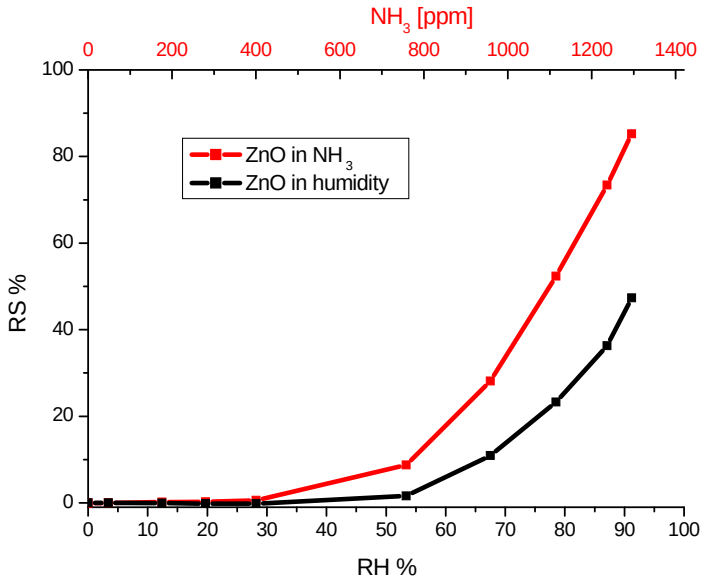

Figure 3.6.5.3. Electrical responses of the sensor based on ZnO prepared by hydrothermal synthesis in function of RH (black line) and of NH_3 concentration (red line).

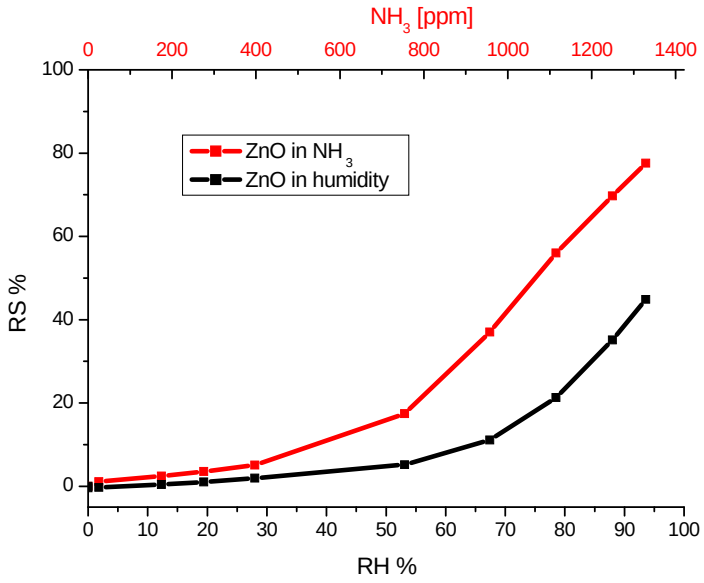

Figure 3.6.5.4. Electrical responses of the sensor based on ZnO prepared by hydrothermal synthesis in function of RH (black line) and of NH_3 concentration (red line).

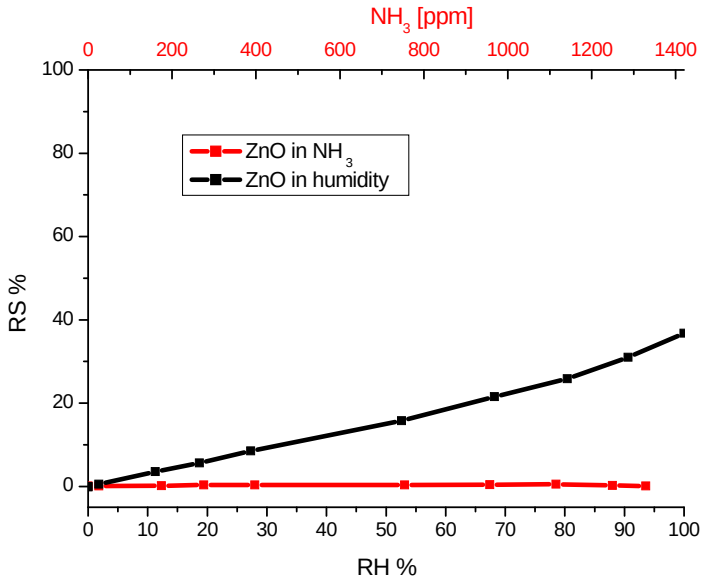

Figure 3.6.5.5Electrical responses of the sensor based on ZnO by hydrothermal synthesis in function of RH (black line) and of NH_3 concentration (red line).

In Figure 3.6.5.4 and 3.6.5.5 we worked in a teflon autoclave at 120°C for 4 hours. In the case of figure 3.6.5.4, during cooling to room temperature we did an isotherm at 60°C for 2 hours while at 40°C in figure 3.6.5.5.

We observed two different electrical response in Figure 3.6.5.4 and 3.6.5.5. The first sensor responded under ammonia gas and humidity while, in the second case, the sensor didn€t responded to ammonia but only to water vapor.

A WO_3 nanopowder was also prepared by hydrothermal synthesis. In this case, an autoclave in teflon was used and warmed at 160°C for 16 hours; in Figure 3.6.5.6 it is possible to observe that the sensor produced with this material didn€t give any electrical response.

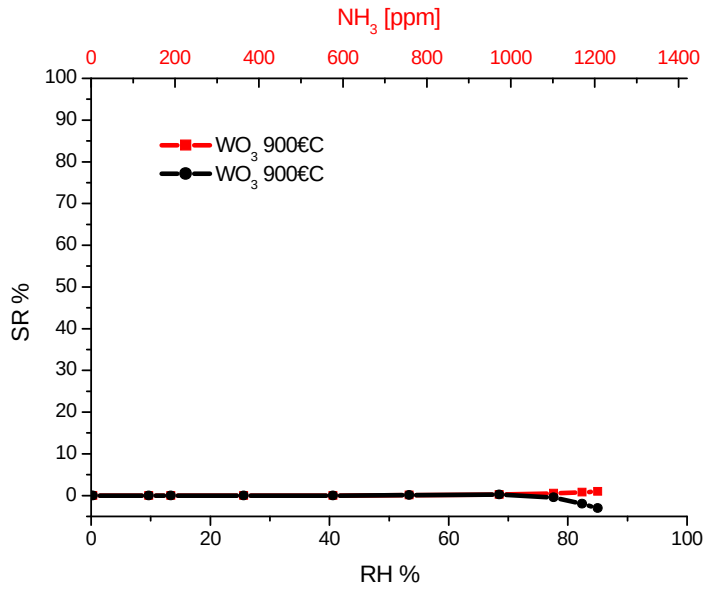

Figure 3.6.5.6. Electrical responses of the sensor based on WO_3 prepared by hydrothermal synthesis in function of RH (black line) and of NH_3 concentration (red line).

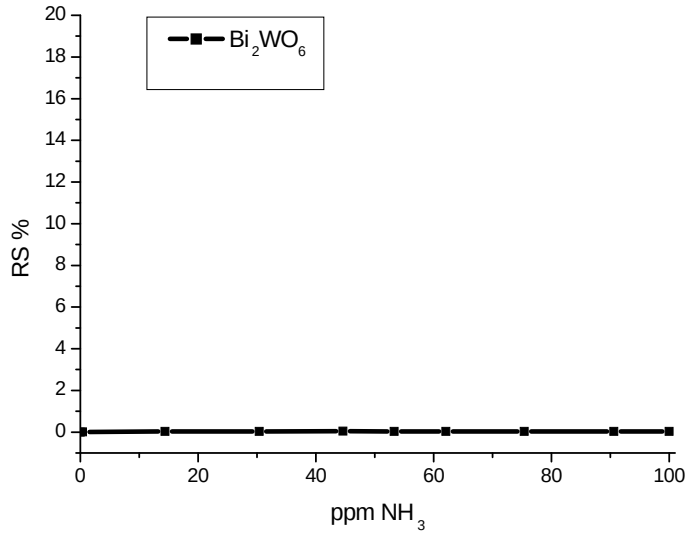

Figure 3.6.5.7. Electrical responses of the sensor based on Bi_2WO_6 prepared by hydrothermal synthesis in function of NH_3 concentration.

It can be observed how the sensor does not give response to ammonia.

3.7 Conclusion

During this Ph.D. thesis research work many ceramic materials have been used for sensors screen printing. These devices are meant to be applied to food industry in order to detect biogenic amines; however, as explained in the first chapter, in preliminary characterizations presented in this chapter, ammonia was chosen as a reference, since this compound is the most simple amino group.

ZnO and other semiconducting oxides were chosen as sensitive layers because it is known from literature that these materials are able to detect ammonia, although usually they are chosen for detections at high temperatures. Several studies have been performed: among them the most promising are those in which sensors are functionalized with carboxyl groups. These devices, however, do not guarantee the measurements repeatability at a distance of few days, probably because of ageing and interactions with the atmosphere's components with time. Another interesting study consists in obtaining sensors starting from nanopowders obtained by hydrothermal synthesis. These sensors, thanks to the greater surface area, are able to detect smaller quantities of ammonia; however, response is still not optimal.

Last study was about the use of a glass ceramic functionalized via plasma with canforquinone and benzophenone. Taking into account the capacity of canforquinone and benzophenone to rip a hydrogen in the presence of UV radiation, it was thought to use them in the presence of UV radiation to make the material sensitive to ammonia.

Bibliography

1- N. Jaydev Dayan, S. R. Sainkar, R. N. Karekar, R. C. Aiyer, Thin Solid Films, 325(1998) 254-258

2- B. Krishnan, V. N. Nampoori, Bull. Mater. Sci. 28(2005) 239-242

3- K.Ram Kumar, Thick Film Deposition and Processing Short Term Course on Thin and Thick Film Hybrid Microelectronics, Bangalore (1986) P 1-12-11-13

4- http://journeytoforever.org/biodiesel_mesh.html

5- D. W. Hamer and J. V. Biggers, •Thick film hybrid microcircuits technology,, John Wiley and Sons Inc. (New York) (1972), pp. 77

6- A. Wei, X. W. Sun, C. X. Xu, Z. L. Dong, Y. Yang, S. T. Tan, and W. Huang, Growth mechanism of tubular ZnO formed in aqueous solution, Nanotechnology 17 (2006), 1740

7- C. Wang, K. Yu, L. Li, Q. Li, and Z. Zhu Synthesis and field emission of two kinds of ZnO nanotubes: tapelike and flat-roofed tubes, Appl. Phys. A 90 (2008), 739

8- C. Badre, T. Pauport, M. Turmine and D. Lincot, A ZnO nanowire array film with stable highly waterepellent properties, Nanotechnology 18 (2007), 365705

9- J. Chen, L. Xu, W. Li and X. Gou, Fe_2O_3 nanotubes in gas sensor and lithium-ion battery applications, Advanced Materials 17 (2005)

10- Y. Wu et al. / Journal of Crystal Growth 292 (2006) 1-8

11- Thesys of M. Previatello, Film nanostrutturati di ossidi di metalli di transizione per sensori ottici di gas, 2011

12- L. Castaneda, A. Maldonado, J.C. Chang, M. Terrones and M.L. Olvera, Composition and morphological characteristics of chemically sprayed fluorine doped zinc oxide thin films deposited on Si(1 0 0), Physica B 390 (2007) 7-16

13- B. Zhang, T. Kong, W. Xu, R. Su, Y. Gao and G. Cheng, Surface Functionalization of Zinc Oxide by Carboxyalkylphosphonic Acid Self-Assembled Monolayers, Langmuir 26(6) (2010), 4514-4522

14- W. Xia, Y. Wang, R. Bergsträßer, S. Kundu and M. Muhler, Surface characterization of oxygen-functionalized multi-walled carbon nanotubes by high resolution X-ray photoelectron spectroscopy and temperature-programmed desorption, Applied Surface Science 254 (2007), pp. 247–250.

15- R.S. Joshi, J.F. Friedrich and M.H. Wagner, Study of carboxylic functionalization of polypropylene surface using the underwater plasma technique, Eur. J. Phys. 54, 249–258 (2009)

16- V. Sciarratta et al. / Surface and Coatings Technology 174–175 (2003) 805–810

17- M. Atilla Tasdelem, B. Kiskan and Y. Yagci, Photoinitiated free radical polymerization using benzoxazines as hydrogen donors, Macromolecular rapid communications, (2006) 1539–1544

18- T. Christensen et al. / Journal of Photochemistry and Photobiology B: Biology 100 (2010) 128–134

19- Zhou Y, et al. Sci China Chem April (2013) Vol.56 No.4

20- Tang JW, Zou ZG, Ye JH. Photocatalytic decomposition of organic contaminants by Bi_2WO_6 under visible light irradiation. Catal Lett, 2004, 92: 53–56

21- T. Bettles, S. Schujman, J. A. Smart, W. Liu and L. Schowalter, UV Light Emitting Diodes- Their Applications and Benefits, Iuva News Vol 9 n. 2 (2007)

PART IV

General Conclusions

During this PhD work many tests were performed with screen-printed sensors to detect ammonia at room temperature, because these devices are meant to be applied to food chemistry, in order to detect biogenic amines . ZnO together with other ceramic oxides were chosen as sensitive layer because it is known in literature that these materials are able to detect ammonia, although they are usually used for NH_3 detection at high temperatures.

Several studies have been performed, among them the most promising are those in which the sensor is functionalized with carboxyl groups. These devices, however, do not guarantee the measurements repeatability at a distance of few days, probably because ammonia tends to react with the carboxyl groups by removing the sensitive group.

Another interesting study was to obtain sensors starting from nanopowders obtained by hydrothermal synthesis. These sensors, thanks to the greater surface area, are able to detect smaller quantities of ammonia, however, the response is still not optimal. The last study performed, was the use of a glassceramic functionalized via plasma with canforquinone and benzophenone. Taking into account the capacity of canforquinone and benzophenone to rip a hydrogen in the presence of UV radiation it was thought to use them in the presence of UV radiation to make the material sensitive to ammonia.

The electrical characterizations have given excellent results, even if they are not actually as good as those reported in the literature: the detection limit was not equal to those reported in the literature. However, it can be concluded that the results obtained are very satisfactory, considering that the processes are simpler and less expensive to implement NH_3 sensor for applications at room temperature and compared with other works in literature.

Future prospects will concern with the research about hydrothermal synthesis of other semiconductor oxides, to verify if it is possible to lower the detection limit of these devices. It is also possible to hypothesized the functionalization of these nanoparticles with carboxyl groups or other materials sensitive to ammonia. Further investigations on glassceramic will also be taken into account, since it is necessary to assess the degree of repeatability of the sensor after several cycles.

Appendix A

A.1 XRD (X-Ray diffraction)

The X-ray diffraction technique allows to detect the phase composition of the sample: in fact, each phase presents specific diffractions peaks, on the basis of the lattice structure and atom position. Moreover, this experimental method is employed to evaluate the structure of the crystalline materials and to measure the crystallite size.
X-ray diffraction analyses were carried out by using the conventional diffractometer Philips PW 1710, with a $CuK\alpha$ radiation (= 1.5405.600 Å) and a Bruker diffractometer equipped with a furnace allowing the samples to be heated up to 1200 °C. A schematic representation of the instrument is shown in Fig. A.1.1.

Figure A.1.1. Scheme of the XRD diffractometer.

The X-ray source consists of a filament that heats the cathode, inducing electrons emission. The presence of two metallic electrodes, with a different potential, implies the acceleration of the electrons towards the anode (in this case, made of copper), which emits the X-ray

beam having a specific wavelength range, on the basis of the metallic component and the applied tension.

The power employed in X-rays production is only 0.1%, whereas the leftover one is converted into heat, which could induce anode melting. To avoid it, a water cooling system is present.

X-rays pass through a monochrometer (in this case, made of nickel), which selects the K radiation of copper. This radiation is then collimated upon the sample.

The instrument presents a goniometer having a Bragg-Brentano geometry, that operates in the „ - 2„ scanning regime, in which the detector (D) and the sample (S) move with respect to the X-rays source (X) in a synchronized way, as schematically presented in Fig. A.1.2.

Figure A.1.2. Mechanism of the goniometer in the diffractometer Philips PW 1710.

In this way, the incident and the diffracted beams form the same angle with the flat surface of the sample, whereas the diffracted beam forms an angle 2„ with the incident one (Fig. A.1.3).

Figure A.1.3. The Bragg–Brentano geometry.

This particular geometry is related to the Bragg equation, employed to evaluate the inter planar distance in the crystalline lattice. In fact, when the X-rays hit the sample surface, they can interact with the lattice atoms, being their wavelength and the inter-atomic distance similar. The lattice atoms are then able to diffract the X-rays beam and a signal is recorded when a positive interference occurs, according to the Bragg equation:

$$n\lambda = 2d\sin\theta \qquad \text{(A.1.1)}$$

where θ is the incident angle, d is the inter-atomic distance, λ is the wavelength of the X-rays beam and n is a number.

On the basis of the inter-atomic distances it is possible to evaluate the geometry and the dimensions of the elementary cell; the whole diffraction pattern allows the identification of the phases through the comparison with the ICDD (International Centre for Diffraction Data) files. In addition, the peak intensity depends on the atom position in the elementary cell: more intense are the signals, more crystalline is the sample.

In this study, XRD was used to investigate the phases present in the produced powders. The average crystallite size was calculated by the line-broadening method, using the Scherrer's equation.

$$D = k\lambda / \beta \cdot \cos\theta \qquad \text{(A.1.2)}$$

where D is the crystalline size, λ is the wavelength of the $CuK\alpha$ line, k is the Scherrer's constant equal to 0.9, and β is the full width at half maximum of the main powder peak, assuming a Gaussian profile.

A.2 Laser granulometry

When a laser beam strikes the particles suspended in a inert medium, the produced diffracted rays present intensity and diffraction angle that depend on the size of the impacted particle.

As illustrated in Fig. A.2.1, a laser granulometer consists of a laser beam source, at a fixed wavelength, and a series of detectors (multidiode detector) to measure the diffracted light as a function of the diffraction angle.

The granulometer Malvern Mastersier 2000 was used to evaluate the particle size distribution of the powders dispersed in ethanol. The Mie theory was used to calculate the particle size distribution. This theory takes into account both the diffraction index and the refractive index of both the sample and the medium.

Figure A.2.1. Schematic representation of a laser granulometer.

A.3 SEM

The SEM (Scanning Electron Microscopy) is a technique that allows a morphological characterization of powdered and massive samples. It uses the electrons for imaging, reaching higher magnifications and greater depth field than the light microscopy.

A schematic representation of an instrument is reported in Fig. A.3.1: from the electron emission source, a heated tungsten filament, the beam is focused on the sample surfaces by a series of electromagnetic lenses. The incident electrons imply electrons emission from the sample surface; they are collected by a suitable detector, during the scanning of a raster pattern, producing a topographical image of the analyzed surface.

Some observations were performed in SE (Secondary Electrons) modality, while, when a phase contrast was needed BSE (Back Scattered Electrons) were also detected.

Figure A.3.1. Schematic representation of a SEM instrument.

The powders and the microstructure of the composite materials were observed by using SEM Hitachi S2300, and ESEM (FEI, XL3O, Eindhoven, Netherlands) exploiting a gold sputtering pretreatment of all samples in order to increase the sample conductivity.
The grains size was measured on polished samples, which were thermally etched at a lower temperature than the sintering one, depending on the specific SEM instrument used for the observation. This thermal etching allows to reveal grain boundary for SEM observation.

A.4 BET analysis

In 1938, Stephen Brunauer, Paul Hugh Emmett, and Edward Teller published an article about the BET theory in a journal [1] for the first time; ,BET, consists of the first initials of their family names.
BET theory aims to explain the physical adsorption of gas molecules on a solid surface and serves as the basis for an important analysis technique for the measurement of the specific surface area of a material.
The concept of the theory is an extension of the Langmuir theory, which is a theory for monolayer molecular adsorption, to multilayer adsorption with the following hypotheses:

1. gas molecules physically adsorb on a solid in layers infinitely;
2. there is no interaction between each adsorption layer;
3. the Langmuir theory can be applied to each layer. The resulting BET equation is expressed by:

$$1/ [(P0/P) \ldots 1] = (c \ldots 1)/ v_m c (P/P0) + 1/v_m c \qquad (A.4.1)$$

where P and P0 are the equilibrium and the saturation pressure of adsorbates at the temperature of adsorption, v is the adsorbed gas quantity (for example, in volume units), vm is the monolayer adsorbed gas quantity and c is the BET constant, which is expressed by:

$$c = \exp((E1 \ldots EL)/ RT) \qquad (A.4.2)$$

E_1 is the heat of adsorption for the first layer, and is E that for the second and higher layers and is equal to the heat of liquefaction.

Equation (A.4.1) is an adsorption isotherm and can be plotted as a straight line with 1/v[(P0/P)† 1] on the yaxis and‡ = P/P_0 on the xaxis according to experimental results (Fig. A.4.1).

Figure A.4.1. Schematic representation of a BET plot.

This plotis called a BET plot. The linear relationship of this equation is maintained only in the range of 0.05 < P / P0 < 0.35. The value of the slope A and the intercept I of the line are used to calculate the monolayer adsorbed gas quantity vm and the BET constant c. The following equations can be used:

$$v_m = 1/(A + I) \quad \text{(A.4.3)}$$

$$c = 1 + (A/I) \quad \text{(A.4.4)}$$

The BET method is widely used in surface science for the calculation of surface areas of solids by physical adsorption of gas molecules. A total surface area Stotal and a specific surface area S are evaluated by the following equation:

$S_{BET,total} = (v_m NS)/V$ (A.4.5)

where vm is in units of volume which are also the units of the molar volume of the adsorbate gas:

$S_{BET} = S_{total}/a$ (A.4.6)

whereN is Avogadro€s number, s is the adsorption cross section of the adsorbing species, V the molar volume of adsorbate gas and a the mass of adsorbent (in g). The BET analyses were carried out by using the ASAP 2010 Micromeritics instrument [2].

A.5 Gas System

In this system, referring to Fig. A.5.1, compressed air was separated into two fluxes: one was dehydrated over a chromatography alumina bed, while the second one was directed through two water bubblers (three if measurements were performed under NH_3 atmosphere), generating, respectively, a dry and a humid flow [3]. Two precision microvalves allowed to recombine the two fluxes into one by means of a mixer and to adjust the RH content while keeping constant the testing conditions: a flow rate of 0.05 L/s. The ammonia flux was obtained by diluting an ammonium hydroxide solution (Fluka, USA) in deionized water (ratio 1:20) into a drechsel through which a known air flow was allowed to bubble. The laboratory apparatus for sensors testing was calibrated in such a way to ensure a constant air flow during electrical measurements and RH (relative humidity) was varied by steps, each one of 3 minutes.

Figure A.5.1. Schematic representation of the laboratory apparatus for sensors testing.

An external alternating voltage (V = 3.6 V at 1 kHz) was applied to each tested sensor, placed into a PVC tube, acting as a variable resistance of the electrical circuit described above. The sensor resistance was determined by a calibration curve (Fig. A.5.2), drawn by substituting the sensors, in the circuit, by known resistances.

Figure A.5.2. Calibration curve for sensors testing: the red fit indicates the range of voltage in which the sensors operated. In the equation, y indicates the resistance, x the voltage.

In particular, the sensors operated from about 1.3 V to 2.4 V, corresponding to about 700 k• to 7 k•: by increasing the electrical resistance, the continuous voltage measured by the multimeter decreased. In order to obtain the fit of the calibration curve, the points in which the resistance was linear with respect to the voltage (VDC) were considered, so those ranging from 1.3 to 2.4 V.

RH values were measured by means of a commercial humidity and temperature probe (Delta Ohm DO9406, Italy, accuracy: ±2% in the 5-90% RH range), while the corresponding NH_3 concentration was determined by means of a commercial ammonia probe (GasAlertMicro5, accuracy: ± 0.1ppm in the 0-100 ppm range) or after 100 ppm of NH_3 was estimated by chemical computation from vapor pressure of ammonia at 25°C diluted into water in a ratio 1:20 [4].

The sensor response, expressed in %, (SR(%)) was defined as the relative variation of the starting resistance comparing it with the resistance measured in gas atmosphere:

$$SR(\%) = 100(|R_0 - R_g|/R_0) \quad \text{(A.5.1)}$$

where R_0 is the original resistance in the presence of air flow and Rg is the resistance after NH_3 exposure until equilibrium, i.e. at saturation of the active surfaces.

A.6 Plasma

For plasma polymerization experiments, a small laboratory batch reactor (Plasmod by March Instruments Inc.) was utilized. A low pressure (1.3 mbar) nitrogen plasma was applied at 50 W for 30 s to samples.

A plasma is defined as a partially or wholly ionised gas with approximately equal amount of positively and negatively charged particles. Near equilibrium plasmas are formed under high temperature conditions and are characterised by thermal equilibrium of its entire range of species. The temperatures required to generate equilibrium plasmas generally range between 4000 and 20,000 K, depending on the ionisation potential of the element. These extreme conditions are not likely to be appropriate for the surface modification of biomaterials constructed from polymers, although they can be used for the evaporation and deposition of bioactive metals and ceramics, such as natural hydroxyapatite based bioglass ceramic composites and zirconia coatings for artificial bones and hard tissues. Non-equilibrium plasmas, on the other hand, can be initiated at substantially lower temperatures, enabling their application for surface cleaning and functionalisation of polymer surfaces. The ion mobility in a low temperature plasma is significantly lower than that of the electrons that transport the energy through the electric field.

The plasma can also be classified according to the pressure at which it is initiated or according to the energy source used to energise the gas.

During plasma surface treatment the substrate is exposed to a reactive environment of a partially ionised gas comprising large concentrations of excited atomic, molecular, ionic, and free radical species Fig. A.6.1. The nature of the interactions between the excited species and the solid surface will determine the type and degree of the chemical and physical modifications that will take place.

The processing conditions, such as power, pressure, gas, etc., and the nature of the substrate will determine whether the surface modification is one of film deposition, substitution, or ablation.

Plasma polymerisation can take place when a monomer, either in vapor phase or at the surface, is fragmented into reactive species that can then recombine and be deposited onto the surface of the substrate. Monomers that do not necessarily contain functionalities associated with conventional thermochemical polymerisation, such as unsaturation or ring structures, can be deposited in this way.

In plasma treatment gases that do not fragment into polymerizable intermediates upon excitation are used. These include air, nitrogen, argon, oxygen, nitrous oxide, helium, tetrafluoromethane, water vapor, carbon dioxide, methane, and ammonia. Exposure to such plasmas can lead to the introduction of chemical functionalities, with the nature of the functionalities being highly dependent on the chemical composition of the biomaterial and the process gas. For instance, plasma oxidation, nitration, hydrolyzation, or amination will increase the surface energy and hydrophilicity of the biomaterial, therefore changing the way in which the biomaterial interacts with its immediate physiological environment.

Free radicals are also created on the surface, since the surface is being bombarded by energetic particles and high energy UV radiation. This can lead to surface ablation, cross linking or surface activation. Ablation is a process by which lower molecular weight species, such as volatile oligomers and monomers, are desorbed. Cross-linking occurs when radicals from one chain on the

surface of the polymer combine with radicals from another polymer chain to form a bond. Surface activation, however, involves the recombination of surface radicals with atoms or chemical groups that are different from those that were originally present at the surface of the biomaterial.

The surface functionalities that arise as a result of plasma treatment can serve as a platform for further surface modification processes, such as the grafting of biomolecules and other functional structures. Further surface modification can be performed in order to tailor the properties of the biomaterial to a specific application.

A number of papers have been published that detail the use of a pulsed plasma technique. This technique allowsthe precise control of chemical functionality and surface morphology and results in a coating with good stability. The plasma duty cycle was found to be an important determinant in controlling the degree of retained surface functionality and, hence, a greater degree of compatibility with biomolecules, bacterial and host cells, and liquid media. Moreover, the surface properties of the coating could be varied using this technique by changing the duty cycle between the ™™pulse on€€ (ion implantation) and ™™pulse off€€ (plasma exposure) periods during treatment, with a high ion implantation/plasma exposure time ratio being achieved by increasing the pulsing frequency and elongating the duration of the pulse [5, 6].

Fig. A.6.1. Surface modification processes that can be achieved using the plasma technique

Bibliography

1. S. Brunauer, P. H. Emmett and E. Teller, J. Am. Chem. Soc., 1938, 60, 309. doi:10.1021/ja01269a023

2. Phd Thesys of A. Cavalieri, Room temperature ammonia sensors for food industry applications, Ph.D. Thesis, 2011.

3. J. M. Tulliani and P. Bonville, Influence of the dopants on the electrical resistance of hematite-based humidity sensors, Ceramics International 31 (2005) 501–507

4. J. H. Perry, Chemical Engineers' Handbook, McGraw-Hill (1963), part 3, p. 66.

5. R.S. Joshi, J.F. Friedrich and M.H. Wagner, Study of carboxylic functionalization of polypropylene surface using the underwater plasma technique, Eur. Phys. J. D 54, 249–258 (2009).

6. V. Sciarratta, U. Vohrer, D. Hegemann, M. Müller, C. Oehr, Plasma functionalization of polypropylene with acrylic acid, Surface and Coatings Technology 174–175 (2003) 805–810